Environmental Science: Nano 8.8 (2021): 2277-2296

DOI: https://doi.org/10.1039/D1EN00284H

Understanding nanoplastics toxicity and their interaction with engineered cationic nanopolymers in microalgae by physiological and proteomic approaches

Please, cite as follows:

Miguel Tamayo-Belda, Juan Vargas-Guerrero, Keila Martin-Betancor, Gerardo Pulido-Reyes, Miguel González-Pleiter, Francisco Leganés, Roberto Rosal, Francisca Fernandez-Piñas, Understanding nanoplastics toxicity and their interaction with engineered cationic nanopolymers in microalgae by physiological and proteomic approaches. Environ. Sci.: Nano, 8, 2277-2296, 2021.

https://doi.org/10.1039/D1EN00284H

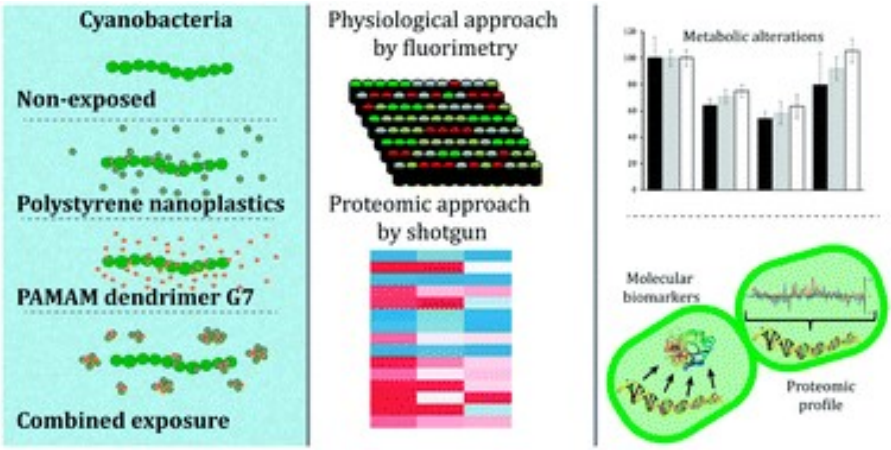

Understanding nanoplastics toxicity and their interaction with engineered cationic nanopolymers in microalgae by physiological and proteomic approaches

Miguel Tamayo-Belda[1], Juan Vargas-Guerrero[1], Keila Martin-Betancor[1], Gerardo Pulido-Reyes[1], Miguel González-Pleiter[1], Francisco Leganés[1], Roberto Rosal[2], Francisca Fernandez-Piñas[1,*]

[1] Department of Biology, Faculty of Science, Universidad Autónoma de Madrid, E-28049, Madrid, Spain.
[2] Department of Chemical Engineering, Universidad de Alcalá, E-28871 Alcalá de Henares, Madrid, Spain

[*] Corresponding author: francisca.pina@uam.es

Abstract

The amount of plastics produced per year is in constant growth, alongside their use in different sectors like textile industry, agriculture or, more recently, in nanotechnology. Under certain environmental conditions, plastics break down into smaller pieces. Those plastics in the nano size range are the most difficult to identify, quantify and remove and therefore, probably prevail in aquatic ecosystems. Likewise, nanomaterial production has been increasing exponentially and therefore, their potential release to the environment poses a threat. There is a lack of knowledge regarding the combined effects of co-occurring nanopolymers on biota. In this work, we have studied the individual toxicity of polystyrene nanoplastics (PS-NPs), as well as their combined effect with Generation 7 PAMAM dendrimers (G7), on the filamentous cyanobacterium *Anabaena* sp. PCC7120, a relevant aquatic primary producer. Exposure to PS-NPs induced the overproduction of reactive oxygen species, lipid peroxidation, membrane disruptions, intracellular acidification, and a decrease in photosynthetic activity. Internalization of the nanoplastics was also observed. Combined exposure to PS-NPs and G7 lowered PS-NPs toxicity and precluded their internalization. This antagonistic interaction was due to the formation of heteroaggregates. Molecular biomarkers (differentially expressed proteins, DEPs) of the toxic effect of nanoplastics, G7 and their binary mixture were identified for the first time. These molecular biomarkers may be envisaged as a molecular signature of the toxic effect of the nanopolymers and could be predictors of cellular damage caused by exposure to nanopolymers.

1. Introduction

The threat of plastic pollution and its potential harmful effects on the environment were already pointed out decades ago but were overlooked for a long time [1]. The production of plastics is expected to globally double in the next 20 years [2–4] and Geyer *et al.* [5]estimated that, up to 2015, 6300 million metric tons of plastic waste has been generated, from which approximately 79 % has accumulated in landfills or in the environment. Due to different environmental factors, plastics fragment into smaller pieces as secondary micro, submicron (sMP, from 100 to < 1000 nm) and nanoplastics (NP, < 100 nm)[6], which might increase their distribution and potential toxicity [7–9]. Nanoplastics may be classified into two categories based on their origin: i) Primary plastics, which are plastics that have reached the environment in the same form as they were produced; and ii) Secondary plastics, which are plastic debris that emerge from fragmentation of the original plastic product as a result of being altered during the time they have been in the environment; therefore, they usually present irregular shapes[6].

Given the possibility of synthesizing polymeric nanoparticles made of different raw plastic materials, research on the potential toxicity of some of them has been addressed in the literature. Polystyrene is one of the most common polymers used for the production of styrofoam, extruded polystyrene for thermal insulation and a wide variety of different products. Polystyrene is prevalent in marine litter because of the buoyancy of most products made from it. Several studies have suggested that polystyrene nanoparticles may be internalized by organisms, producing different effects like developmental abnormalities, mitochondrial damage, and inflammatory reactions[10]. Polystyrene is the only polymer for which its secondary nanoparticles or oligomers produced during ageing have been detected in environmental samples. Both Saido *et al*. and Amamiya *et al.*[11,12]detected several oligomers of polystyrene (identified as products of polystyrene decomposition) in samples of sand and seawater of the North-West Pacific Ocean[11,12]. Most of the toxicological studies to date have been performed with polystyrene nanoplastics (hereafter, PS-NPs) [13–28], since they are routinely synthesized for several biomedical applications[29,30].

Dendrimers belong to the family of dendritic architectures that include many hyperbranched polymers. All dendritic architectures are branched molecules growing from a central core and sharing

properties like a high number of reactive groups, low viscosity, and high solubility. Some dendritic compounds find large volume applications; in particular, hyperbranched poly(ethyleneimine) has been used as a dispersant in oil spills and for the curing of epoxy resins[31,32]. Poly(amidoamine) (PAMAM) dendrimers are made by repetitively branched amidoamine internal structure with terminal primary amines and internal tertiary amines that share a basic chemical similarity with dendritic structures containing amines, namely their positive charge at neutral or near to neutral pH. As for their environmental relevance, apart from their medical uses, PAMAM dendrimers are applied as chelating agents in water and wastewater treatment, among other uses[33–41].

In this context, and given the wide range of potential applications, the OECD has included PAMAM dendrimers in the list of nanoparticles to be screened for possible toxicological effects in both environmental[42–48] and mammalian systems.[49] Organisms in their natural environment are generally exposed to mixtures of different substances, often including multiple rather than single pollutants;[50], exposure scenarios should therefore consider factors such as heteroaggregation, adsorption or possible antagonistic/synergistic effects. To date, no study has assessed the effect of the combined exposure of organisms to nanoplastics and polymeric engineered nanomaterials. The reason for combining polystyrene nanoparticles and PAMAM dendrimers is their belonging to entirely different families of nanomaterials. Polystyrene is aromatic while PAMAM is aliphatic, and both bear different charges in aqueous suspension; while polystyrene nanoparticles display a negative change due to the preferential adsorption of hydroxide ions, PAMAM dendrimers are positively charged as a consequence of the protonation of their amine moieties.
In this work, the effects of virgin fluorescent PS-NPs on the filamentous cyanobacterium *Anabaena* sp. PCC 7120 (hereinafter *Anabaena*) have been thoroughly studied using both physiological and proteomic approaches. This cyanobacterium, given its ecological relevance in freshwaters as primary producer, has been regularly used as a model for ecotoxicological studies, including in the field of nanotoxicology.[47,48,51,52] Furthermore, a combined toxicity study has been undertaken by using PS-NPs and poly(amidoamine) dendrimers of generation 7 (hereafter G7) to evaluate their potential interaction towards *Anabaena* by means of the Isobologram-Combination Index (CI) method.[53,54] Physiological studies were carried out by measuring the formation of reactive oxygen species (ROS), membrane integrity, cytoplasmic membrane potential, intracellular pH, lipid peroxidation, and photosynthesis. Potential internalization of PS-NPs and/or adhesion to cellular envelopes was observed by confocal microscopy, which allows tracking the fluorescence of PS-NPs. To dig deeper into the mechanisms of toxicity, as well as to determine potential molecular biomarkers of toxicity with PS-NPs, both individually and combined with dendrimers, a shotgun proteomic approach was also used.

2. Materials and methods

(EC_{10}, EC_{50} and EC_{90}, respectively) were calculated by the dose–response package using R-Studio software, version 0.99.902. The concentrations corresponding to the EC_{50} for both PS-NPs and G7 were used to study the mechanisms of toxic action. For dry weight determinations, 1 L of grown culture was collected by centrifugation and dilutions were made, culture density of the dilutions was determined spectrophotometrically at 750 nm. For dry-weight determinations, collected cells were washed and dried at 70 ºC for 24 h. To relate culture density and dry-weight, the following calibration curve was obtained and applied: mg Dry Weight/ml = 0.396 X OD750nm – 0.004. No toxicity was expected by the G7 stock suspension medium (pure water) and in the case of PS-NPs, the highest concentration tested was filtered through 50 kDa (removing all the particles higher than ~ 5 nm) and the nanoplastic-free suspension was tested, finding no significant growth inhibition or chlorophyll a content decrease (Fig. S1).

2.1. Photosynthetic pigment concentrations

Photosynthetic pigment concentrations were determined after 72 h exposure of *Anabaena* to increasing concentrations of PS-NPs (from 1 mg/L to 200 mg/L) and G7 (from 1 mg/L to 30 mg/L), under constant shaking and illumination. Chlorophyll *a* concentration was estimated spectrophotometrically after extraction in 1 mL aqueous solution of methanol (90 %, w/v) at 4 °C for 24 h in darkness.[56] For phycobiliprotein extraction, 1 mL of culture was centrifuged and the pellet was resuspended by adding 950 µL of pure water and 50 µL of toluene. After shaking for 1 min, the samples were incubated for 24 hours in darkness at 4 °C. Phycocyanin concentration was determined following.[57] DRC for PS-NPs and G7 in terms of chlorophyll *a* and phycocyanin concentration as well as the EC_{10}, EC_{50} and EC_{90} were also analysed using the R-Studio software package.

2.2. Mixture toxicity bioassays

For testing the combined toxicity of G7 and PS-NPs, *Anabaena* was exposed simultaneously to the individual growth inhibition EC_{50} of both nanopolymers and to their combination in a constant ratio 1:1 as previously described.[53,54] The

DRC of the mixture was described in terms of growth inhibition, but also of chlorophyll *a* and phycocyanin concentration decrease. Each experiment was conducted in triplicate. The effect of the nanopolymer mixture was determined using the median-effect equation based on the mass-action law.[58] For each effect level, the combination index was calculated according using the equation:

$$^{n}(\mathrm{Cl})_x = \sum_{j=1}^{n} \frac{(D)_j}{(D_x)_j} = \sum_{j=1}^{n} \frac{(D_x)_{j1-n} \frac{D_j}{\sum_1^n [D]}}{(D_m)_j \left[\frac{(f_{ax})_j}{1-(f_{ax})_j}\right]^{1/mj}}$$

Where $^{n}(CI)_x$ is the combination index of n compounds for a given *fa*, which is the fraction affected by dose D (e.g. 0.50 if growth is inhibited by 50%). $(Dx)_{1-n}$ is the sum of the doses of the n compounds that exert x% inhibition (growth and pigment concentration in this study) in combination; $([D]_j / \sum_1^n [D])$ is the proportion of the dose of each compound that exerts x% of growth or pigment content inhibition in combination, and $(Dm)_j (fa_x)_j / [1 - (fa_x)_j]^{1/mj}$ is the dose of each compound separately that exerts inhibition of x%. From the equation CI < 1, CI = 1 and CI > 1 indicate synergism, an additive effect and antagonism, respectively. Data corresponding to the parameters of the dose-effect curve and the CI values for each effect level were determined by the software CompuSyn (ComboSyn, Inc.).

2.3. Physiological study

2.3.1 Fluorimetry analysis

The mechanism of action of both nanopolymers, singly and in combination, was measured in *Anabaena* cultures, exposed for 72 h at the concentration corresponding to the EC_{50} of each nanopolymer, in triplicate using fluorimetry. After 72 h of treatment, samples were analysed in a microplate reader Fluoroskan Ascent® fluorometer (Thermo Fisher Scientific) with an excitation laser (488 nm) and 4 detectors corresponding to 4 wavelength range channels: 505-550 (FL1), 550-600 (FL2), 600- 645 (FL3) and> 645 (FL4) following.[59] Five fluorescent probes were used to evaluate four physiological parameters (incubation times and concentrations were adapted from Tamayo *et al.* 2019[48]: reactive oxygen species (ROS) formation by dihydrorhodamine 123 (DHR 123) for H_2O_2 formation at a final concentration of 30 µM, and dichlorofluorescein diacetate (H_2 DCF DA), a non-specific probe that reveals the formation of both reactive oxygen and nitrogen species at a final concentration of 100 µM, incubated for 10-15 min, channel FL1; membrane integrity (propidium iodide (PI) at a final concentration of 7.5 µM, incubated for 10 min, channel FL3); Cytoplasmic membrane potential (Bis- (1,3-Dibutylbarbituric Acid) bis-(1,3-dibutylbarbituric acid) trimethine oxonol (DiBAC4 (3)) at a final concentration of 5 µM, incubated for 10 min, channel FL1); intracellular pH (2', 7'-Bis-(2-carboxyethyl)-5(6) -carboxyfluorescein, acetoxymethyl ester (BCECF AM) at a final concentration of 9.5 µM, incubated for 40 min, channels FL1 and FL3). The fluorescence of chlorophyll *a* and of three independent PS-NP suspensions (in the absence of cells) was subtracted from the total fluorescence of the treatments when overlapping with the emission of the fluorochrome used. Aliquots of 200 µL were placed in 96-well plates with the corresponding fluorochrome (from Thermo Fisher Scientific, Waltham, Massachusetts). Five technical replicates were made for each treatment and ten measurements were carried out for each plate. The responses of the cyanobacterial cells to the treatments with each fluorochrome were expressed as percentage with respect to the control (non-exposed cyanobacterial cells)

2.3.2. Lipid peroxidation

Lipid peroxidation was determined in terms of thiobarbituric acid reactive substances (TBARS) following the protocol described by Ortega-Villasante *et al.* 2005[73] with minor modifications.[74] Cyanobacterial cells were harvested by centrifugation (3000 rpm) and resuspended in 3 ml (0.67 % w/v) of trichloroacetic acid (TCA) solution and then broken by ultrasonication at 400 mA for 120 s. The suspension was centrifuged at 13 000 rpm for 30 min and 2 mL of the supernatant was mixed with 2 mL of 0.5 % thiobarbituric acid (TBA) in 20 % TCA. The mixture was heated at 90˚C in a hot block for 30 min, cooled to 25 °C, and centrifuged at 13 000 rpm for 5 min. The absorbance of the supernatant was measured at 532 nm. The value for nonspecific absorbance at 600 nm was subtracted. The amount of TBARS was calculated by using the extinction coefficient of 155 mM^{-1} cm^{-1}. Lipid peroxidation was expressed as malondialdehyde (MDA) content percentage with respect to the control (non-exposed cyanobacterial cells).

2.3.3. Photosynthesis

Photosynthetic oxygen evolution was measured at 28 °C under saturating actin light (300 µmol photons m^{-2} s^{-1}) with a Clark-type oxygen electrode (Hansatech) according to Leganés *et al.* 2014[62]. Photosynthetic rates were relativized to chlorophyll *a* and represented as percentage with respect to control (non-exposed cells).[63]

2.4. Proteomic analysis

The protein extracts from three independent replicates of *Anabaena* exposed to PS-NPs, G7 and their binary mixture for 72h were digested, labelled, fractioned, and quantified following the steps specified in Supplementary Material. Differentially expressed proteins (DEPs) were detected based on a fold change (FC) of > 1.2 or < 0.83 and a $p < 0.01$;[64] DEPs were clustered from the protein-protein interaction network (PPI) analysis using the MCL algorithm,[65] tuned to an inflation parameter = 3 (output is listed in Table S1), and subsequently adapted based on GO, using UniProt, STRING software version 11.0 and ALCOdbCyano, as shown in Fig. S2.[66] In order to compare protein alteration patterns between treatments, Pearson correlation coefficient (*r*) and the coefficient of determination (R^2) were calculated by category, considering the FC of each DEP, between PS-NPs and G7 individual treatments (PS-NPs:G7), PS-NPs and binary mixture treatments, (PS-NPs:Mix) and G7 and binary mixture treatments (G7:Mix).[67,68]

2.5. Confocal microscopy

A Confocal Laser Scanning Microscope LSM510 coupled to an inverted microscope Axiovert200 M (Zeiss) was used to visually track the fluorescence of PS-NPs in *Anabaena* exposed for 72 h to PS-NPs individually and in combination with G7. A volume of 7 µL of each sample was directly taken and observed without any fixation procedures, in order to prevent masking, the interactions between the particles and the cyanobacterium filaments. The excitation laser was set at 488 nm and the emission filter at 665 nm for chlorophyll *a* fluorescence and 535 nm for fluorescence of the PS-NPs. The obtained images were visualized with ZEN 2.3 SP1 (black), V.14.0.0.201 (Carl Zeiss, Germany).

2.6. Data analysis

Means and standard deviation values were calculated for each treatment from three independent experiments. To determine significant differences between with respect to controls, as well as among treatments, data were analysed using ANOVA by means of R software (v. 3.3.1). Significant differences were assessed using multiple-range Tukey's HSD test. $p < 0.05$ was considered statistically significant.

3. Results

3.1. Physicochemical characterization of PS-NPs and G7 dendrimers

The physicochemical characterization of PS-NPs and G7 dendrimers was carried out by studying the size (measured by DLS) and the net surface charge (by calculating the ζ-potential by ELS) of both nanopolymers individually and in combination. Size measurements were carried out both in AA / 8 + N medium (cyanobacterial growth medium) and pure water in the absence of cells. The concentrations used for the measurement were 100 mg/L for PS-NPs and 10 mg/L for G7. The DLS and ζ -potential give information on both the particle size in suspension and the stability of the particles. PS-NP particle numbers were studied in the range of 0.1 to 300 mg/L by MADLS® technique. Based on particle counts, a regression equation was obtained to calculate the concentration of particles. The theoretical number of PS-NPs particles (assuming spherical shape, the manufacturer specified PS-NPs density and assuming monodispersity) was also evaluated. Both sets of data agreed. Accordingly, the experimental equation based on MADLS data was used to convert mass concentration in mg/L into particle concentration in particles/cm^3 (Fig. 1A; Fig. S3). Both linear regression equations, the empirical and the theoretical, showed high positive correlation ($R^2 = 0.963$); hence, highly accurate data of PS-NPs particle number may be obtained from their concentration (mg/L) by using the following equation:

$$[\text{PS-NPs}]\ (\text{particle number/mL}) = 1.07 \times 10^{11} \times [\text{PS-NPs}]\ (\text{mg/L})$$

G7 particle number was also estimated, but only at the theoretical level given that G7 has a well-defined polymeric structure and the molecular weight is provided by the manufacturer. As shown in Fig. S4, the number of G7 particles may be easily calculated from their concentration in terms of mass as well as in terms of molarity using:

$$[\text{G7}]\ (\text{particle number/mL}) = 6 \times 10^{14}\ [\text{G7}]\ (\mu\text{M})$$

$$[\text{G7}]\ (\text{particle number/mL}) = 5\times 10^{12}\ [\text{G7}]\ (\text{mg/L})$$

The micro-FTIR spectra (Fig. 1B) present the characteristic bands of single PS-NPs and G7 whilst the suspension containing both nanopolymers shows characteristic peaks from each one (specific spectra information is under the subheading; Figure 1B specific information is in the Supplementary Material). The DLS measurements of particle hydrodynamic size, transformed to volume distribution, of both nanopolymers in pure water after filtration through a 100 nm filter are in good agreement with the data provided by the manufacturers, namely 8 nm in the case of G7 and 24 nm for PS-NPs (Table S2). The DLS size, by intensity distribution, of G7 in aqueous solution also showed a peak of about 300 nm (Fig. 1 C(a)). The presence of aggregates of PAMAM dendrimers in aqueous solution and in AA/8+N medium at close to neutral pH has been reported elsewhere [47]. The results are consistent with the formation of aggregates from G7, which would coexist with a certain number of free

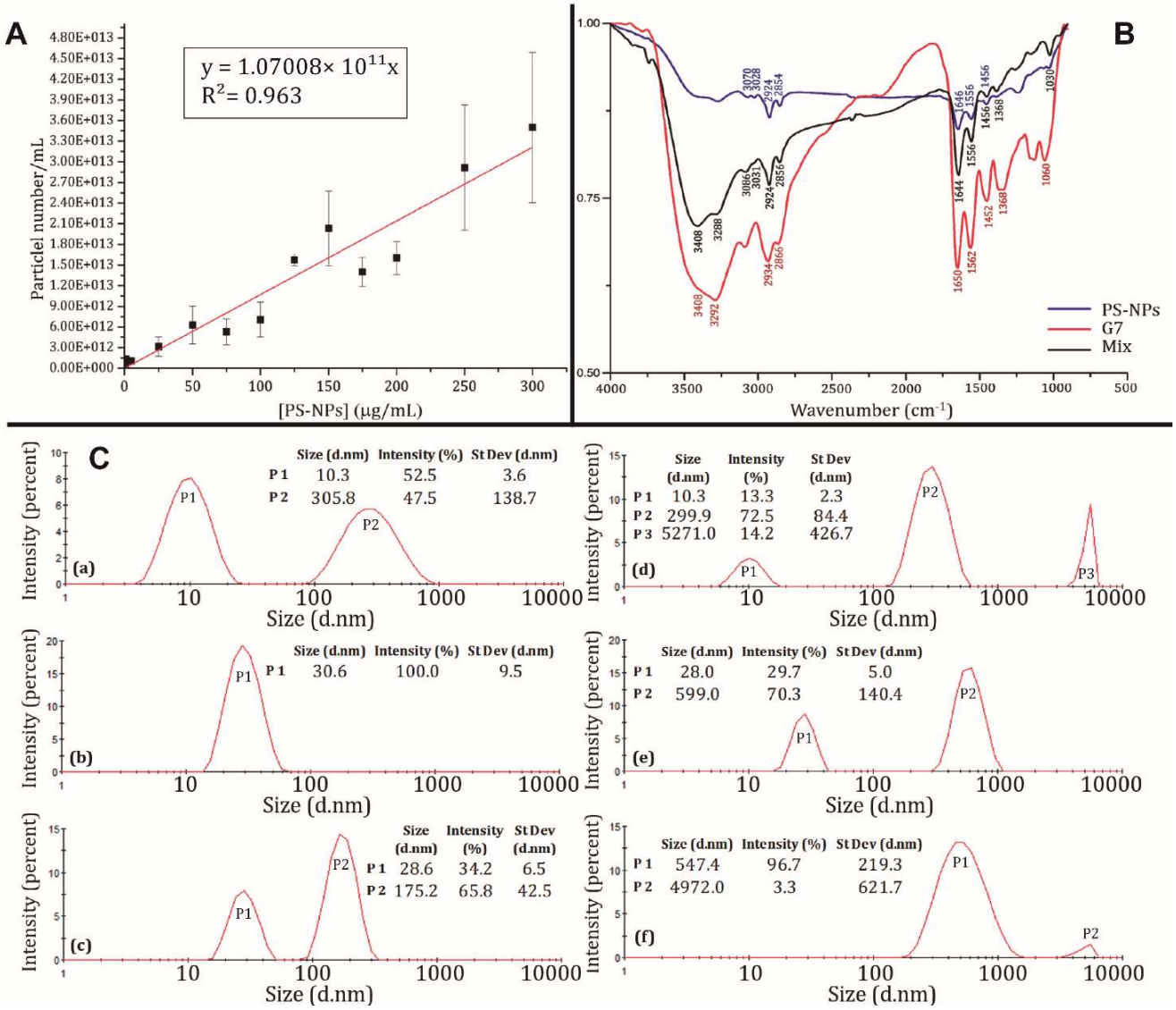

Figure 1: A: MADLS® measurements of PS-NPs numbers in pure water, the linear regression equation, and the coefficient of determination (R^2). B: µFTIR spectra of PS-NPs (blue) G7 PAMAM dendrimers (red) and their mixture (black). The three highly concentrated suspensions (~1000 mg L^{-1} corresponding to ~1.07×10^{14} and ~5×10^{15} PS-NPs and G7 particles ml^{-1}, respectively) were dried over potassium bromide discs and measured by transmission using a 50 mm^2 spot. C: DLS intensity distribution plots (size is shown as diameter in nanometers) with representative peaks (P) of G7, PS-NPs and their mixture (PS-NPs + G7) in pure water (C(a), C(b) and C(c), respectively) and in the cyanobacterial culture medium AA/8+N (C(d), C(e) and C(f), respectively). Measurements were conducted at 100 mg L^{-1} for PS-NPs and 10 mg L^{-1} for G7 (~1.07×10^{13} and ~5×10^{13} particles ml^{-1}, respectively) after filtering by 100 nm filter (the mixture was filtered separately).

G7 molecules. While PS-NPs present a single peak in pure water (Fig. 1C(b)), the size measurement of the G7 and PS-NPs mixture, also in pure water, yielded a peak at about 30 nm, which corresponded an excess of PS-NPs, together with a peak centred at 175 nm (Fig. 1C(c)). Such aggregates are most probably formed by the interaction of negatively charged PS-NPs with the positively charged G7. In AA/8+N medium, after filtration through 100 nm filters, the peaks from PS-NPs and G7 are also clearly visible together with other particles from the background colloid. The results are shown in Fig. 1C(d) and (e). The obtained DLS sizes are consistent with some degree of heteroaggregation with particles from the background colloid. In the mixture, characteristic peaks from the single particles disappear and a peak of about 550 nm appears, probably as a result of heteroaggregation between positively and negatively charged particles (Fig. 1C(f).

In order to elucidate the cause of such heteroaggregation processes, the ζ-potential was measured by ELS in AA / 8 + N culture medium. As shown in Table S2, PS-NPs present a negative surface charge (-19.8 mV), unlike G7 dendrimers, which present a similar but positive charge (20.8 mV). This analysis provides relevant information when predicting the interactions between both nanopolymers in mixtures. In this regard, the ζ-potential of the PS-NPs and G7 mixture showed a significant decrease in absolute value (under 17 mV), reflecting a loss of the suspension stability and probably inducing the observed heteroaggregation.

3.2. Effect of PS-NPs, G7 and their mixture on growth and pigment concentrations of *Anabaena*

Fig. S5 A and B show the dose response curves (DRC) of *Anabaena* growth when exposed singly to both PS-NPs and G7 as well as the DRC of their mixture (Fig. S5 C, D and E); subsequently, the values corresponding to the EC_{10}, EC_{50} and EC_{90} of PS-NPs and their mixture were determined (Table S3). DRC of the individual exposures of both nanopolymers in terms of chlorophyll *a* and phycocyanin concentrations are shown in Fig. S6. Attending to growth inhibition, the EC_{50} of PS-NPs (~ 64 mg/L, corresponding to ~ 6.85×10^{12} PS-NPs particles ml^{-1}) is higher than the EC_{50} of G7 (~ 8 mg/L according to Tamayo-Belda *et al.*[48], corresponding to ~ 4×10^{13} G7 particles ml^{-1}), indicating that lower toxicity is exerted by the PS-NPs, which also exhibited higher surface areas (at the concentration corresponding to the EC_{50}) than G7 (Table S4).

The combination of the concentrations corresponding to the EC_{50} for growth inhibition of each nanopolymer at a constant ratio of 1:1 was used to obtain the dose-response curve of the mixture after 72 h exposure of *Anabaena*. Fig. S7 shows the CI–f_a plot. A clear antagonistic behavior was observed throughout the whole range of effect levels, meaning that their combined toxicity is lower than the sum of the individual toxicities. As the affected fraction increases, the CI values decrease for growth inhibition and phycocyanin concentration, which means that the interaction between both nanopolymers tend to be additive, whilst for chlorophyll *a* concentration the CI value keeps constant and therefore displays an antagonistic behavior along the whole range of effect levels. Table 1 shows the dose-effect curve parameters (*Dm*, *m* and *r*) of the two nanopolymers singly and in their binary combination, as well as the mean combination index (CI) values of the PS-NPs and G7 mixture. *Dm*, the dose required to produce the median effect (analogous to the EC_{50}), also referred as potency, is higher for growth inhibition than for pigment concentration. Pigment concentration therefore seems to be a more sensitive endpoint than growth inhibition for both PS-NPs and G7 nanopolymer toxicity. *m* indicates the shape of the dose-effect plot ($m = 1$, $m > 1$, and $m < 1$ indicate hyperbolic, sigmoidal and negative sigmoidal dose-effect curves, respectively), which is negative in all cases, corresponding to a negative sigmoidal dose-effect curve shape; the linear correlation coefficients (*r*-values) of the median-effect plots is > 0.9 in all cases, indicating good conformity of the data to the median-effect principle, which qualifies for further studies using this method

3.3. Physiological study

So far, results support that PS-NPs inhibit the growth of *Anabaena* and decrease its pigment concentrations*;* in order to investigate the mechanism of toxic action, several physiologically relevant parameters such as ROS formation, lipid peroxidation, membrane integrity, membrane potential, intracellular pH and photosynthetic activity (by measuring oxygen evolution) were studied. The concentrations of nanopolymers corresponding to the EC_{50} of growth inhibition were used. For comparison, the single effects of G7 were measured simultaneously to those of PS-NPs and their mixture, basically obtaining the same results as previously published [48].

Table 1: Dose-effect related parameters and mean combination index (CI) values (as a function of fractional growth inhibition, chlorophyll *a* and phycocyanin concentration decrease) of polystyrene nanoplastics (PS-NPs) and PAMAM dendrimer of generation 7 (G7), individually and in their binary combination.

Endpoint	Particle/Combo	Dose-effect parameters			CI Values		
		Dm	*m*	*r*	EC_{10}	EC_{50}	EC_{90}
Growth inhibition	PS-NPs	60.5	-7.22	0.979	-	-	-
	G7	3.75	-4.35	0.991	-	-	-
	PS-NPs + G7	95.3	-2.66	0.985	4.75 ± 0.12	3.12 ± 0.06	2.07 ± 0.07
[Chlorophyll *a*] decrease	PS-NPs	52.3	-5.15	0.929	-	-	-
	G7	2.94	-2.44	0.923	-	-	-
	PS-NPs + G7	87.3	-3.38	0.908	3.45 ± 0.33	3.47 ± 0.26	3.70 ± 0.68
[phycocyanin] decrease	PS-NPs	54.9	-7.59	0.967	-	-	-
	G7	3.69	-4.24	0.942	-	-	-
	PS-NPs + G7	104	-3.21	0.943	4.79 ± 0.46	3.91 ± 0.18	2.76 ± 0.26

The parameters *Dm, m* and *r* are the antilog of x-intercept, the slope and the linear correlation coefficient of the median-effect plot, which refers to the shape of the dose-effect curve, the potency (EC_{50}), and conformity of the data to the mass-action law, respectively.[112] *Dm* and *m* values are used for calculating the CI values, where: CI <1, =1, and >1 indicate synergism, additive effect and antagonism, respectively. EC_{10}, EC_{50} and EC_{90}, are the doses required to inhibit each endpoint; 10, 50 and 90%, respectively. Computer software CompuSyn was used for automated calculation and simulation.

3.3.1. Effect on reactive oxygen species formation

It is well known that exposure to different nanoparticles may trigger the overproduction of intracellular ROS, exposing the cell to oxidative stress when an imbalance in its redox homeostasis occurs and, subsequently, compromising the integrity of different cellular components, such as the plasma membrane or the photosynthetic apparatus. H_2DCF DA and DHR123 probes were used to study the levels of intracellular ROS (Fig. 2A, B). Both H_2DCF DA and DHR123 fluorescence showed a statistically significant increase (150 % and 200 % ($p < 0.001$), respectively, compared with the control) when *Anabaena* was exposed to PS-NPs. The combined exposure to PS-NPs and G7 induced a significant increase on the fluorescence of DHR123 but not H_2DCF DA, with respect to the control. This shows that the presence of PS-NPs by itself is able to induce ROS overproduction, however, in co-exposure with G7, ROS overproduction is lower than that induced by the individual exposure to PS-NPs or G7 nanopolymers. This is in agreement with the observed antagonistic interaction resulting in less growth inhibition and pigment content. This antagonistic behaviour is probably linked to the observed heteroaggregation of both nanopolymers when mixed.

3.3.2. Effect on membrane integrity

Potential damage of the cytoplasmic membranes was analyzed using two different approaches. Firstly, an imbalance in intracellular ROS formation may lead to membrane damage by structural lipid peroxidation. Analysis of lipid peroxidation was performed by quantification of TBARS, end products of lipid peroxidation, predominantly malondialdehyde (Fig. 2C). Both PS-NPs and G7 led to a similar level of membrane lipid peroxidation as a significant increase ~175 % ($p < 0.001$) of TBARS was observed after individual exposure to PS-NPs and G7, with respect to the control. Higher TBARS increase (300 % with respect to the control) was observed when exposed to the PS-NPs and G7 mixture, probably indicating an abrasion effect of the nanopolymer aggregates on the cellular envelopes (see below under Intracellular tracking of fluorescent PS-NPs). Secondly, PI was used since it is unable to pass through intact cell membranes, however, when the integrity of the cell membrane fails, PI is able to enter and stain nucleic acids, which then emit fluorescence, allowing the discrimination of cells presenting damages in their cytoplasmic membrane.[48,69] The results in Fig. 2D also show a similar level of alteration in cytoplasmic membrane integrity produced by individual exposure to PS-NPs and G7, as revealed by a PI fluorescence increase of around 400 % with respect to the control ($p < 0.001$). In this case, the nanopolymer mixture induced around a 200 % increase in fluorescence with respect to the control, corroborating the observed antagonistic interaction.

3.3.3. Effect on cytoplasmic membrane potential

The cytoplasmic membrane potential is mainly regulated by two factors: the ionic permeability of the membrane and the transmembrane ionic gradient. DiBAC4 (3) fluorochrome was used to detect changes in the membrane potential. After being excited, this fluorochrome varies between decreasing or increasing fluorescence emission in the case of hyperpolarization or depolarization, respectively, of the cytoplasmic membrane. The three treatments caused a significant increase ($p < 0.001$) in fluorescence and therefore cytoplasmic membrane depolarization, with respect to the control (Fig. 2E). The effect of both PS-NPs and G7 exposure was similar, with a fluorescence of ~ 430% ($p < 0.001$) with respect to the control. The mixture caused a slightly lower increase of DiBAC4 (3) fluorescence (~ 350% ($p < 0.001$) with respect to the control), meaning that the potential abrasion of heteroaggregates on cell envelopes (see below under Intracellular tracking of fluorescent PS-NPs) may alter also cytoplasmic membrane potential.

3.3.4. Effect on intracellular pH

Intracellular pH may vary (usually it is acidified) after pollutant exposure.[48,70,71] The green/red BCECF fluorescence intensity ratio (green fluorescence is pH dependent, whereas red fluorescence is pH independent) was used to measure intracellular pH variations after each treatment. This ratio increases when intracellular pH increases and decreases when it decreases (within the physiological pH range). In this case, the three treatments triggered a significant acidification of the intracellular pH of *Anabaena* (Fig. 2F) which is revealed by a significant decrease (around 50 %) in the red: green ratio, with respect to the control ($p < 0.001$), after exposure with PS-NPs, G7 and also with their mixture, which correlates with the negative effects triggered by the heteroaggregates on lipid peroxidation and cytoplasmic membrane potential.

3.3.5. Effect on photosynthetic activity

Figure 2G shows the effect of both nanopolymers applied singly and in combination on the photosynthetic activity measured as oxygen evolution and photosynthetic pigment contents. It was measured in cyanobacterial cells exposed over 72 h to the EC_{50} of PS-NPs and their mixture with G7. Exposure to PS-NPs induced a significant decrease, of 65 %, in photosynthetic activity with

respect to the control. In contrast, the combined exposure of PS-NPs and G7 triggered a slight but not significant decrease in oxygen evolution of *Anabaena*, revealing an antagonistic behavior of both nanopolymers when combined towards photosynthesis. This probably means that the heteroaggregates do not contact the thylakoid membranes, as they are not internalized (see below under Intracellular tracking of fluorescent PS-NPs).

3.4. Effect on protein expression

Proteomic approaches have allowed the global identification and differential quantification of expressed proteins of cyanobacterial cells under different environmental stresses.[72] Given the physiological changes induced by the presence of both nanopolymers and their co-exposure, their effects at the molecular level were explored, specifically, on the cyanobacterial proteome. Firstly, 1102 proteins were identified by shotgun proteomic analysis and their differential expression was quantified from both controls and the three treatments (PS-NPs, G7 and their mixture) on *Anabaena*. From the total identified proteins, the expression of 118 proteins were significantly modified by one of the three treatments, when considering DEPs to be those with FC <0.83 or >1.2, p <0.01 (Table S5). DEPs were then allocated into one of nine categories (Fig. S2): Oxidative stress response (8 DEPs); Stress response (9 DEPs); Surface location (21 DEPs); Carbon metabolism and energy (18 DEPs); Organo-nitrogen metabolism (19 DEPs); Nucleic acid metabolism (14 DEPs); Photosynthesis (11 DEPs); Signal domain (9 DPEs); and Non clustered proteins (6 DEPs). A heatmap showing the expression level of each protein by category is in Fig. 3A (a heatmap including the phylogenetic relationship between DEPs is shown in Figure S9).

3.4.1. Oxidative stress response

As shown in Fig. 3B(a), proteins involved in oxidative stress were upregulated by each of the three treatments. Among them, five DEPs were at least two FC increased by PS-NPs, G7 or both: three peroxiredoxins (All1154, Alr4642 and Alr0672), a thioredoxin (All0737) and a DpsA-like protein (alr3808 gene), which could also be involved in nutrient stress response. Exposure to the mixture caused a smaller number of alterations than single exposure, corroborating the antagonistic behavior of both nanopolymers.

3.4.2. Stress response

This group of DEPs is mainly represented by chaperone proteins like ClpB2, DnaK2, GroL1, GroL2 and three poorly described heat shock proteins denoted as Alr0286, Alr1809 and Alr2323 whose function, presumably, would also be related to ensuring correct protein folding. These DEPs were slightly upregulated after exposure to PS-NPs and G7, whilst they were downregulated after the combined exposure (Fig. 3C(a)), with the exception of ClpP3, a probable ATP-dependent protease proteolytic subunit involved in efficient protein homeostasis, which is upregulated specifically under the mixture exposure.

3.4.3. Surface location

In this category, in order to study envelope-membrane related alterations, we allocated the unconnected DEPs from the PPI (Protein-Protein Interaction Network) whose cellular location is peripheral (transmembrane, periplasmic or belonging to the exoproteome). A general downregulation of these proteins is observed upon exposure to PS-NPs and the mixture, while G7 induced both up and downregulation to a similar extent (Fig. 3D(a)). The expression of eight proteins were altered by more than two FC by one of the treatments: Alr1540 (which presents a peptidoglycan binding domain); All7121 and Alr4821 (two integral components of the membrane, All7121 (which presents Cytochrome c-like domain); Alr0397, Alr4028 and Alr4029 (TonB-dependent transporters, with at least alr0397 having siderophore uptake activity),[73] and Alr0474 (belonging to the *Anabaena* exoproteome)[74] . In contrast, Alr4280 (a component of a putative ABC exporter homologous to the DevBCA heterocyst-specific glycolipid exporter, which is essential for antibiotic resistance in *Anabaena*)[75] was upregulated specifically after exposure to PS-NPs and the mixture. There were two other components of ABC transporters that were upregulated, Alr0140 following exposure to both nanopolymers and All2358 that was only upregulated after G7 exposure.

3.4.4. Carbon metabolism and energy

DEPs clustered in this category were unconnected to the PPI but most of them are enzymes involved in different carbon and energy related metabolic processes. Both PS-NPs and G7 exposure induced an upregulation of these DEPs, while the response to the mixture showed no clear trend (Fig. 3E(a)). There were eight proteins altered more than two FC and from these, seven were clearly upregulated by the three treatments: six presented different catalytic activities like epimerase, dehydrogenase, oxidoreductase or ATPase (All5295, Alr0663, CysA, Alr4380, Alr4566, Alr7200), and one was related to the intracellular inorganic carbon concentrating mechanism (CcmK); the metabolic activity of the cyanobacterium appears to be enhanced when exposed to the nanopolymers or

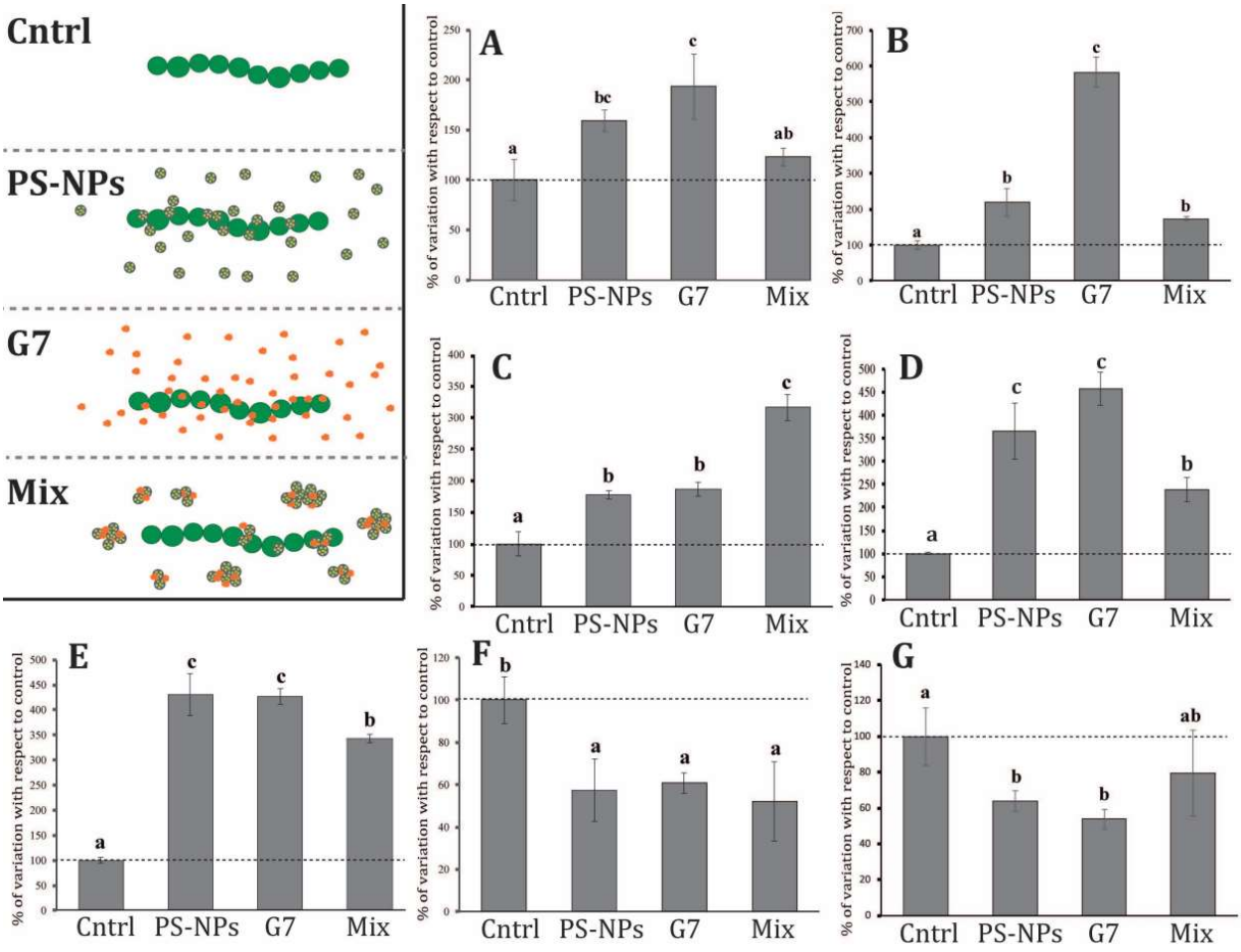

Figure 2: Physiological responses of *Anabaena* sp. PCC7120 after exposure to PAMAM dendrimer of generation 7 (G7), Polystyrene nanoparticles (PS-NPs), the binary mixture (Mix) and non-exposed cultures (Cntrl). Measurements were conducted by fluorimetry using a set of fluorochromes to evaluate: intracellular ROS formation by using two different fluorochromes, H_2DCF DA for general oxidative stress (A) and DHR 123 for H_2O_2 formation (B), lipid peroxidation by quantification of TBARS (C), membrane integrity by propidium iodide (D), cytoplasmic membrane potential by DiBAC$_4$(3) (E), intracellular pH using BCECF AM (F) and photosynthesis as oxygen evolution (G). Results are presented as percentage of variation of the relevant physiological parameters ± SD with respect to control (100% is indicated by the dashed line). Different letters indicate treatments that are significantly different (Tukey's HSD, $p < 0.05$). Non-relativized data are shown in Fig. S8.

their mixture. In contrast, one DEP was strongly downregulated by the three treatments, the protein All2127, which presents an aldolase-type TIM barrel domain as well as a radical SAM core domain that could generate radical species by reductive cleavage of S-adenosyl-L-methionine through an unusual Fe-S centre.

3.4.5. Organo-nitrogen metabolism

Proteins allocated to this group are slightly interconnected, but all of them are related to different aspects of biosynthesis/catalysis/modification of proteins or other molecules containing nitrogen, as well as with nitrogen assimilation. As shown in Fig. 3F(a) upregulation is the most common response after the individual exposure with each nanopolymer. Several DEPs were altered by more than two FC: Alr2927 and Alr0669 (related to peptidase activity); All0666 (related to envelope homeostasis, which co-occurs with all0665, a protein containing a peptidase domain) and the closely related protein All0667; All4737, Alr3804 (deoxyhypusine synthase homologue); asl0662 (involved in nitrate transport); Alr0668 and Alr3301 (associated with heterocyst differentiation) and GlnA, responsible for nitrogen assimilation.

3.4.6. Nucleic acid metabolism

Tight relationships between DEPs were found in this category. At least half of the proteins were upregulated after exposure to the three treatments whilst only a few were downregulated (Fig. 3G(a)). Most of them are ribosomal proteins (Rpl1, RplN, RpsD RpsE RpsG RpsN), which were upregulated together with the transcriptional regulator Alr4692 and the chromosome partition protein from the ParB family, Alr7083. In contrast, two DNA-directed RNA polymerase subunits (RpoB and

RpoC2) were downregulated, together with the DNA-binding transcription factor Alr7311.

3.4.7. Photosynthesis

DEPs found in this category are essential for the phototrophic metabolism of *Anabaena*: two proteins are part of the photosystem reaction centers I and II (Psal and PsbB, respectively) and one associated with them (alr1129); six proteins related to the phycobilisomes (PecA, PecB, PecC, CPCg3, ApcE and All7348); one involved in the electron transfer chain (Ndhl); and one implicated in zeta-carotene biosynthesis (All7255). Around 50 % of these proteins were strongly downregulated upon PS-NPs, G7 and combined exposures (Fig. 3H(a)), specifically ApcE and PecA were modified more than two FC. On the other hand, a slight upregulation of CpcG3 (phycobilisome rod-core linker polypeptide), Ndh1 (NAD(P)H-quinone oxidoreductase subunit I) and PsaL (photosystem I reaction center subunit XI) was observed upon exposure to PS-NPs and, more strongly, All7348 (thylakoid membrane protein with 2 iron, 2 sulfur cluster binding and chlorophyllide *a* oxygenase activity), when exposed to the binary mixture. These results corroborate the observed alteration in the photosynthetic process.

3.4.8. Signal domain

In this category, those DEPs unconnected by the PPI that present a signal domain are compiled. Most of these proteins were barely modified by the treatments, however, PS-NPs and the mixture appear to induce downregulation of four proteins (All1755, all1783, Alr7326 and Alr7345) while the G7 exposure trend was to upregulate the other four proteins (All4130, Alr0490, Alr1548 and Alr3932). Remarkably, one protein, whose levels were altered more than two FC (All0050), showed a strong downregulation after the three treatments (Fig. 3I(a)).

3.4.9. Global proteome alteration pattern

Finally, it is interesting to study the global proteome alteration pattern, which may allow a better understanding of the observed effects of single or combined nanopolymer exposures on *Anabaena*. The response pattern induced by PS-NP single exposure clearly differed (r = 0.25-0.3) from that of G7 with respect to Oxidative stress, Surface location and Nucleic acid metabolism (Fig. 3B(b) D(b) G(b)). However, the pattern was substantially similar (r = 0.7-0.9) in the categories of Carbon metabolism and energy, Organo-nitrogen metabolism and Signal domain in both treatments (Fig. 3E(b), F(b), I(b)). The pattern induced by exposure to the binary mixture significantly differed from G7 exposure in most categories except Stress response (r = 0.5) and Signal domain categories (r = 0.9) but was similar to the response caused by PS-NPs. Global correlation analysis (Fig. 3J(a) and J(b)) revealed that the protein alteration pattern after single exposure to G7 or PS-NPs, with the exception of the above-described categories, was quite similar, showing a strong positive correlation (r = 0.81). The correlation between each nanopolymer applied singly and their mixture was less significant (r = 0.61 and r = 0.14 for PS-NPs and G7, respectively). These results also point out that the PS-NPs toxicological behavior prevailed over the G7 one in the mixture (r = 0.61 > r = 0.14).

The Venn diagram gives a global overview of those DEPs up-or down regulated by the three different treatments and was constructed considering those DEPs with FC <0.5 or >2, p <0.01 (Fig. S10). DEPs altered specifically by each treatment (PS-NPs, G7 and their binary mixture) as well as those proteins whose response overlaps between treatments are shown in the table below the Venn diagram; these DEPs could be considered as molecular biomarkers of the toxicity of these treatments towards the cyanobacterium.

3.5. Intracellular tracking of fluorescent PS-NPs

Exterior cell envelope damage (including to the cytoplasmic membrane) and potential internalization of PS-NPs may be altered upon exposure to PS-NPs or their mixture with G7. In this context, confocal microscopy was used to locate PS-NPs distribution in the cell and surrounding areas, including adhesion to the cell envelopes as well as their potential intracellular location. This approach allowed discrimination between mechanisms that might imply the internalization of the nanopolymer and those based on surface level interactions. Fig. 4 shows filaments exposed to PS-NPs whose green fluorescence allows nanoparticle tracking. Firstly, the morphological characteristics of *Anabaena* cells were affected by 72 h of individual exposure to PS-NPs and to its mixture with G7. Within filaments, cells acquired aberrant morphologies; they were distorted and in general, they appeared swollen and therefore bigger than the control cells (Fig. 4A, B, C and D). As also shown in the Fig. 4C and D, exposure to only PS-NPs caused their accumulation on cell envelopes, more clearly seen on the junctions between cells within the same filament. Furthermore, internalization of the PS-NPs is observed clearly in the inner periphery of the cell (yellow dots in an intermediate Z section in Fig. 4D; the yellow colour results from overlapping of the green fluorescence of the PS-NPs with the red fluorescence of chlorophyll molecules in the inner

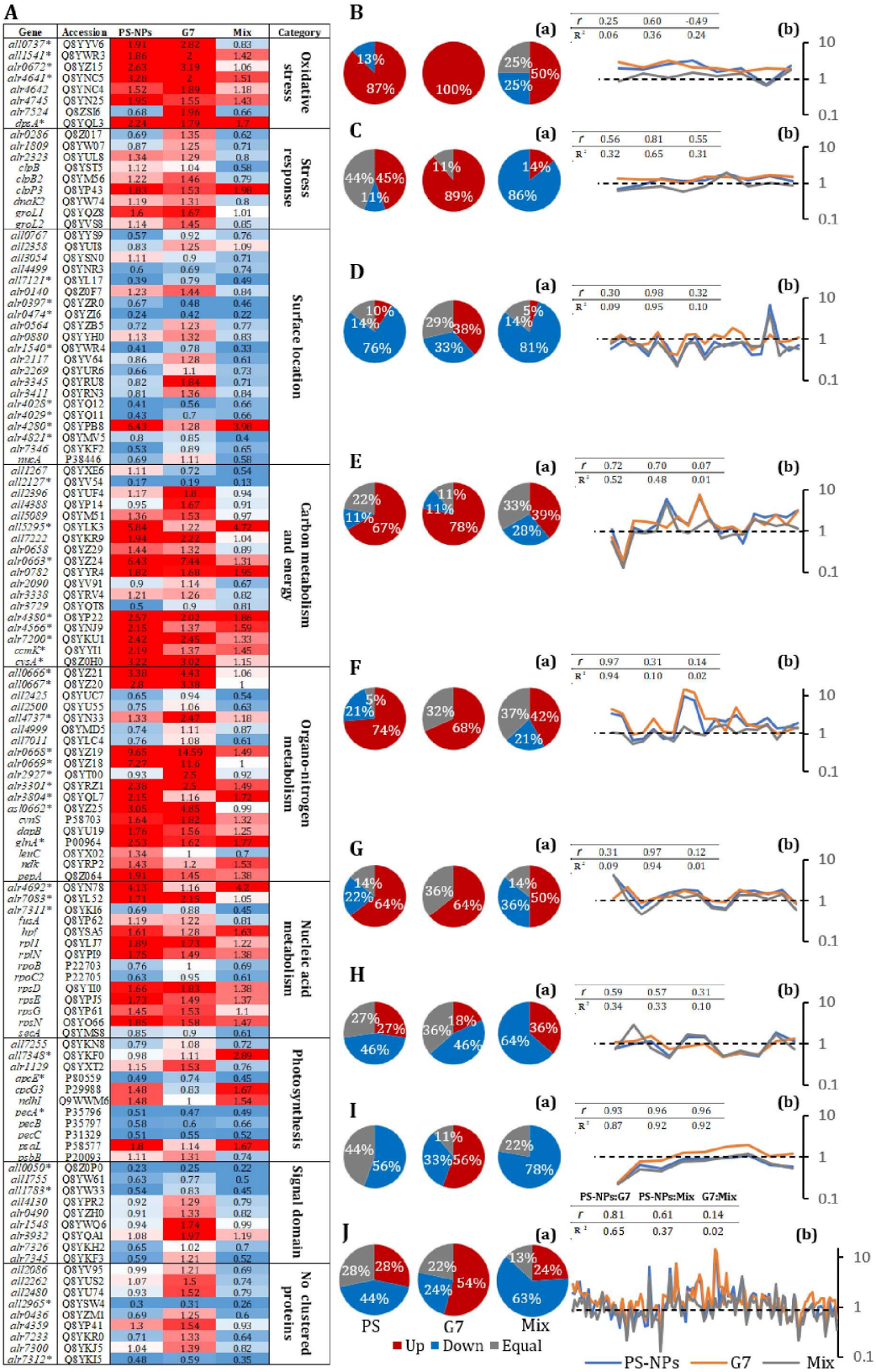

Gene	Accession	PS-NPs	G7	Mix	Category
all0737*	Q8YYV6	1.91	2.82	0.83	Oxidative stress
all1541*	Q8YWR3	1.86	2	1.42	
alr0672*	Q8YZ15	2.63	3.19	1.06	
alr4641*	Q8YNC5	3.28	2	1.51	
alr4642	Q8YNC4	1.52	1.89	1.18	
alr4745	Q8YN25	1.95	1.55	1.43	
alr7524	Q8ZSI6	0.68	1.96	0.66	
dps4*	Q8YQL3	2.24	1.79	1.7	
alr0286	Q8ZD17	0.69	1.35	0.62	Stress response
alr1809	Q8YW07	0.87	1.25	0.71	
alr2323	Q8YUL8	1.34	1.29	0.8	
clpB	Q8YST5	1.12	1.04	0.58	
clpB2	Q8YMS6	1.22	1.46	0.79	
clpP3	Q8YP43	1.83	1.53	1.98	
dnaK2	Q8YW74	1.19	1.31	0.8	
groL1	Q8YQZ8	1.6	1.67	1.01	
groL2	Q8YVS8	1.14	1.45	0.85	
all0767	Q8YYS9	0.57	0.92	0.76	Surface location
all2358	Q8YUI8	0.83	1.25	1.09	
all3054	Q8YSN0	1.11	0.9	0.71	
all4499	Q8YNR3	0.6	0.69	0.74	
all7121*	Q8YL17	0.39	0.79	0.49	
alr0140	Q8ZDF7	1.23	1.44	0.84	
alr0397*	Q8YZR0	0.67	0.48	0.46	
alr0474*	Q8YZI6	0.24	0.42	0.22	
alr0564	Q8YZB5	0.72	1.23	0.77	
alr0880	Q8YYH0	1.13	1.32	0.83	
alr1546*	Q8YWR4	0.41	0.78	0.33	
alr2117	Q8YV64	0.86	1.28	0.61	
alr2269	Q8YUR6	0.66	1.1	0.73	
alr3345	Q8YRU8	0.82	1.84	0.71	
alr3411	Q8YRN3	0.81	1.36	0.84	
alr4028*	Q8YQ12	0.41	0.56	0.66	
alr4029*	Q8YQ11	0.43	0.7	0.66	
alr4280*	Q8YPB8	6.43	1.28	3.98	
alr4821*	Q8YMV5	0.8	0.85	0.4	
alr7346	Q8YKF2	0.53	0.89	0.65	
nucA	P38446	0.69	1.11	0.58	
all1267	Q8YXE6	1.11	0.72	0.54	Carbon metabolism and energy
all2127*	Q8YV54	0.17	0.19	0.13	
all2396	Q8YUF4	1.17	1.8	0.94	
all4388	Q8YP14	0.95	1.67	0.91	
all5089	Q8YM51	1.36	1.53	0.97	
all5295*	Q8YLK3	5.84	1.22	4.72	
all7222	Q8YKR9	1.94	2.22	1.04	
alr0658	Q8YZ39	1.44	1.32	0.89	
alr0663*	Q8YZ24	6.43	7.44	1.31	
alr0782	Q8YYR4	1.82	1.68	1.06	
alr2090	Q8YV91	0.9	1.14	0.67	
alr3338	Q8YRV4	1.21	1.26	0.82	
alr3729	Q8YQT8	0.5	0.9	0.81	
alr4380*	Q8YP22	2.57	2.02	1.86	
alr4566*	Q8YNJ9	2.15	1.37	1.59	
alr7200*	Q8YKU1	2.42	2.45	1.33	
ccmK*	Q8YYI1	2.19	1.37	1.45	
cysA*	Q8Z0H0	3.22	3.02	1.15	
all0666*	Q8YZ21	3.38	4.43	1.06	Organo-nitrogen metabolism
all0667*	Q8YZ20	2.8	3.38	1	
all2425	Q8YUC7	0.65	0.94	0.54	
all2500	Q8YU55	0.75	1.06	0.63	
all4737*	Q8YN33	1.33	2.47	1.18	
all4999	Q8YMD5	0.74	1.11	0.87	
all7011	Q8YLC4	0.76	1.08	0.61	
alr0668*	Q8YZ19	9.65	14.59	1.49	
alr0669*	Q8YZ18	7.22	11.6	1	
alr2927*	Q8YT00	0.93	2.5	0.92	
alr3301*	Q8YRZ1	2.38	2.5	1.49	
alr3804*	Q8YQL7	2.15	1.16	1.72	
asl0662*	Q8YZ25	3.05	4.85	0.99	
cynS	P38703	1.64	1.82	1.32	
dapB	Q8YU19	1.76	1.56	1.25	
glnA*	P00964	2.53	1.62	1.72	
lexC	Q8YX02	1.34	1	0.7	
ndk	Q8YRP2	1.43	1.2	1.53	
pepA	Q8Z064	1.91	1.45	1.38	
alr4692*	Q8YN78	4.13	1.16	4.2	Nucleic acid metabolism
alr7083*	Q8YL52	1.71	2.15	1.05	
alr7311*	Q8YKI6	0.69	0.88	0.45	
fusA	Q8YP62	1.19	1.22	0.81	
hpf	Q8YSA5	1.61	1.28	1.63	
rpl1	Q8YLJ7	1.89	1.73	1.22	
rplN	Q8YPI9	1.75	1.49	1.38	
rpoB	P22703	0.76	1	0.69	
rpoC2	P22705	0.63	0.95	0.61	
rpsD	Q8YTI0	1.66	1.83	1.38	
rpsE	Q8YPJ5	1.73	1.49	1.37	
rpsG	Q8YP61	1.45	1.53	1.1	
rpsN	Q8YO66	1.65	1.58	1.47	
secA	Q8YMS8	0.85	0.9	0.61	
all7235	Q8YKN8	0.79	1.08	0.72	Photosynthesis
all7348*	Q8YKF0	0.98	1.11	2.89	
alr1129	Q8YXT2	1.15	1.53	0.76	
apcE*	P80559	0.49	0.74	0.45	
cpcG3	P29988	1.48	0.83	1.67	
ndhI	Q9WWM6	1.48	1	1.54	
psaA*	P35796	0.51	0.47	0.49	
psaB	P35797	0.58	0.6	0.66	
psaC	P31329	0.51	0.55	0.52	
psaL	P58577	1.8	1.14	1.67	
psbB	P20093	1.11	1.31	0.74	
all0050*	Q8Z0P0	0.23	0.25	0.22	Signal domain
all1755	Q8YW61	0.63	0.77	0.5	
all1783*	Q8YW33	0.54	0.83	0.45	
all4130	Q8YPR2	0.92	1.29	0.79	
alr0490	Q8YZH0	0.91	1.33	0.82	
alr1548	Q8YWQ6	0.94	1.74	0.99	
alr3932	Q8YQA1	1.08	1.97	1.19	
alr7326	Q8YKH2	0.65	1.02	0.7	
alr7345	Q8YKF3	0.59	1.21	0.52	
all2086	Q8YV95	0.99	1.21	0.69	No clustered proteins
all2262	Q8YUS2	1.07	1.5	0.74	
all2480	Q8YU74	0.93	1.52	0.79	
all2965*	Q8YSW4	0.3	0.31	0.26	
alr0436	Q8YZM1	0.69	1.25	0.6	
alr4559	Q8YP41	1.3	1.54	0.93	
alr7233	Q8YKR0	0.71	1.33	0.64	
alr7300	Q8YKJ5	1.04	1.39	0.82	
alr7312*	Q8YKI3	0.48	0.59	0.35	

Figure 3: A: heatmap representing the proteomic response of *Anabaena* sp. PCC7120 after its exposure to polystyrene nanoparticles (PS-NPs), PAMAM dendrimer of generation 7 (G7) and the combination of both nanopolymers (Mix); only those proteins with changes with respect to the control (FC <0.83 or >1.2, p <0.01) are shown. B(a): Pie charts representing the proportion of differential expressed proteins up/down regulated (DEPs) into the Oxidative stress category; C(a): Stress response pie charts; D(a): Surface location pie charts; E(a): Carbon metabolism and energy pie charts; F(a): Organo-nitrogen metabolism pie charts; G(a): Nucleic acid metabolism pie charts; H(a): Photosynthesis pie charts; I(a): Signal domain pie charts; J(a): pie charts for global response in which all DEPs are included. B(b): referred to as the Oxidative stress category, differential expression pattern plot, representing DEPs (X axis) vs Fold change (Y axis) after exposure of *Anabaena* to PS-NPs, G7 and Mix; the correlation coefficient between expression patterns is represented by the Pearson correlation coefficient (r) and the proportion of the variation explained by the linear regression is estimated by the coefficient of determination (R^2); C(b): Stress response plot; D(b): Surface location plot; E(b): Carbon metabolism and energy plot; F(b): Organo-nitrogen metabolism plot; G(b): Nucleic acid metabolism plot; H(b): Photosynthesis plot; I(b): Signal domain plot; J(b): plot representing the global differential expression pattern in which all DEPs are included.

thylakoid membranes); this may account for the observed toxic effects of PS-NPs. When *Anabaena* was exposed to the binary mixture of PS-NPs and G7 (Fig. 4E and F), clear aggregates were observed which were located on the cell surfaces; these aggregates may interact with the cell envelopes and with the junctions between cells and cause abrasion that might explain the observed effect of the mixture on membrane lipid peroxidation. In this case, no clear PS-NP internalization was observed, although there was potential abrasion on cell envelopes; in this context, and after six days of exposure, a clear fragmentation of cyanobacterial filaments was evident with the heteroaggregates of PS-NPs and G7 adhered to sites of filament fragmentation (Fig. S11).

4. Discussion

Since the increase in production of plastics as a versatile material for the production of everyday items in the mid-twentieth century, the amount of plastic that is in the environment is estimated at about 5000 million tons.[5] The occurrence of nanoplastics in the environment may arise from the direct release of commercial products containing nanoplastics,[76] as well as through the fragmentation of conventional products that, once they become waste, are degraded by the action of different environmental factors.[7] In parallel, during the last decades, the use of engineered nanoparticles has increased due to the advances in nanotechnology, and their spilling may become an environmental threat too.[77] Amongst the nanoparticles, Naha *et al.* 2018[78] highlighted dendrimers as potential environmental pollutant of special concern. Within nanoplastics, PS-NP toxicity has been observed in different environmentally relevant organisms, such as *Microcystis aeruginosa*, *Daphnia pulex*, *Brachionus plicatilis*, *Halomonas alkaliphila* or *Scenedesmus obliquus*, in a range of concentrations between 1 and 320 mg/L.[79] The range of concentrations where an effect is observed may depend on the model organism used but also on the particle size and the surface functionalization (when functionalized, a positive surface charge results in higher toxicity due to the affinity with the negatively charged groups of the cytoplasmic membranes). In this context, the toxicity of G7 PAMAM dendrimer, which presents a high density of surface positive charges[48], is clearly higher than that of PS-NPs. The EC_{50} for PS-NPs exposure in *Anabaena* is in good correlation with the growth inhibition results obtained by Sendra *et al.* 2019[80] in diatoms exposed to 50 nm PS-NPs, as well as with the report by Baudrimont *et al.* 2019[81] with *Scenedesmus subspicatus*, exposed to natural and reference polyethylene nanoplastics, and to those reported by Huang *et al.* 2019[82] with *Chlamydomonas reinhardtii*, exposed to carboxylic modified PS-NPs (20nm). Nevertheless, it is significantly lower than that found by Sjollema *et al.* 2016[83] in the alga *Dunaliella tertiolecta* exposed to uncharged PS-NPs (50 nm). Regarding cyanobacteria specifically, Feng *et al.* 2019[84] described high toxicity in *Synechococcus elongatus,* triggered by strongly cationic PS-NPs-NH_2 (50 nm), which correlates better with G7 toxicity, whilst they did not find significant toxicity below 100 mg/L sulfonic-modified anionic PS-NPs (50 nm). PS-NPs induced an increase in ROS levels in *Anabaena*, which is consistent with lipid peroxidation and concomitant membrane integrity damage, and is also consistent with photosynthetic activity inhibition.[85] ROS overproduction, photosynthetic inhibition and membrane damage have been previously reported to be triggered by PS-NPs, or PS-NPs in binary mixtures with other pollutants, in several unicellular photosynthetic organisms.[24,80,86–88]

While the interaction between nanoparticles and combined toxicity has seldom been reported,[82,87,89–93] eventually, given their increased use, both types of nanopolymers might co-occur in aquatic environments. In this study, we observed an antagonistic interaction for PS-NPs and G7 along all the range of effect levels meaning that their combined toxicity is less than the sum of individual toxicities. This antagonistic behavior is corroborated by the results from mechanistic studies and by the measured heteroaggregation by DLS. Thus, the binary mixture alleviates the observed individual toxicity by heteroaggregation, as previously observed with copper nanoparticles and carbon nanotubes on the marine microalgae *Skeletonema costatum*, and with silver and hematite nanoparticles on *Escherichia coli*. [91,92]

PS-NPs were internalized, and, as previously shown, G7 are internalized to a larger extent[48]. PS-NPs are bigger in size than G7 and are negatively charged, which might hinder their internalization. Interestingly, when PS-NPs and G7 co-occurred, their heteroaggregates were observed on the cell surfaces, which could cause abrasion of cell envelopes and in the long-term cause membrane damage as shown by the increased lipid peroxidation and filament fragmentation after mixture treatment. Feng *et al.* 2020[64] did not observe positively charged PS-NPs (50 nm) internalization in *Microcystis aeruginosa*, but observed the physical interaction of PS-NPs and the cytoplasmic membrane, which might be triggering cell envelope damage. Rodea-Palomares *et al.* 2010[53] and Rodea-Palomares *et al.* 2015[47] observed abrasion of *Anabaena* cell envelopes when the cyanobacterium was exposed to cerium oxide nanoparticles and lower generation PAMAM dendrimers, respectively, with concomitant ROS

overproduction and membrane integrity impairment. Pulido-Reyes *et al.* 2019[94] and Hurtado-Gallego *et al.* 2019[63] also described membrane damage and ROS overproduction caused by the exposure of *Chlamydomonas reinhardtii* to cerium oxide (uncoated and coated by polyvinylpyrrolidone) and superparamagnetic iron oxide nanoparticles, respectively. A loss in membrane integrity and membrane potential by increasing membrane permeability, therefore impairing the ion gradients, may not only damage membranes, but also may induce acidification of the intracellular pH, jeopardizing cell viability.[48,84,95,96]

For the first time, this study correlates these physiological alterations with proteomic changes in *Anabaena* exposed to PS-NPs, G7 or their mixture. Regarding PS-NPs, the upregulation of DEPs related to oxidative stress and stress response is well correlated with the observed ROS overproduction. Moreover, the impairment observed on photosynthetic activity is supported by a significant downregulation of several photosynthesis-related DEPs and in agreement with the photosynthesis reduction observed by Bhattacharya *et al.* 2010[86], exposing *Chlorella* and *Scenedesmus* to amidine and carboxyl PS-NPs (20 nm) and Feng *et al.* 2020[64], exposing *Microcystis aeruginosa* to positively charged PS-NPs (50 nm). Surface localized proteins are the primary barrier that may interact with PS-NPs resulting in membrane disruption[84] ; in this regard, the proteomic analysis reveals a clear downregulation of surface-located DEPs. In contrast, Feng *et al.* 2020[64] reported a clear upregulation of several transmembrane proteins, mostly related with transport; it should be taken into account that some of the upregulated DEPs allocated into carbon and metabolism (like CysA) are also surface-located proteins involved in transport.

The general upregulation observed after PS-NPs exposure on the DEPs related to carbon, energy, nitrogen and nucleic acid metabolism might be a response to the structural damage caused by interaction with the nanopolymer, mainly related to the maintenance of the cell envelope structural integrity, as described by Mirzajani *et al.* 2013[97] when *Bacillus thuringiensis* was exposed to silver nanoparticles. In addition, novel G7 effects on *Anabaena* obtained in this study, through the proteomic analysis, are consistent with those obtained by Tamayo *et al.* 2019[48].

Specifically, the analysis denotes the upregulation of DEPs allocated into the categories of oxidative stress and stress responses (mostly heat-shock proteins), as well as, similarly to PS-NPs, of carbon, energy, nitrogen and nucleic acid metabolism, together with the downregulation of photosynthesis related proteins. Similar results were observed by Qian *et al.* 2016[98] on *Chlamydomonas vulgaris* exposed to silver nanoparticles. Furthermore, G7 exposure caused substantial upregulation of surface-located DEPs (Fig. 3 D (a)), so that, the response to G7 seems to correlate better with that observed by Feng *et al.* 2020[64] probably since both nanopolymers are cationic. Based on the heatmap (FC <0.83 or >1.2, p <0.01), there are 21 DEPs characteristic of the combined treatment; however, to focus on clearly distinctive DEPs of the mixture in comparison with single exposures, a Venn diagram was made according to FC <0.5 or >2 (p <0.01). As discussed below, four mixture-distinctive DEPs, that could be potential molecular biomarkers, were identified.

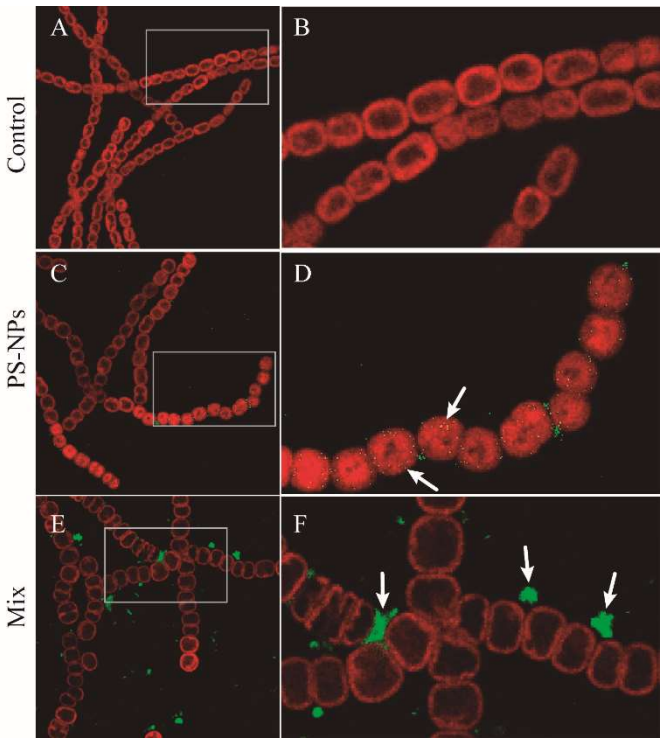

Figure 4. Confocal microscopy images (intermediate Z section where fluorescent PS-NPs are clearly visible) of the fluorescence overlay in red (chlorophyll a) and in green (fluorescent PS-NPs) of the *Anabaena* sp. PCC7120 control: A and B; exposed to the EC_{50} of the polystyrene nanopolymer (PS-NPs): C and D and the mixture (Mix): E and F. The arrows in D indicate internalization of PS-NPs and in F heteroaggregates of PS-NPs and G7 adhered to the cell envelopes.

Looking at the expression pattern of the DEPs by category (Fig. 3 B-J) both the anionic PS-NPs and the cationic G7 caused similar alterations in DEPs associated with the carbon, energy, and nitrogen metabolism categories, which agrees with the response to the structural damages caused by

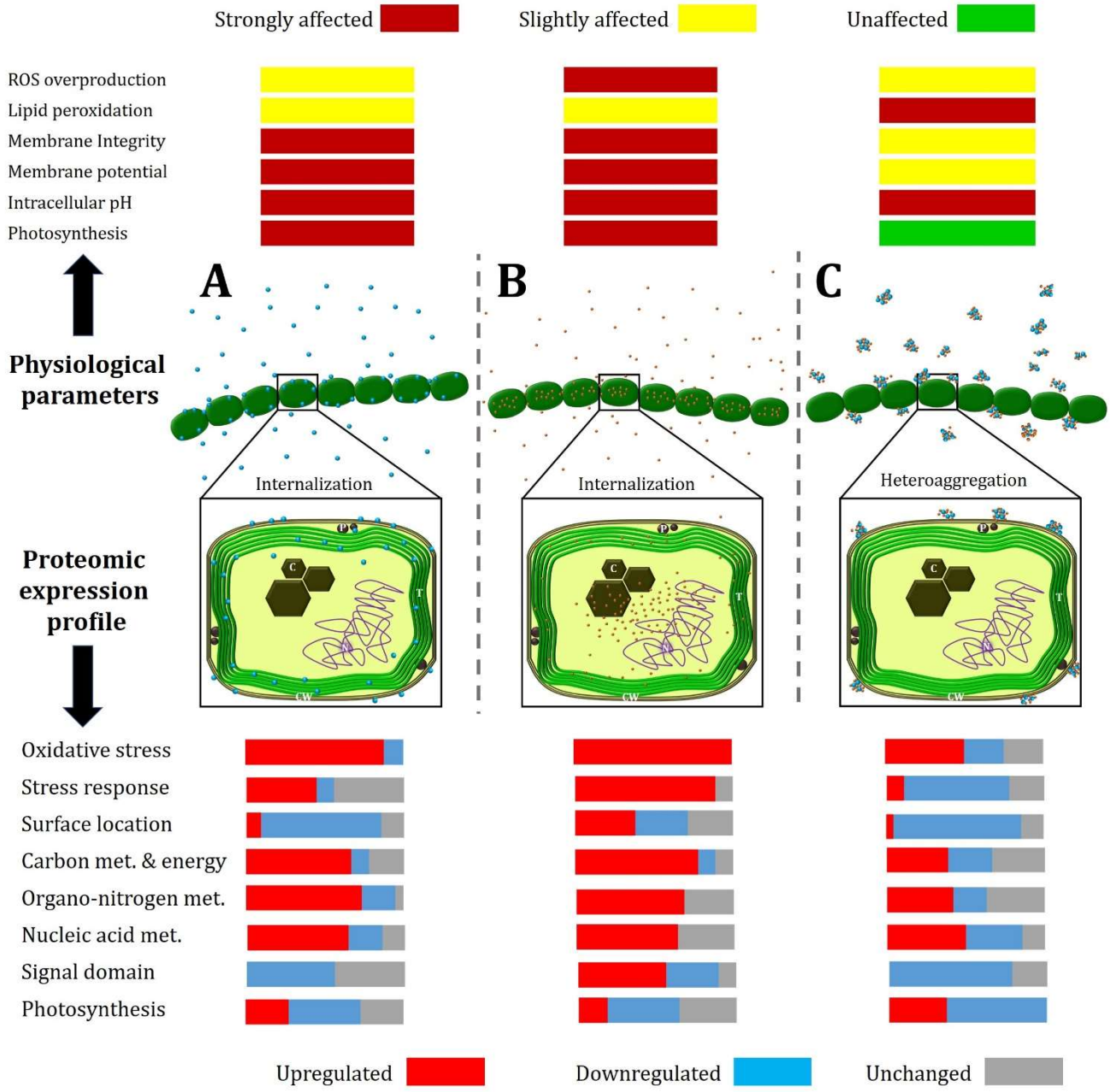

Figure 5. Proposed mechanistic scheme for the effects of PS-NPs (A), G7 PAMAM dendrimers (B) and the PS-NPs and G7 mix (C) on the cyanobacterium Anabaena sp. PCC7120. The degree of alteration of relevant targeted physiological parameters by each treatment is shown alongside the changes in proteomic expression profiles. Both PS-NPs and G7 PAMAM dendrimers were internalized into Anabaena cells but PS-NPs and G7 formed heteroaggregates on the cell surfaces when mixed. CW: Cell Wall, T: Thylakoids, C: Carboxysome, P: polyphosphate granules, N: Nucleoid.

interaction with the nanopolymers. However, despite both inducing a general upregulation of stress response (mostly heat-shock proteins) and oxidative stress response categories, the low correlation between PS-NPs and G7 DEPs whose expression is altered in each group (r = 0.25 and r = 0.56, respectively) probably reveals different mechanisms involved in the cellular response to both nanopolymers. This also correlates with the dissimilar pattern observed in the nucleic acid category (r = 0.31). Nevertheless, when globally comparing the DEPs between PS-NPs and G7 applied singly, the similarity is higher between PS-NPs and G7 (r = 0.81) than between PS-NPs or G7 with their mixture (r = 0.61 and r = 0.14, respectively). This means that the cyanobacterial proteomic response is more similar when cells are exposed to the nanopolymers individually than when exposed to the mixture, which is a completely different situation due to the heteroaggregates formation, which increases their size by more than one order of magnitude and reduces toxicity (antagonistic behaviour).

Finally, certain DEPs may be considered a signature of exposure and/or effect (molecular biomarkers) towards a toxin, in this case PS-NPs, PAMAM G7 and their mixture. The importance of the altered expression patterns in cells or organisms exposed to nanoplastics in the environment has been recently highlighted .[64,88,99–103] In this regard,

ABC transporters, especially those related to multidrug resistance, might be potential biomarkers for nanoparticle toxicity.[104] Several proteins involved in cellular biotransformation mechanisms, such us cytochrome P450 in human cells or impairment of AChE activity in the immune cells of sea urchins have been also highlighted.[105,106] The DEPs identified in this study might be useful as molecular biomarker candidates for future studies related to nanoplastics toxicity. Thus, regarding PS-NPs toxicity, based on the Venn diagram (Fig. S10), the most clearly modified DEPs (unmodified by G7) are GlnA, CcmK, Alr4641, Alr4566, DpsA and Alr3804. Among these, the proteins that are most differentially modified between PS-NPs and G7 exposures are Alr3804 (a deoxyhypusine synthase required in the homospermidine biosynthetic pathway, which is essential for *Anabaena* diazotrophic growth)[107] and Alr4641 (a peroxiredoxin (2-cys-prx)). In this context, a bioreporter bioluminescent strain based on the promoter region of the alr4641 gene, able to report on oxidative stress induced by aquatic pollutants, has previously been constructed and validated in environmental samples by our research group.[108] In addition, there are three DEPs strongly upregulated (FC > 4) by both single exposure to PS-NPs and exposure to the mixture with G7: Alr4280 (a component of a putative ABC exporter), All5295 (a protein containing a NAD-dependent epimerase/dehydratase domain) and Alr4692 (Multi antibiotic resistance transcriptional regulator). On the other hand, there are five DEPs (All7222, Alr7083, All0737, Alr2927, All4737) specifically upregulated (FC > 2) by G7 exposure. From these, the most useful as biomarkers are probably the chromosome partitioning protein from ParB family Alr7083, and the thioredoxin reductase All0737, responsible for redox homeostasis through a pivotal role in antioxidant defence systems in *Anabaena*.[109] Some of the most highly upregulated DEPs by both nanopolymers when applied singly, but not by their mixture, are: Alr0663 (FC > 6), a glycoside hydrolase identified in the outer membrane of *Anabaena* which could be more susceptible to undergoing alteration through direct contact with nanopolymers; [110] CysA (FC > 3), part of the ABC transporter complex CysAWTP involved in sulfate/thiosulfate import and responsible for energy coupling to the transport system and Alr4380, a delta-aminolevulinic acid dehydratase involved in porphyrin and chlorophyll metabolism, whose accumulation has been reported to occur during oxidative stress induction in plants by cadmium.[111] Regarding combined exposure, four DEPs (All7348, All1783, Alr7311, Alr4821) are clearly modified only by the mixture. Two of them might serve as molecular biomarkers that are specifically distinctive of the mixture: All7348, upregulated (FC > 2), is an integral component of the membrane that presents 2 iron and 2 sulfur cluster binding and chlorophyllide *a* oxygenase activity and Alr7311 that is downregulated (FC < 0.5), is a protein with DNA binding transcription factor activity that presents a RNA polymerase sigma-70 like domain. As a summary, Fig. 5 shows a proposed mechanistic scheme for the observed alterations in relevant physiological parameters of the three treatments: PS-NPs (A), G7 PAMAM dendrimers (B) and PS-NPs and G7 mix (C). Both PS-NPs and G7 dendrimers were internalized into the cyanobacterial cell while both nanopolymers formed heteroaggregates onto cell surfaces when mixed, which may lead to cell envelope abrasion and membrane damage in the long term. The main changes in proteomic expression profiles are also shown.

5. Conclusions

This study reveals novel mechanisms of nanopolymer toxicity (nanoplastics and PAMAM dendrimers) when applied singly and in combination in a relevant aquatic primary producer, which sustains the life of more complex aquatic organisms. The interaction between both polymers turned out to be antagonistic due to the formation of heteroaggregates; these heteroaggregates in general lowered the toxic effects compared with each nanopolymer when applied singly. They tended, however, to adhere to the cell envelopes, probably causing abrasion, which in the long term might damage them, perhaps irreversibly as shown by the increased filament fragmentation. Molecular biomarkers (differentially expressed proteins, DEPs) of toxic effect of nanoplastics, PAMAM dendrimers and their binary mixture have been identified for the first time. These molecular biomarkers may be envisaged as a molecular signature of the toxic effect of the nanopolymers and could be predictors of cellular damage caused by exposure to nanopolymers. However, more studies of these interactions are needed in aquatic environments as many pollutants, including different types of nanoparticles, may co-occur and a deep understanding of their combined effects will shed light on the intricate effect of polluted waters on biota.

Acknowledgements

We thank the financial support provided by the Spanish Ministry of Science, Innovation and Universities (CTM2016-74927-C2- 1/2-R). MTB thanks the award of pre-doctoral grants to the Spanish Ministry of Education. The authors gratefully acknowledge the support of IESMAT during physicochemical characterization of the nanopolymers and the CBM support for the proteomic analysis: “Protein Identification,

characterization and quantitation by LC-MS/MS" was carried out in the 'CBMSO PROTEINCHEMISTRY FACILITY', that belongs to ProteoRed, PRB3-ISCIII,supported by grant PT17/0019, of the PE I+D+i 2013-2016, funded byISCIII and ERDF" . We would like to thank Dr. Robyn Wright for her kind help in English language editing of the manuscript.

References

1 J.G.B. Derraik, The pollution of the marine environment by plastic debris: A review, Mar. Pollut. Bull., **2002**, 44, 842–852.
2 Directive (EU) 2019/904 of the European Parliament and of the Council of 5 June 2019 on the reduction of the impact of certain plastic products on the environment., Publ. Off. EU, **2019**, 155, 1–19.
3 Plastics–the Facts 2019: An analysis of European plastics production, demand and waste data, PlasticsEurope: Association of Plastics Manufacturers, Brussels, **2019**.
4 World Economic Forum and Ellen MacArthur Foundation, The New Plastics Economy: Rethinking the future of plastics Background to key statistics from the report, **2016**, 1–4.
5 R. Geyer, J.R. Jambeck, K.L. Law, Production, use, and fate of all plastics ever made, Sci. Adv., **2017**, 25–29.
6 N. B. Hartmann, T. Hu, R. C. Thompson, M. Hassello, A. Verschoor, A. E. Daugaard, S. Rist, T. Karlsson, N. Brennholt, M. Cole, M.P. Herrling, M.C. Hess, N.P. Ivleva, A.L. Lusher, M. Wagner, Are we speaking the same language? Recommendations for a definition and categorization framework for plastic debris, Environ. Sci. Technol., **2019**, 53, 1039−1047.
7 K. Mattsson, S. Jocic, I. Doverbratt, L.A. Hansson, Nanoplastics in the Aquatic Environment, Elsevier Inc., **2018**.
8 A.L. Andrady, The plastic in microplastics: A review, Mar. Pollut. Bull., **2017**, 119, 12–22.
9 A.A. Koelmans, E. Besseling, W.J. Shim, Nanoplastics in the aquatic environment, Mar. Anthropog. Litter, **2015**, 329– 344.
10 K. Kik, B. Bukowska, P. Sicińska, Polystyrene nanoparticles: Sources, occurrence in the environment, distribution in tissues, accumulation and toxicity to various organisms, Environ. Pollut., **2020**, 262, 114297.
11 K. Saido, K. Koizumi, H. Sato, N. Ogawa, B.G. Kwon, S. Y. Chung, T. Kusui, M. Nishimura, Y. Kodera, New analytical method for the determination of styrene oligomers formed from polystyrene decomposition and its application at the coastlines of the North-West Pacific Ocean, Sci. Total Environ., **2014**, 473–474, 490–495.
12 K. Amamiya, K. Saido, S.Y. Chung, T. Hiaki, D.S. Lee, B.G. Kwon, Evidence of transport of styrene oligomers originated from polystyrene plastic to oceans by runoff, Sci. Total Environ., **2019**, 667, 57–63.
13 P. Rosenkranz, Q. Chaudhry, V. Stone, T.F. Fernandes, A comparison of nanoparticle and fine particle uptake by *Daphnia magna*, Environ. Toxicol. Chem., **2009**, 28, 2142–2149.
14 I. Paul-Pont, C. Lacroix, C. González-Fernández, H. Hégaret, C. Lambert, N. Le-Goïc, L. Frère, A.L. Cassone, R. Sussarellu, C. Fabioux. J. Guyomarch. M.Albentosa, A. Huvet, P. Soudant, Exposure of marine mussels *Mytilus* spp. to polystyrene microplastics: Toxicity and influence on fluoranthene bioaccumulation, Environ. Pollut., **2016**, 216, 724–737.
15 H. Liu, H. Shao, Z. Guo, D. Wang, Nanopolystyrene exposure activates a fat metabolism related signaling- mediated protective response in *Caenorhabditis elegans*, NanoImpact, **2020**, 17, 100204.
16 Sökmen, T. Ö., Sulukan, E., Türkoğlu, M., Baran, A., Özkaraca, M., & Ceyhun, S. B. (2020). Polystyrene nanoplastics (20 nm) are able to bioaccumulate and cause oxidative DNA damages in the brain tissue of zebrafish embryo (Danio rerio). Neurotoxicology, 77, 51-59.
17 Q. Chen, M. Gundlach, S. Yang, J. Jiang, M. Velki, D. Yin and H. Hollert, Quantitative investigation of the mechanisms of microplastics and nanoplastics toward zebra fish larvae locomotor activity, Sci. Total Environ., **2017**, 584–585, 1022–1031.
18 A.C. Greven, T. Merk, F. Karagöz, K. Mohr, M. Klapper, B. Jovanović, D. Palić, Polycarbonate and polystyrene nanoplastic particles act as stressors to the innate immune system of fathead minnow (*Pimephales promelas*). Environ. Toxicol. Chem., **2016**, 35, 3093-3100.
19 M. Cole, P. Lindeque, E. Fileman, C. Halsband, T.S. Galloway, The impact of polystyrene microplastics on feeding, function and fecundity in the marine copepod *Calanus helgolandicus*, Environ. Sci. Technol., **2015**, 49, 1130−1137.
20 M. Al-Sid-Cheikh, S.J. Rowland, K. Stevenson, C. Rouleau, T.B. Henry, R.C. Thompson, Uptake, whole-body distribution, and depuration of nanoplastics by the scallop *Pecten maximus* at environmentally realistic concentrations, Environ. Sci. Technol., **2018**, 52, 14480–14486.
21 C.C. Parenti, A. Ghilardi, C. Della Torre, S. Magni, L. Del Giacco, A. Binelli, Evaluation of the infiltration of polystyrene nanobeads in zebra fish embryo tissues after short-term exposure and the related biochemical and behavioural effects, Environ. Pollut., **2019**, 254, 112947.
22 Ó. Herrero, G. Morcillo, R. Planelló, Transcriptional deregulation of genetic biomarkers in *Chironomus riparius* larvae exposed to ecologically relevant concentrations of di(2-

ethylhexyl) phthalate (DEHP), PLoS One, **2017**, 12, 6–8.
23 E. Bergami, S. Pugnalini, M.L. Vannuccini, L. Manfra, C. Faleri, F. Savorelli, K.A. Dawson, I. Corsi, Long-term toxicity of surface-charged polystyrene nanoplastics to marine planktonic species *Dunaliella tertiolecta* and *Artemia franciscana*, Aquat. Toxicol., **2017**, 189, 159–169.
24 E. Besseling, B. Wang, M. Lu, A.A. Koelmans, Nanoplastic affects Growth of *S. obliquus* and Reproduction of *D. magna*, Environ. Sci. Technol., **2014**, 48, 12336−12343.
25 A. Reynolds, M. Giltrap, G. Chambers, Evaluation of non-invasive toxicological analysis of nano-polystyrene in relative in vivo conditions, Environ. Sci. Nano, **2019**, 6, 2832–2849.
26 Z. Liu, P. Yu, M. Cai, D. Wu, M. Zhang, Y. Huang, Polystyrene nanoplastic exposure induces immobilization, reproduction, and stress defense in the freshwater cladoceran *Daphnia pulex*, Chemosphere, **2019**, 215, 74–81.
27 Z. Liu, M. Cai, P. Yu, M. Chen, D. Wu, M. Zhang, Y. Zhao, Age-dependent survival, stress defense, and AMPK in *Daphnia pulex* after short-term exposure to a polystyrene nanoplastic, Aquat. Toxicol., **2018**, 204, 1–8.
28 R. Cui, S. W. Kim, Y. An, Polystyrene nanoplastics inhibit reproduction and induce abnormal embryonic development in the freshwater crustacean *Daphnia galeata*, Sci. Rep., **2017**, 1–10.
29 Q. Chaudhry, M. Scotter, J. Blackburn, B. Ross, A. Boxall, L. Castle, R. Aitken, R. Watkins, Applications and implications of nanotechnologies for the food sector, Food Addit. Contam. Part A Chem. Anal. Control. Expo. Risk Assess., **2008**, 25, 241–258.
30 H. Bouwmeester, P.C.H. Hollman, R.J.B. Peters, Potential health impact of environmentally released micro- and nanoplastics in the human food production chain: Experiences from nanotoxicology, Environ. Sci. Technol., **2015**, 49, 8932–8947.
31 M. Salehi, R. Rodriguez, A. Boettcher, S. Powers, N. Geitner, D.A. Ladner, S. Rikard, A.J. Whelton, Impact of dispersant on early life stages of the water flea Daphnia magna and the eastern oyster *Crassostrea virginica*, J. Appl. Toxicol., **2017**, 37, 1464–1470.
32 F. Román, P. Colomer, Y. Calventus; J.M. Hutchinson, Study of hyperbranched poly(ethyleneimine) polymers of different molecular weight and their interaction with epoxy resin, Materials, **2018**, 11, 1–26.
33 M.S. Diallo, S. Christie, P. Swaminathan, J.H. Johnson, W.A. Goddard, Dendrimer enhanced ultrafiltration. 1. Recovery of Cu(II) from aqueous solutions using PAMAM dendrimers with ethylene diamine core and terminal NH_2 groups, Environ. Sci. Technol., **2005**, 39, 1366–1377.
34 A. Alighardashi, Z. Kashitarash-Esfahani, F. Najafi, A. Afkhami, N. Hassani, Development and Application of Graphene oxide/poly-amidoamines dendrimers (GO/PAMAMs) nano-composite for nitrate removal from aqueous solutions. Environ. Process. **2015**, 5, 41–64.
35 I. Gopalakrishnan, R.S. Samuel, K. Sridharan, Nanomaterials-based adsorbents for water and wastewater treatments, In: Emerging Trends of Nanotechnology in Environment and Sustainability, K. Sridharan (Ed.), Springer, **2018**, pp. 89–98.
36 C. Deraedt, G. Melaet, W.T. Ralston, R. Ye, G.A. Somorjai, Platinum and other transition metal nanoclusters (Pd, Rh) stabilized by PAMAM dendrimer as excellent heterogeneous catalysts: Application to the methylcyclopentane (MCP) hydrogenative isomerization, Nano Lett., **2017**, 17, 1853–1862.
37 G. Ou, J. Zhao, P. Chen, C. Xiong, F. Dong, B. Li, X. Feng, Fabrication and application of noble metal nanoclusters as optical sensors for toxic metal ions, Anal. Bioanal. Chem., **2018**, 410, 2485–2498.
38 S. Akbari, R.M. Kozłowski, A review of application of amine-terminated dendritic materials in textile engineering, J. Text. Inst., **2018**, 1–8.
39 M. Dodangeh, R. Tang, K. Gharanjig, Improving the photostability of curcumin using functional star-shaped polyamidoamine dendrimer: Application on PET, Mater. Today Commun., **2019**, 21, 100620.
40 M. Dodangeh, K. Gharanjig, R. Tang, I. Grabchev, Dyes and pigments functionalization of PAMAM dendrimers with curcumin: Synthesis, characterization, fluorescent improvement and application on PET polymer, Dye. Pigment., **2020**, 174, 108081.
41 I. Sohail, I.A. Bhatti, A. Ashar, F.M. Sarim, M. Mohsin, R. Naveed, M. Yasir, M. Iqbal, A. Nazir, Polyamidoamine (PAMAM) dendrimers synthesis, characterization and adsorptive removal of nickel ions from aqueous solution, J. Mater. Res. Technol., **2020**, 9, 498–506.
42 P. Fernández Freire, A. Peropadre, R. Rosal, J. M. Pérez Martín, M.J. Hazen, Toxicological assessment of third generation (G3) poly (amidoamine) dendrimers using the *Allium cepa* test, Sci. Total Environ., **2016**, 563–564, 899–903.
43 A.N. Petit, P. Eullaffroy, T. Debenest, F. Gagné, Toxicity of PAMAM dendrimers to *Chlamydomonas reinhardtii*, Aquat. Toxicol., **2010**, 100, 187–193.
44 A.N. Petit, T. Debenest, P. Eullaffroy, F. Gagné, Effects of a cationic PAMAM dendrimer on photosynthesis and ROS production of

Chlamydomonas reinhardtii, Nanotoxicology, **2012**, 6, 315–326.
45 C. Blaise, F. Gagné, J. Auclair, D. Maysinger, P. Sutthivaiyakit, Ecotoxicity of a potential drug nano-formulation: PAMAM-dendrimer and minocycline, J. Xenobiotics, **2014**, 4, 85–87.
46 P.C. Naha, M. Davoren, A. Casey, H.J. Byrne, An ecotoxicological study of poly(amidoamine) dendrimers-toward quantitative structure activity relationships, Environ. Sci. Technol., **2009**, 43, 6864–6869.
47 S. Gonzalo, I. Rodea-Palomares, F. Leganés, E. García-Calvo, R. Rosal, F. Fernández-Piñas, First evidences of PAMAM dendrimer internalization in microorganisms of environmental relevance: A linkage with toxicity and oxidative stress, Nanotoxicology, **2015**, 9, 706–718.
48 M. Tamayo-Belda, M. González-Pleiter, G. Pulido-Reyes, K. Martin-Betancor, F. Leganés, R. Rosal, F. Fernández-Piñas, Mechanism of the toxic action of cationic G5 and G7 PAMAM dendrimers in the cyanobacterium, Environ. Sci. Nano, **2019**, 6, 863–878.
49 OECD, Series on the Safety of Manufactured Nanomaterials, No. 27 List of manufactured nanomaterials and List of endpoints for phase one of the sponsorship programme for the testing of manufactured nanomaterials: Revision, **2010**.
50 A.L. Barrán-Berdón, I. Rodea-Palomares, F. Leganés, F. Fernández-Piñas, Free Ca^{2+} as an early intracellular biomarker of exposure of cyanobacteria to environmental pollution, Anal. Bioanal. Chem., **2011**, 400, 1015–1029.
51 G. Pulido-Reyes, I. Rodea-Palomares, S. Das, T.S. Sakthivel, F. Leganes, R. Rosal, S. Seal and F. Fernández-Piñas, Untangling the biological effects of cerium oxide nanoparticles: the role of surface valence states., Sci. Rep., **2015**, 5, 15613.
52 M. González-Pleiter, M. Tamayo-Belda, G. Pulido-Reyes, G. Amariei, F. Leganés, R. Rosal, F. Fernández-Piñas, Secondary nanoplastics released from a biodegradable microplastic severely impact freshwater environments, Environ. Sci. Nano, **2019**, 6, 1382–1392.
53 I. Rodea-palomares, A.L. Petre, K. Boltes, F. Leganés, J.A. Perdigón-Melón, R. Rosal, F. Fernández-Piñas, Application of the combination index (CI)-isobologram equation to study the toxicological interactions of lipid regulators in two aquatic bioluminescent organisms, Water Res., **2010**, 44, 427–438.
54 I. Martín-de-Lucía, M. C. Campos-Mañas, A. Agüera, F. Leganés, F. Fernández-Piñas, R. Rosal, Combined toxicity of graphene oxide and wastewater to the green alga Chlamydomonas, Environ. Sci. Nano, **2018**, 5, 1729–1744.
55 M.B. Allen, D.I. Arnon, Studies on nitrogen-fixing blue-green algae, Plant Physiol., **1955**, 366–372.
56 S. Ahmed, Estimation of total chlorophyll and total carotenoid contents for strains of *Anabaena* and *Gloeocapsa* through spectrophotometer, Biol. Sci., **2016**, 70–71.
57 E. Blumwald, E. Tel-Or, Structural aspects of the sdaptation of *Nostoc muscorum* to salt, Arch. Microbiol., *1982*, 132, 163–167.
58 T.C. Chou, P. Talalay, Quantitative analysis of dose-effect relationships: the combined effects of multiple drugs or enzyme inhibitors, Adv. Enzyme Regul., **1984**. 22, 27–55.
59 M. Ameri, A. Baron-Sola, R. A. Khavari-Nejad, N. Soltani, F. Najafi, A. Bagheri, F. Martínez, L.E. Hernández, Aluminium triggers oxidative stress and antioxidant response in the microalgae *Scenedesmus* sp, J. Plant Physiol., **2020**, 246–247, 153114.
60 C. Ortega-Villasante, R. Rellán-Álvarez, F.F. Del Campo, R.O. Carpena-Ruiz, L.E. Hernández, Cellular damage induced by cadmium and mercury in *Medicago sativa*, J. Exp. Bot., **2005**, 56, 2239–2251.
61 A. Elbaz, Y.Y. Wei, Q. Meng, Q. Zheng, Z.M. Yang, Mercury-induced oxidative stress and impact on antioxidant enzymes in *Chlamydomonas reinhardtii*, Ecotoxicology, **2010**, 19, 1285–1293.
62 F. Leganés, F. Martínez-Granero, M.Á. Muñoz-Martín, E. Marco, A. Jorge, L. Carvajal, T. Vida, M. González-Pleiter, F. Fernández-Piñas, Characterization and responses to environmental cues of a photosynthetic antenna-deficient mutant of the filamentous cyanobacterium *Anabaena* sp. PCC 7120, J. Plant Physiol., **2014**, 171, 915–926.
63 J Hurtado-Gallego, G. Pulido-Reyes, M. González-Pleiter, G. Salas, F. Leganés, R. Rosal, F. Fernández-Piñas, Toxicity of superparamagnetic iron oxide nanoparticles to the microalga *Chlamydomonas reinhardtii*, Chemosphere, **2020**, 238, 2–11.
64 L. Feng, X. Sun, F. Zhu, Y. Feng, J. Duan, F. Xiao, X. Li, Y. Shi, Q. Wang, J. Sun, X. Liu, J. Liu, L. Zhou, S. Wang, Z. Ding, H. Tian, T.S. Galloway, X. Yuan, Nanoplastics promote microcystin synthesis and release from cyanobacterial *Microcystis aeruginosa*, Environ. Sci. Technol., **2020**, 54, 6, 3386–3394.
65 S. Van Dongen, C. Abreu-Goodger, Using MCL to extract clusters from networks, Bact. Mol. Networks, **2012**, 804, 281–295.
66 Y. Aoki, Y. Okamura, H. Ohta, K. Kinoshita, T. Obayashi, ALCOdb: Gene coexpression database for microalgae, Plant Cell Physiol., **2016**, 57, 1–9.
67 T. Obayashi, K. Kinoshita, Rank of correlation coefficient as a comparable measure for biological significance of gene coexpression, DNA Research, **2009**, 16, 249–260.
68 J. L. Rodgers, W.A. Nicewander, Thirteen ways to look at the correlation coefficient, Am. Stat., **1988**, 42, 59–66.

69 R. Prado, C. Rioboo, C. Herrero, Á. Cid, Characterization of cell response in *Chlamydomonas moewusii* cultures exposed to the herbicide paraquat: Induction of chlorosis, Aquat. Toxicol., **2011**, 102, 10–17.
70 G. Thiel, Redox-state of intactNitella cells: dependency on intracellular pH and photosynthesis, Protoplasma, **1994**, 179, 26–33.
71 M. Gonzalez-Pleiter, C. Rioboo, M. Reguera, I. Abreu, F. Leganes, Á. Cid, F. Fernandez-Piñas, Calcium mediates the cellular response of *Chlamydomonas reinhardtii* to the emerging aquatic pollutant triclosan, Aquat. Toxicol., **2017**, 186, 50–66.
72 N. Battchikova, D. Muth-Pawlak, E. Aro, Proteomics of cyanobacteria: current horizons, Curr. Opin. Biotechnol., **2018**, 54, 65–71.
73 O. Mirus, S. Strauss, K. Nicolaisen, A. Von Haeseler, E. Schleiff, TonB-dependent transporters and their occurrence in cyanobacteria, BMC Biol., **2009**, 25, 1–25.
74 P. Oliveira, N.M. Martins, M. Santos, N.A.S. Couto, P. C. Wright, P. Tamagnini, The *Anabaena* sp. PCC 7120 Exoproteome: Taking a peek outside the box, Life, **2015**, 5, 130–163.
75 D. Shvarev, C.N. Nishi, I. Maldener, Two DevBCA-like ABC transporters are involved in the multidrug resistance of the cyanobacterium *Anabaena* sp. PCC 7120, FEBS Lett., **2019**, 593, 1818–1826.
76 L.M. Hernández, N. Youse, N. Tufenkji, Are there nanoplastics in your personal care products? Environ. Sci. Technol., **2017**, 4, 280–285.
77 M. Bundschuh, J. Filser, S. Lüderwald, M.S. Mckee, G. Metreveli, G.E. Schaumann, R. Schulz, S. Wagner, Nanoparticles in the environment: where do we come from, where do we go to? Environ. Sci. Eur., **2018**, 30, 1–17.
78 P.C. Naha, S.P., Mukherjee, H.J. Byrne, Toxicology of engineered nanoparticles: Focus on poly(amidoamine) dendrimers, Int. J. Environ. Res. Public Health, **2018**, 15, 338.
79 M. Shen, Y. Zhang, Y. Zhu, B. Song, G. Zeng, D. Hu, X. Wen, X. Ren, Recent advances in toxicological research of nanoplastics in the environment: A review, Environ. Pollut., **2019**, 252, 511–521.
80 Sendra, M., Staffieri, E., Yeste, M. P., Moreno-Garrido, I., Gatica, J. M., Corsi, I., Blasco, J. Are the primary characteristics of polystyrene nanoplastics responsible for toxicity and ad/absorption in the marine diatom Phaeodactylum tricornutum? Environ. Pollut, **2019**, 249, 610-619.
81 M. Baudrimont, A. Arini, C. Guégan, Z. Venel, J. Gigault, B. Pedrono, J. Prunier, L. Maurice, A. Ter Halle, A. Feurtet-Mazel, Ecotoxicity of polyethylene nanoplastics from the North Atlantic oceanic gyre on freshwater and marine organisms (microalgae and filter-feeding bivalves), Environ. Sci. Pollut. Res., **2019**, 27, 3746–3755.
82 B. Huang, Z. Wei, L. Yang, K. Pan, A. Miao. Combined toxicity of silver nanoparticles with hematite or plastic nanoparticles toward two freshwater algae, Environ. Sci. Technol., **2019**, 53, 3871−3879.
83 S.B. Sjollema, P. Redondo-Hasselerharm, H.A. Leslie, M.H. Kraak, A.D. Vethaak, Do plastic particles affect microalgal photosynthesis and growth?, Aquat. Toxicol., **2016**, 170, 259–261.
84 L. Feng, J. Li, E. G. Xu, X. Sun, F. Zhu, Z. Ding, H. Tian, S. Dong, P. Xia and X. Yuan, Short-term exposure to positively charged polystyrene nanoparticles causes oxidative stress and membrane destruction in cyanobacteria, Environ. Sci. Nano, **2019**, 6, 3072–3079.
85 A. Latifi, M. Ruiz and C.C. Zhang, Oxidative stress in cyanobacteria, FEMS Microbiol. Rev., **2009**, 33, 258–278.
86 P. Bhattacharya, S. Lin, J.P. Turner, P.C. Ke, Physical adsorption of charged plastic nanoparticles affects algal photosynthesis, J. Phys. Chem. C, **2010**, 114, 16556–16561.
87 Q. Zhang, Q. Qu, T. Lu, M. Ke, Y. Zhu, M. Zhang, Z. Zhang, B. Du, X. Pan, L. Sun, H. Qian, The combined toxicity effect of nanoplastics and glyphosate on Microcystis aeruginosa growth, Environ. Pollut., **2018**, 243, 1106–1112.
88 Y. Liu, Z. Wang, S. Wang, H. Fang, N. Ye, D. Wang, Ecotoxicological effects on *Scenedesmus obliquus* and *Danio rerio* co-exposed to polystyrene nano-plastic particles and natural acidic organic polymer, Environ. Toxicol. Pharmacol., **2019**, 67, 21–28.
89 N. Ye, Z. Wang, S. Wang, W.J.G.M. Peijnenburg, Toxicity of mixtures of zinc oxide and graphene oxide nanoparticles to aquatic organisms of different trophic level: particles outperform dissolved ions, Nanotoxicology, **2018**, 0, 1–16.
90 V. Iswarya, M. Bhuvaneshwari, S. A. Alex, S. Iyer, G. Chaudhuri, P. T. Chandrasekaran, G.M. Bhalerao, S. Chakravarty, A.M. Raichur, N. Chandrasekaran, A. Mukherjee, Combined toxicity of two crystalline phases (anatase and rutile) of titania nanoparticles towards freshwater microalgae: *Chlorella* sp, Aquat. Toxicol., **2015**, 161, 154–169.
91 K.A. Huynh, J.M. Mcca, K.L. Chen, Heteroaggregation reduces antimicrobial activity of silver nanoparticles: Evidence for nanoparticle−cell proximity effects, Environ. Sci. Technol., **2014**, 1(9), 361–366.
92 N. Ye, Z. Wang, H. Fang, S. Wang, F. Zhang, Combined ecotoxicity of binary zinc oxide and copper oxide nanoparticles to Scenedesmus obliquus to *Scenedesmus obliquus*, J. Environ. Sci. Heal. Part A, **2017**, 0, 1–6.

93 Y. Liu, S. Wang, Z.Wang, N. Ye, H.Zang, D. Wang, TiO_2, SiO_2 and ZrO_2 nanoparticles synergistically provoke cellular oxidative damage in freshwater microalgae, nanomaterials, **2018**, 8, 95.
94 G. Pulido-Reyes, M. Briffa, J. Hurtado-Gallego, T. Yudina, F. Leganés, V. Puntes, E. Valsami-Jones, Internalization and toxicological mechanisms of uncoated and PVP-coated cerium oxide nanoparticles in the freshwater alga *Chlamydomonas reinhardtii*, Environ. Sci. Nano, **2019**, 6, 1959–1972.
95 T.M. Nolte, N.B. Hartmann, J.M. Kleijn, J. Garnæs, D. Van De Meent, A.J. Hendriks, A. Baun, The toxicity of plastic nanoparticles to green algae as influenced by surface modification, medium hardness and cellular adsorption, Aquat. Toxicol., **2020**, 183, 11–20.
96 G. Rossi, J. Barnoud, L. Monticelli, Polystyrene nanoparticles perturb lipid membranes, J. Phys. Chem. Lett. Lett., **2014**, 5, 241−246.
97 F. Mirzajani, H. Askari, S. Hamzelou, Y. Schober, A. Römpp, A. Ghassempour, B. Spengler, Proteomics study of silver nanoparticles toxicity on *Bacillus thuringiensis*, Ecotoxicol. Environ. Saf., **2014**, 100, 122–130.
98 H. Qian, K. Zhu, H. Lu, M. Lavoie, S. Chen, Z. Zhou, Z. Deng, J. Chen, Z. Fu, Contrasting silver nanoparticle toxicity and detoxification strategies in *Microcystis aeruginosa* and *Chlorella vulgaris*: New insights from proteomic and physiological analyses, Sci. Total Environ., **2016**, 572, 1213–1221.
99 M. Qu, K. Xu, Y. Li, G. Wong, D. Wang, Using acs-22 mutant *Caenorhabditis elegans* to detect the toxicity of nanopolystyrene particles, Sci. Total Environ., **2018**, 643, 119–126.
100 S. L. Lim, C.T. Ng, L. Zou, Y. Lu, J. Chen, B. Huat, H. Shen, C.N. Ong, Targeted metabolomics reveals differential biological effects of nanoplastics and nano-ZnO in human lung cells, Nanotoxicology, **2019**, 0, 1–16.
101 Z. Liu, Y. Huang, Y. Jiao, Q. Chen, D. Wu, P. Yu, Y. Li, M. Cai, Y. Zhao, Polystyrene nanoplastic induces ROS production and affects the MAPK-HIF-1/NFkB-mediated antioxidant system in *Daphnia pulex*, Aquat. Toxicol., **2020**, 220, 105420.
102 Z. Liu, Y. Jiao, Q. Chen, Y. Li, J. Tian, Y. Huang, M. Cai, D. Wu and Y. Zhao, Two sigma and two mu class genes of glutathione S-transferase in the water flea *Daphnia pulex*: Molecular characterization and transcriptional response to nanoplastic exposure, Chemosphere, **2020**, 248, 126065.
103 W. Zhang, Z. Liu, S. Tang, D. Li, Q. Jiang and T. Zhang, Transcriptional response provides insights into the effect of chronic polystyrene nanoplastic exposure on *Daphnia pulex*, Chemosphere, **2020**, 238, 124563.
104 M.N. Moore, Do nanoparticles present ecotoxicological risks for the health of the aquatic environment?, Environ. Int., **2006**, 32, 967–976.
105 A. Sereemaspun, P. Hongpiticharoen, R. Rojanathanes, P. Maneewattanapinyo, S. Ekgasit, W. Warisnoicharoen, Inhibition of human cytochrome P450 enzymes by metallic nanoparticles: a preliminary to nanogenomics, Int. J. Pharmacol., **2008**, 4, 492-495.
106 C. Falugi, M.G. Aluigi, M.C. Chiantore, D. Privitera, P. Ramoino, M.A. Gatti, A. Fabrizi, A. Pinsino, V. Matranga, Toxicity of metal oxide nanoparticles in immune cells of the sea urchin, Mar. Environ. Res., **2012**, 76, 114–121.
107 M. Burnat, B. Li, S. H. Kim, J. Anthony, Homospermidine biosynthesis in the cyanobacterium Anabaena requires a deoxyhypusine synthase homologue and is essential for normal diazotrophic growth, Mol. Microbiol., **2018**, 109, 763–780.
108 J. Hurtado-Gallego, A. Redondo-López, F. Leganés, R. Rosal, F. Fernández-Piñas, Peroxiredoxin (*2-cys-prx*) and catalase (*katA*) cyanobacterial-based bioluminescent bioreporters to detect oxidative stress in the aquatic environment, Chemosphere, **2019**, 236, 124395.
109 S. Mihara, K. Yoshida, A. Higo, T. Hisabori, Functional significance of NADPH-thioredoxin reductase C in the antioxidant defense system of cyanobacterium, Plant Cell Physiol., **2017**, 58, 86–94.
110 S. Moslavac, Outer membrane proteins of *Anabaena* sp. strain PCC 7120, PhD Diss, Ludwig-Maximilians-Universität, 2007.
111 G.O. Noriega, K.B. Balestrasse, A. Batlle, M.L. Tomaro, Cadmium induced oxidative stress in soybean plants also by the accumulation of d-aminolevulinic acid, Biometals, **2007**, 20, 841–851.
112 T. Chou, Theoretical basis, experimental design, and computerized simulation of synergism and antagonism in drug combination Studies, Pharmacol. Rev., **2006**, 58, 621–681.

SUPPLEMENTARY INFORMATION

Understanding nanoplastics toxicity and their interaction with engineered cationic nanopolymers in microalgae by physiological and proteomic approaches

Miguel Tamayo-Belda[1], Juan Vargas-Guerrero[1], Keila Martin-betancor[1], Gerardo Pulido-Reyes[1], Miguel González-Pleiter[1], Francisco Leganés[1], Roberto Rosal[2], Francisca Fernandez-Piñas[1,*]

[1] Department of Biology, Faculty of Science, Universidad Autónoma de Madrid, E-28049, Madrid, Spain.
[2] Department of Chemical Engineering, Universidad de Alcalá, E-28871 Alcalá de Henares, Madrid, Spain

[*] Corresponding author: francisca.pina@uam.es

Proteomic analysis

In-Gel Digestion (Stacking gel)

The protein extracts from three independent replicates of *Anabaena* exposed to PS-NPs, G7 and their binary mixture for 72h plus the control non-exposed cyanobacterial cells were suspended in a volume up to 50 µl of sample buffer, and then applied onto 1.2 cm wide wells of a conventional SDS-PAGE gel (0.75 mm thick, 4% stacking, and 10% resolving). The run was stopped as soon as the front entered 3 mm into the resolving gel, so that the whole proteome became concentrated in the stacking/resolving gel interface. The unseparated protein bands were visualized by Coomassie staining, excised, cut into cubes (2 x 2 mm), and placed in 0.5 ml microcentrifuge tubes.[1] The gel pieces were destained in acetonitrile:water (ACN:H_2O, 1:1), reduced and alkylated (disulfide bonds from cysteinyl residues were reduced with 10 mM DTT for 1 h at 56 ºC, and then thiol groups were alkylated with 10 mM iodoacetamide for 30 min at room temperature in darkness) and digested *in situ* with sequencing-grade trypsin (Promega, Madison, WI) as described by Shevchenko et al.[2] with minor modifications. The gel pieces were dehydrated by removing all liquid using sufficient ACN. Acetonitrile was pipetted out and the gel pieces were dried in a speedvac. The dried gel pieces were re-hydrated in 100 mM Tris-HCl pH 8, 10mM $CaCl_2$ with 60 ng/µl trypsin at 5:1 protein:enzyme (w/w) ratio. The tubes were kept on ice for 2 h and incubated at 37 ºC for 12 h. Digestion was stopped by the addition of 1% trifluoroacetic acid (TFA). Whole supernatants were dried and desalted onto OMIX Pipette tips C18 (Agilent Technologies) prior to mass spectrometric analysis.

TMT labelling and high pH fractionation

The resultant peptide mixture from desalted protein tryptic digest (50 µg) was labelled using chemicals from the TMT six plex Isobaric Mass Tagging Kit (Thermo Fisher Scientific, MA, USA) (Reagents 126 for the Control sample, 128 for the 65 sample, 130 for the 45 sample and 131 for the Mix sample) essentially as described by manufacturer. Briefly, peptides were dissolved in 50 µL of 100 mM triethylammonium bicarbonate (TEAB), adjusted to pH 8. For labelling, each TMT reagent

was dissolved in 41 µL of ACN and added to the respective peptide mixture and then incubated at room temperature for one hour. Labelling was stopped by the addition of 8 µL 5% hydroxylamine. Whole supernatants were dried and the four samples were mixed to obtain the "4plex-labeled mixture". The mixture was analyzed by RP-LC-MS/MS to check the efficiency of the labelling.[3]

Fractionation

The sample was then fractionated using the Pierce High pH Reversed-Phase Peptide Fractionation Kit (Thermo Fisher Scientific, MA, USA), as described with minor modifications. The sample was re-hydrated in 0.1% TFA and then loaded onto an equilibrated, high-pH, reversed-phase fractionation spin column. A step gradient of increasing ACN concentrations (5-80%) in a volatile high-pH (Triethylamine (0.1%)) is then applied to the columns to elute bound peptides into nine different fractions collected by centrifugation. The fractions obtained from high-pH, reversed-phase 4plex-labeled mixture were dried and stored until analysis by mass spectrometry for quantification.

Quantitative analysis by reverse phase-liquid chromatography RP-LC-MS/MS

The fractions were resuspended in 10 µl of 0.1% formic acid and analyzed by RP-LC-MS/MS in an Easy-nLC II system coupled to an ion trap LTQ-Orbitrap-Velos-Pro hybrid mass spectrometer (Thermo Scientific). The peptides were concentrated (on-line) by reverse phase chromatography using a 0.1mm × 20 mm C18 RP precolumn (Proxeon), and then separated using a 0.075mm x 250 mm C18 RP column (Proxeon) operating at 0.3 µl/min. Peptides were eluted using a 90-min dual gradient. The gradient profile was set as follows: 5−25% solvent B for 68 min, 25−40% solvent B for 22min, 40−100% solvent B for 2 min and 100% solvent B for 18 min (Solvent A: 0,1% formic acid in water, solvent B: 0,1% formic acid, 80% ACN in water). ESI ionization was done using a Nano-bore emitters Stainless Steel ID 30 µm (Proxeon) interface at 2.1 kV spray voltage with S-Lens of 60%.

The instrument method consisted of a data-dependent top-20 experiment with an Orbitrap MS1 scan at a resolution (m/Δm) of 30,000 followed by either twenty high energy collision dissociation (HCD) MS/MS mass-analyzed in the Orbitrap at 7,500 (Δm/m) resolution. MS2 experiments were performed using HCD to generate high resolution and high mass accuracy MS2 spectra.
The minimum MS signal for triggering MS/MS was set to 500. The lock mass option was enabled for both MS and MS/MS mode and the polydimethylcyclosiloxane ions (protonated $(Si(CH_3)_2O))_6$; m/z 445.120025) were used for internal recalibration of the mass spectra.

Peptides were detected in survey scans from 400 to 1600 amu (1 µscan) using an isolation width of 1.3 u (in mass-to-charge ratio units), normalized collision energy of 40% for HCD fragmentation, and dynamic exclusion applied for 60 seconds periods. Charge-state screening was enabled to reject unassigned and singly charged protonated ions.[4]

Quantitative data analysis

Peptide identification from raw data (a single search was performed with all nine raws from the fractionation) was carried out using PEAKS Studio X+ search engine (Bioinformatics Solutions Inc., Waterloo, Ontario, Canada). Database searches were performed against uniprot-*Nostoc* (*Anabaena)* sp. PCC 7120 (6070 entries; UniProt release 12/2019) (decoy-fusion database). The following constraints were used for the searches: tryptic cleavage after Arg and Lys (semi-specific), up to two missed cleavage sites, and tolerances of 20 ppm for precursor ions and 0.05 Da for MS/MS fragment ions and the searches were performed allowing optional Met oxidation and Cys

carbamidomethylation and fixed TMT 6plex reagent labelling at the N-terminus and lysine residues. False discovery rates (FDR) for peptide spectrum matches (PSM) was limited to 0.01. Only those proteins with at least two distinct peptides and at least one unique peptide being discovered from LC/MS/MS analyses were considered reliably identified and sent to be quantified.

The quantitation of TMT labelled peptides was performed with PEAKS Studio X+ search engine, selected "Reporter Ion Quantification TMT" under the "Quantifications" options. Auto normalization mode was used that calculates a global ratio from the total intensity of all labels in all quantifiable peptides. The -10LgP, Quality and Reporter Ion Intensity (1.7e4) were used for Spectrum filter and Significance (20, PEAKSQ method) was used for peptide and protein abundance calculation. For the Protein quantification, protein groups for peptide uniqueness were considered, using only unique peptides for protein quantification and the modified peptides were excluded.[3,5]

Table S1: Data displayed by STRING MCL clustering (inflation parameter = 3)

Cluster number	cluster color	Gene count	Protein name	Protein identifier
1	Red	12	FusA	103690.1713
1	Red	12	SecA	103690.1713
1	Red	12	Rps7	103690.1713
1	Red	12	Rps4	103690.1713
1	Red	12	Rps5	103690.1713
1	Red	12	RpsN	103690.1713
1	Red	12	Hpf	103690.1713
1	Red	12	DapB	103690.1713
1	Red	12	RpoC2	103690.1714
1	Red	12	Rpl1	103690.1713
1	Red	12	RplN	103690.1713
1	Red	12	RpoB	103690.1714
2	Lime Green	9	DnaK2	103690.1713
2	Lime Green	9	ClpP3	103690.1713
2	Lime Green	9	Alr0286	103690.1714
2	Lime Green	9	GroL2	103690.1713
2	Lime Green	9	ClpB2	103690.1713
2	Lime Green	9	Alr1809	103690.1713
2	Lime Green	9	Alr2323	103690.1713
2	Lime Green	9	GroL1	103690.1713
2	Lime Green	9	17132093	103690.1713
3	Cyan	5	Alr4642	103690.1713
3	Cyan	5	All0737	103690.1713
3	Cyan	5	All1541	103690.1714
3	Cyan	5	Alr4641	103690.1713
3	Cyan	5	Alr4745	103690.1713
4	Medium Purple	5	PecA	103690.1713
4	Medium Purple	5	CpcG3	103690.1713
4	Medium Purple	5	PecC	103690.1713

4	Medium Purple	5	ApcE	103690.1713
4	Medium Purple	5	PecB	103690.1713
5	Medium Purple (2)	4	NdhI	103690.1714
5	Medium Purple (2)	4	PsbB	103690.1714
5	Medium Purple (2)	4	Alr1129	103690.1713
5	Medium Purple (2)	4	All0107	103690.1714
6	Orchid	2	Alr0668	103690.1713
6	Orchid	2	Alr0669	103690.1713
7	Purple	2	All1267	103690.1713
7	Purple	2	Alr0782	103690.1713
8	Pink	2	All0667	103690.1713
8	Pink	2	All0666	103690.1713
9	Pale Violet Red	2	PepA	103690.1714
9	Pale Violet Red	2	Ndk	103690.1713
10	Brown	2	Alr3411	103690.1713
10	Brown	2	Alr1548	103690.1714
11	Dark Golden Rod	2	Alr4029	103690.1713
11	Dark Golden Rod	2	Alr4028	103690.1713
12	Yellow	2	Alr2117	103690.1713
12	Yellow	2	All3054	103690.1713
13	Olive	2	Alr0490	103690.1713
13	Olive	2	All2127	103690.1713
14	Green Yellow	1	All4499	103690.1713
15	Green	1	Alr2269	103690.1713
16	Light Green	1	GlnA	103690.1713

Table S2: Particle hydrodynamic size, based on volume distribution, determined by DLS and ζ-potential measured by ELS in pure water and in culture medium (AA/8 + N) with their 95% confidence intervals.

	Size (nm)		ζ-Potential (mV)
	Pure water (pH 6.5)	AA/8 + N (pH 7.4)	AA/8 + N (pH 7.4)
Without nanoparticles	--	1.8 ± 1.1	-19.4 ± 1.6
PS-NPs	23.8 ± 0.6	24.9 ± 1.1	-19.8 ± 0.7
G7*	7.6 ± 0.3*	10.1 ± 1.1*	20.8 ± 1.1*
Mix	27.3 ± 3.3	527.1 ± 69.4	-17.0 ± 0.9

* In agreement with Tamayo-Belda *et al.* after filtration through a 100 nm filter.[55]

Table S3: Effective concentrations of polystyrene nanoplastics (PS-NPs) both individually and in mixture with PAMAM dendrimers of generation 7 (Mix) that induced 10%, 50% and 90% of growth inhibition, chlorophyll *a* and phycocyanin concentration decrease and the model type fitted on *Anabaena* sp. PCC7120 for 72 h.

Measured parameter	Model Fitted (PS-NPs / Mix)	Effective concentration	PS-NPs (mg/mL)	Mix (Constant ratio dilutions)
Growth (mg of dry weight/mL)	W1.3 / W1.4	EC_{10}	46.12 ± 2.08	0.59 ± 0.06
		EC_{50}	64.40 ± 0.90	1.39 ± 0.06
		EC_{90}	81.26 ± 3.29	3.25 ± 0.13
Chlorophyll *a* (mg/mL)	LL.2 / W1.3	EC_{10}	40.51 ± 1.21	0.56 ± 0.09
		EC_{50}	59.35 ± 0.65	1.22 ± 0.07
		EC_{90}	75.71 ± 1.25	1.99 ± 0.16
Phycocyanin (mg/mL)	LL.5 / W2.3	EC_{10}	40.03 ± 2.36	0.94 ± 0.19
		EC_{50}	59.47 ± 1.17	1.47 ± 0.18
		EC_{90}	76.53 ± 2.15	2.31± 0.43

Table S4: Surface and volume related properties of polystyrene nanoplastics (PS-NPs), PAMAM dendrimers of generation 7 (G7) and their mixture (Mix) in AA/8+N.

Particle/Combo	**PS-NPs**	**G7**	**Mix**
Radius (nm)	12	4	264
Surface area (nm^2)	1.81E+03	2.01E+02	8.76E+05
Volume (nm^3)	7.24E+03	2.68E+02	7.71E+07
Surf. area/Volume	0.250	0.750	0.011
Concentration ($\mu g\ mL^{-1}$)	64.4	3.9	64.4 (PS-NPs) 3.92 (G7)
Concentration (particle number mL^{-1})	6.89E+12	1.96E+13	7.15E+08
Total Surface area ($nm^2\ mL^{-1}$)	1.25E+16	3.94E+15	6.27E+14
Total Volume ($nm^3\ mL^{-1}$)	4.99E+16	5.25E+15	5.51E+16
Total Surf. area/Volume	0.250	0.750	0.011

Table S5: Protein description data from Uniprot

Category	Gene	Accession	Length	Protein names & description
Oxidative stress	all0737*	Q8YYV6	483	Thioredoxin reductase (EC 1.8.1.9); Biological process: cell redox homeostasis [GO:0045454]; removal of superoxide radicals [GO:0019430]; Cellular component: cell [GO:0005623]; cytoplasm [GO:0005737]; Associated terms: cell [GO:0005623]; cytoplasm [GO:0005737]; thioredoxin-disulfide reductase activity [GO:0004791]; cell redox homeostasis [GO:0045454]; removal of superoxide radicals [GO:0019430]; Molecular function: thioredoxin-disulfide reductase activity [GO:0004791]; Domain features: DOMAIN 339-483; note="Thioredoxin"; evidence="ECO:0000259|PROSITE:PS51352"; Keywords: FAD; Flavoprotein; Oxidoreductase; Redox-active center; Protein families: Class-II pyridine nucleotide-disulfide oxidoreductase family
	all1541*	Q8YWR3	251	Peroxiredoxin 2 family protein/glutaredoxin Biological process: cell redox homeostasis [GO:0045454]; Cellular component: cell [GO:0005623]; Associated terms: cell [GO:0005623]; electron transfer activity [GO:0009055]; protein disulfide oxidoreductase activity [GO:0015035]; cell redox homeostasis [GO:0045454]; Molecular function: electron transfer activity [GO:0009055]; protein disulfide oxidoreductase activity [GO:0015035]; Domain features: DOMAIN 4-168; note="Thioredoxin"; evidence="ECO:0000259|PROSITE:PS51352"
	alr0672*	Q8YZ15	433	Alr0672 protein; Molecular function: peroxidase activity;[6] Domain features: DOMAIN 273-418; note="acidPPc"; evidence="ECO:0000259|Pfam:PF01569"
	alr4641*	Q8YNC5	203	Peroxiredoxin ; Biological process: cell redox homeostasis [GO:0045454]; Cellular component: cell [GO:0005623]; Associated terms: cell [GO:0005623]; peroxiredoxin activity [GO:0051920]; cell redox homeostasis [GO:0045454]; Molecular function: peroxiredoxin activity [GO:0051920]; Domain features: DOMAIN 11-169; note="Thioredoxin"; evidence="ECO:0000259|PROSITE:PS51352"
	alr4642	Q8YNC4	213	Alr4642 protein ; Biological process: cell redox homeostasis [GO:0045454]; Cellular component: cell [GO:0005623]; Associated terms: cell [GO:0005623]; antioxidant activity [GO:0016209]; oxidoreductase activity [GO:0016491]; cell redox homeostasis [GO:0045454]; Molecular function: antioxidant activity [GO:0016209]; oxidoreductase activity [GO:0016491]; Domain features: DOMAIN 63-213; note="Thioredoxin"; evidence="ECO:0000259|PROSITE:PS51352"
	alr4745	Q8YN25	475	Dihydrolipoyl dehydrogenase (EC 1.8.1.4) ; Biological process: cell redox homeostasis [GO:0045454]; Cellular component: cell [GO:0005623]; Associated terms: cell [GO:0005623]; dihydrolipoyl dehydrogenase activity [GO:0004148]; electron transfer activity [GO:0009055]; flavin adenine dinucleotide binding [GO:0050660]; cell redox homeostasis [GO:0045454]; Molecular function: dihydrolipoyl dehydrogenase activity [GO:0004148]; electron transfer activity [GO:0009055]; flavin adenine dinucleotide binding [GO:0050660]; Domain features: DOMAIN 7-338; note="Pyr_redox_2"; evidence="ECO:0000259|Pfam:PF07992"; DOMAIN 357-469; note="Pyr_redox_dim"; evidence="ECO:0000259|Pfam:PF02852"; Keywords: FAD; Flavoprotein; NAD; Nucleotide-binding; Oxidoreductase; Redox-active center; Protein families: Class-I pyridine nucleotide-disulfide oxidoreductase family

	alr7524	Q8ZSI6	193	Alr7524 protein; {ECO:0000250}; Associated terms: peroxiredoxin activity [GO:0051920]; Molecular function: peroxiredoxin activity [GO:0051920]; Domain features: DOMAIN 57-123; note="CMD"; evidence="ECO:0000259|Pfam:PF02627"; Keywords: Plasmid
	dpsA*	Q8YQL3	184	Nutrient stress-induced DNA-binding protein; Function: Involved in protection of chromosomal DNA from damage under nutrient-limited and oxidative stress conditions. Binds heme (By similarity); Biological process: cellular iron ion homeostasis [GO:0006879]; Cellular component: cell [GO:0005623]; Associated terms: cell [GO:0005623]; DNA binding [GO:0003677]; ferric iron binding [GO:0008199]; oxidoreductase activity, oxidizing metal ions [GO:0016722]; cellular iron ion homeostasis [GO:0006879]; Molecular function: DNA binding [GO:0003677]; ferric iron binding [GO:0008199]; oxidoreductase activity, oxidizing metal ions [GO:0016722]; Keywords: DNA-binding; Heme; Iron; Metal-binding; Protein families: Dps family
Stress response	alr0286	Q8Z017	150	Small heat shock protein; Domain features: DOMAIN 33-146; note="SHSP"; evidence="ECO:0000259|PROSITE:PS01031" Keywords: Stress response; Protein families: Small heat shock protein (HSP20) family
	alr1809	Q8YW07	155	Heat shock protein, class I; Domain features: DOMAIN 43-155; note="SHSP"; evidence="ECO:0000259|PROSITE:PS01031" Keywords: Stress response; Protein families: Small heat shock protein (HSP20) family
	alr2323	Q8YUL8	658	Heat shock protein ; Biological process: protein folding [GO:0006457]; Associated terms: ATP binding [GO:0005524]; unfolded protein binding [GO:0051082]; protein folding [GO:0006457]; Molecular function: ATP binding [GO:0005524]; unfolded protein binding [GO:0051082]; Domain features: DOMAIN 25-178; note="HATPase_c"; evidence="ECO:0000259|SMART:SM00387" Keywords: Stress response
	clpB	Q8YST5	839	Endopeptidase Clp ATP-binding chain; Subcellular location: Cytoplasm {ECO:0000305}; Biological process: protein metabolic process [GO:0019538]; Associated terms: ATP binding [GO:0005524]; protein metabolic process [GO:0019538]; Molecular function: ATP binding [GO:0005524]; Domain features: DOMAIN 432-467; note="UVR"; evidence="ECO:0000259|PROSITE:PS50151" Keywords: ATP-binding; Chaperone; Coiled coil; Nucleotide-binding; Repeat; Protein families: ClpA/ClpB family
	clpB2	Q8YM56	872	Chaperone protein ClpB 2; Function: Part of a stress-induced multi-chaperone system, it is involved in the recovery of the cell from heat-induced damage, in cooperation with DnaK, DnaJ and GrpE. Acts before DnaK, in the processing of protein aggregates. Protein binding stimulates the ATPase activity; ATP hydrolysis unfolds the denatured protein aggregates, which probably helps expose new hydrophobic binding sites on the surface of ClpB-bound aggregates, contributing to the solubilization and refolding of denatured protein aggregates by DnaK (By similarity). {ECO:0000250}; Subcellular location: Cytoplasm {ECO:0000255|HAMAP-Rule:MF_00444}; Biological process: protein metabolic process [GO:0019538]; protein refolding [GO:0042026]; response to heat [GO:0009408]; Cellular component: cytoplasm [GO:0005737]; Associated terms: cytoplasm [GO:0005737]; ATP binding [GO:0005524]; protein metabolic process [GO:0019538]; protein refolding [GO:0042026]; response to heat [GO:0009408]; Molecular function: ATP binding [GO:0005524]; Domain features: DOMAIN 6-148; note="Clp R"; evidence="ECO:0000255|PROSITE-ProRule:PRU01251"

				Keywords: ATP-binding; Chaperone; Coiled coil; Cytoplasm; Nucleotide-binding; Repeat; Stress response; Protein families: ClpA/ClpB family
	clpP3	Q8YP43	197	Probable ATP-dependent Clp protease proteolytic subunit 3 (EC 3.4.21.92) (Endopeptidase Clp 3) involved in the efficient protein homeostasis;[7] Function: Cleaves peptides in various proteins in a process that requires ATP hydrolysis. Has a chymotrypsin-like activity. Plays a major role in the degradation of misfolded proteins. {ECO:0000255|HAMAP-Rule:MF_00444}; Cellular component: cytoplasm [GO:0005737]; Associated terms: cytoplasm [GO:0005737]; serine-type endopeptidase activity [GO:0004252]; Molecular function: serine-type endopeptidase activity [GO:0004252]; Keywords: Cytoplasm; Hydrolase; Protease; Serine protease; Protein families: Peptidase S14 family
	dnaK2	Q8YW74	633	Chaperone protein dnaK2 (HSP70-2) (Heat shock 70 kDa protein 2) (Heat shock protein 70-2); Function: Acts as a chaperone. {ECO:0000250}; Subcellular location: Cytoplasm {ECO:0000255|HAMAP-Rule:MF_00600}; Biological process: protein folding [GO:0006457]; Associated terms: ATP binding [GO:0005524]; unfolded protein binding [GO:0051082]; protein folding [GO:0006457]; Molecular function: ATP binding [GO:0005524]; unfolded protein binding [GO:0051082]; Keywords: ATP-binding; Chaperone; Nucleotide-binding; Phosphoprotein; Stress response; Protein families: Heat shock protein 70 family
	groL1	Q8YQZ8	544	60 kDa chaperonin 1 (GroEL protein 1) (Protein Cpn60 1); Function: Prevents misfolding and promotes the refolding and proper assembly of unfolded polypeptides generated under stress conditions. {ECO:0000255|HAMAP-Rule:MF_00600}; Subcellular location: Cytoplasm {ECO:0000255|HAMAP-Rule:MF_00600}; Biological process: protein refolding [GO:0042026]; Cellular component: cytoplasm [GO:0005737]; Associated terms: cytoplasm [GO:0005737]; ATP binding [GO:0005524]; unfolded protein binding [GO:0051082]; protein refolding [GO:0042026]; Molecular function: ATP binding [GO:0005524]; unfolded protein binding [GO:0051082]; Keywords: ATP-binding; Chaperone; Cytoplasm; Nucleotide-binding; Protein families: Chaperonin (HSP60) family
	groL2	Q8YVS8	560	60 kDa chaperonin 2 (GroEL protein 2) (Protein Cpn60 2); Function: Prevents misfolding and promotes the refolding and proper assembly of unfolded polypeptides generated under stress conditions. {ECO:0000255|HAMAP-Rule:MF_00600}; Biological process: protein refolding [GO:0042026]; Cellular component: cytoplasm [GO:0005737]; Associated terms: cytoplasm [GO:0005737]; ATP binding [GO:0005524]; unfolded protein binding [GO:0051082]; protein refolding [GO:0042026]; Molecular function: ATP binding [GO:0005524]; unfolded protein binding [GO:0051082]; Keywords: ATP-binding; Chaperone; Cytoplasm; Nucleotide-binding; Protein families: Chaperonin (HSP60) family
Surface location	alr1540*	Q8YWR4	128	Alr1540 protein; Transmembrane; Domain features: DOMAIN 22-77; note="PG_binding_1"; evidence="ECO:0000259|Pfam:PF01471"
	all0767	Q8YYS9	185	All0767 protein; Cellular component: integral component of membrane [GO:0016021]; Associated terms: integral component of membrane [GO:0016021]; Keywords: Membrane; Transmembrane; Transmembrane helix
	all2358	Q8YUI8	326	Phosphonate ABC transport phosphonate binding component; Transmembrane; Biological process: transmembrane transport [GO:0055085]; Cellular component: ATP-binding cassette (ABC)

				transporter complex [GO:0043190]; Associated terms: ATP-binding cassette (ABC) transporter complex [GO:0043190]; transmembrane transport [GO:0055085]
	all3054	Q8YSN0	1038	All3054 protein; Transmembrane; ; Cellular component: integral component of membrane [GO:0016021]; Associated terms: integral component of membrane [GO:0016021]; Domain features: DOMAIN 54-281; note="PBP_domain"; evidence="ECO:0000259|Pfam:PF12849" Keywords: Membrane; Transmembrane; Transmembrane helix
	all7121*	Q8YL17	694	All7121 protein; Cellular component: integral component of membrane [GO:0016021]; Associated terms: integral component of membrane [GO:0016021]; electron transfer activity [GO:0009055]; heme binding [GO:0020037]; metal ion binding [GO:0046872]; Molecular function: electron transfer activity [GO:0009055]; heme binding [GO:0020037]; metal ion binding [GO:0046872]; Domain features: DOMAIN 163-351; note="Cytochrome c"; evidence="ECO:0000259|PROSITE:PS51007"; DOMAIN 473-649; note="Cytochrome c"; evidence="ECO:0000259|PROSITE:PS51007" Keywords: Heme; Iron; Membrane; Metal-binding; Plasmid; Transmembrane; Transmembrane helix
	alr0140	Q8Z0F7	552	Periplasmic oligopeptide-binding protein of oligopeptide ABC transporter; Subcellular location: Cell outer membrane {ECO:0000256|RuleBase:RU003357, ECO:0000256|SAAS:SAAS01009251}; Biological process: transmembrane transport [GO:0055085]; Cellular component: ATP-binding cassette (ABC) transporter complex [GO:0043190]; Associated terms: ATP-binding cassette (ABC) transporter complex [GO:0043190]; transmembrane transport [GO:0055085]; Domain features: DOMAIN 96-459; note="SBP_bac_5"; evidence="ECO:0000259|Pfam:PF00496"
	alr0397*	Q8YZR0	867	Alr0397 protein; Cellular component: cell outer membrane [GO:0009279]; Associated terms: cell outer membrane [GO:0009279]; siderophore uptake transmembrane transporter activity [GO:0015344]; signaling receptor activity [GO:0038023]; Molecular function: siderophore uptake transmembrane transporter activity [GO:0015344]; signaling receptor activity [GO:0038023]; Domain features: DOMAIN 71-167; note="AMIN"; evidence="ECO:0000259|Pfam:PF11741"; DOMAIN 199-301; note="Plug"; evidence="ECO:0000259|Pfam:PF07715"; DOMAIN 400-865; note="TonB_dep_Rec"; evidence="ECO:0000259|Pfam:PF00593" Keywords: Cell outer membrane; Membrane; Receptor; TonB box; Protein families: TonB-dependent receptor family
	alr0474*	Q8YZI6	596	Alr0474 protein
	alr0564	Q8YZB5	397	Alr0564 protein ; Biological process: peptidoglycan turnover [GO:0009254]; Cellular component: outer membrane [GO:0019867]; Associated terms: outer membrane [GO:0019867]; hydrolase activity, hydrolyzing O-glycosyl compounds [GO:0004553]; peptidoglycan turnover [GO:0009254]; Molecular function: hydrolase activity, hydrolyzing O-glycosyl compounds [GO:0004553]; Domain features: DOMAIN 154-295; note="MltA"; evidence="ECO:0000259|SMART:SM00925" Keywords: Signal
	all4499	Q8YNR3	546	All4499 protein ; Biological process: carbohydrate transport [GO:0008643]; Cellular component: integral component of membrane [GO:0016021]; Associated terms: integral component of membrane [GO:0016021]; porin activity [GO:0015288]; carbohydrate transport [GO:0008643]; Molecular function: porin activity [GO:0015288]; Domain features: DOMAIN 55-119;

				note="SLH"; evidence="ECO:0000259|PROSITE:PS51272" Keywords: Coiled coil; Signal; Protein families: OprB family
	alr3411	Q8YRN3	190	Alr3411 protein; Identify in the outer membrane fraction.[8]
	alr0880	Q8YYH0	702	Oligopeptidase A; Transmembrane; Associated terms: metal ion binding [GO:0046872]; metalloendopeptidase activity [GO:0004222]; Molecular function: metal ion binding [GO:0046872]; metalloendopeptidase activity [GO:0004222]; Domain features: DOMAIN 235-696; note="Peptidase_M3"; evidence="ECO:0000259|Pfam:PF01432" Keywords: Coiled coil; Hydrolase; Metal-binding; Metalloprotease; Protease; Zinc; Protein families: Peptidase M3 family
	alr2117	Q8YV64	603	Alr2117 protein; Cellular component: integral component of membrane [GO:0016021]; Associated terms: integral component of membrane [GO:0016021]; Keywords: Coiled coil; Membrane; Transmembrane; Transmembrane helix
	alr2269	Q8YUR6	833	Alr2269 protein; Cellular component: outer membrane [GO:0019867]; Associated terms: outer membrane [GO:0019867]; Domain features: DOMAIN 315-378; note="POTRA_2"; evidence="ECO:0000259|Pfam:PF08479"; DOMAIN 405-466; note="POTRA"; evidence="ECO:0000259|Pfam:PF07244"; DOMAIN 493-833; note="Bac_surface_Ag"; evidence="ECO:0000259|Pfam:PF01103" Keywords: 3D-structure; Signal
	alr3345	Q8YRU8	340	Alr3345 protein; Cellular component: outer membrane-bounded periplasmic space [GO:0030288]; Associated terms: outer membrane-bounded periplasmic space [GO:0030288]
	alr4028*	Q8YQ12	287	Alr4028 protein; Domain features: DOMAIN 93-201; note="Plug"; evidence="ECO:0000259|Pfam:PF07715" Keywords:
	alr4029*	Q8YQ11	258	Alr4029 protein; Domain features: DOMAIN 2-255; note="TonB_dep_Rec"; evidence="ECO:0000259|Pfam:PF00593" Keywords: Receptor
	alr4280*	Q8YPB8	436	Alr4280 protein; Transmembrane; Domain features: DOMAIN 74-127; note="Biotin_lipoyl_2"; evidence="ECO:0000259|Pfam:PF13533" Keywords: Coiled coil
	alr4821*	Q8YMV5	352	Alr4821 protein; Cellular component: integral component of membrane [GO:0016021]; Associated terms: integral component of membrane [GO:0016021]; Keywords: Coiled coil; Membrane; Transmembrane; Transmembrane helix
	alr7346	Q8YKF2	262	Alr7346 protein; Subcellular location: Periplasm. Note=Periplasmic or loosely attached to the cytoplasmic or the outer membrane; Domain features: DOMAIN 6-258; note="DUF3598"; evidence="ECO:0000259|Pfam:PF12204" Keywords: Plasmid
	nucA	P38446	274	Nuclease (EC 3.1.30.-) (Endonuclease); Pathway: Carbohydrate metabolism; tricarboxylic acid cycle; isocitrate from oxaloacetate: step 2/2. {ECO:0000256|PIRNR:PIRNR036687}; Function: Catalyzes the degradation of both RNA and DNA; has the potential to act as an endonuclease; Cellular component: periplasmic space [GO:0042597]; Associated terms: periplasmic space [GO:0042597]; endonuclease activity [GO:0004519]; metal ion binding [GO:0046872]; nucleic acid binding [GO:0003676]; Molecular function: endonuclease activity [GO:0004519]; metal ion binding [GO:0046872]; nucleic acid binding [GO:0003676]; Keywords: 3D-structure; Endonuclease; Hydrolase; Magnesium; Manganese; Metal-binding; Nuclease; Periplasm; Plasmid; Signal; Protein families: DNA/RNA non-specific endonuclease family
Carbon metabolism and energy	all1267	Q8YXE6	876	Aconitate hydratase B (EC 4.2.1.3) (EC 4.2.1.99) (2-methylisocitrate dehydratase) ; Biological process: tricarboxylic acid cycle [GO:0006099]; Cellular component: cytosol [GO:0005829]; Associated terms: cytosol [GO:0005829]; 2-

				methylisocitrate dehydratase activity [GO:0047456]; 4 iron, 4 sulfur cluster binding [GO:0051539]; aconitate hydratase activity [GO:0003994]; citrate dehydratase activity [GO:0047780]; metal ion binding [GO:0046872]; tricarboxylic acid cycle [GO:0006099]; Molecular function: 2-methylisocitrate dehydratase activity [GO:0047456]; 4 iron, 4 sulfur cluster binding [GO:0051539]; aconitate hydratase activity [GO:0003994]; citrate dehydratase activity [GO:0047780]; metal ion binding [GO:0046872]; Domain features: DOMAIN 4-175; note="Aconitase_B_N"; evidence="ECO:0000259|Pfam:PF11791"; DOMAIN 187-390; note="Aconitase_2_N"; evidence="ECO:0000259|Pfam:PF06434"; DOMAIN 479-825; note="Aconitase"; evidence="ECO:0000259|Pfam:PF00330" Keywords: 4Fe-4S; Iron; Iron-sulfur; Lyase; Metal-binding; Tricarboxylic acid cycle; Protein families: Aconitase/IPM isomerase family
	all2127*	Q8YV54	452	All2127 protein; Associated terms: 4 iron, 4 sulfur cluster binding [GO:0051539]; catalytic activity [GO:0003824]; metal ion binding [GO:0046872]; Molecular function: 4 iron, 4 sulfur cluster binding [GO:0051539]; catalytic activity [GO:0003824]; metal ion binding [GO:0046872]; Domain features: DOMAIN 96-239; note="Radical_SAM"; evidence="ECO:0000259|Pfam:PF04055" Keywords: 4Fe-4S; Iron; Iron-sulfur; Metal-binding; S-adenosyl-L-methionine
	all2396	Q8YUF4	454	All2396 protein; Keywords:
	all4388	Q8YP14	493	All4388 protein; Cellular component: membrane [GO:0016020]; Associated terms: membrane [GO:0016020]; polysaccharide transmembrane transporter activity [GO:0015159]; Molecular function: polysaccharide transmembrane transporter activity [GO:0015159]; Domain features: DOMAIN 380-433; note="SLBB"; evidence="ECO:0000259|Pfam:PF10531" Keywords: Signal
	all5089	Q8YM51	478	Phosphoglucomutase/phosphomannomutase ; Biological process: carbohydrate metabolic process [GO:0005975]; Associated terms: intramolecular transferase activity, phosphotransferases [GO:0016868]; magnesium ion binding [GO:0000287]; carbohydrate metabolic process [GO:0005975]; Molecular function: intramolecular transferase activity, phosphotransferases [GO:0016868]; magnesium ion binding [GO:0000287]; Domain features: DOMAIN 8-141; note="PGM_PMM_I"; evidence="ECO:0000259|Pfam:PF02878"; DOMAIN 162-268; note="PGM_PMM_II"; evidence="ECO:0000259|Pfam:PF02879"; DOMAIN 277-382; note="PGM_PMM_III"; evidence="ECO:0000259|Pfam:PF02880"; DOMAIN 418-468; note="PGM_PMM_IV"; evidence="ECO:0000259|Pfam:PF00408" Keywords: Isomerase; Magnesium; Metal-binding; Protein families: Phosphohexose mutase family
	all5295*	Q8YLK3	334	All5295 protein; Associated terms: catalytic activity [GO:0003824]; coenzyme binding [GO:0050662]; Molecular function: catalytic activity [GO:0003824]; coenzyme binding [GO:0050662]; Domain features: DOMAIN 7-234; note="Epimerase"; evidence="ECO:0000259|Pfam:PF01370"
	all7222	Q8YKR9	348	All7222 protein; Domain features: DOMAIN 94-198; note="CbiA"; evidence="ECO:0000259|Pfam:PF01656" Keywords: Plasmid
	alr0658	Q8YZ29	461	UDP-glucose 6-dehydrogenase (EC 1.1.1.22) ; Biological process: polysaccharide biosynthetic process [GO:0000271]; D binding [GO:0051287]; UDP-glucose 6-dehydrogenase activity [GO:0003979]; polysaccharide biosynthetic process [GO:0000271]; Molecular function: NAD binding [GO:0051287]; UDP-glucose 6-dehydrogenase activity [GO:0003979]; Domain features: DOMAIN

				344-446; note="UDPG_MGDP_dh_C"; evidence="ECO:0000259|SMART:SM00984" Keywords: NAD; Oxidoreductase; Protein families: UDP-glucose/GDP-mannose dehydrogenase family
	alr0663*	Q8YZ24	632	Alr0663 protein ; Biological process: carbohydrate metabolic process [GO:0005975]; Associated terms: catalytic activity [GO:0003824]; carbohydrate metabolic process [GO:0005975]; Molecular function: catalytic activity [GO:0003824]; Domain features: DOMAIN 55-504; note="Aamy"; evidence="ECO:0000259|SMART:SM00642"
	alr0782	Q8YYR4	235	Ribulose-phosphate 3-epimerase (EC 5.1.3.1) ; Biological process: carbohydrate metabolic process [GO:0005975]; pentose-phosphate shunt [GO:0006098]; Associated terms: metal ion binding [GO:0046872]; ribulose-phosphate 3-epimerase activity [GO:0004750]; carbohydrate metabolic process [GO:0005975]; pentose-phosphate shunt [GO:0006098]; Molecular function: metal ion binding [GO:0046872]; ribulose-phosphate 3-epimerase activity [GO:0004750]; Keywords: Carbohydrate metabolism; Cobalt; Isomerase; Manganese; Metal-binding; Zinc; Protein families: Ribulose-phosphate 3-epimerase family
	alr2090	Q8YV91	602	Alr2090 protein; Domain features: DOMAIN 406-469; note="SLH"; evidence="ECO:0000259|PROSITE:PS51272"; DOMAIN 470-529; note="SLH"; evidence="ECO:0000259|PROSITE:PS51272"; DOMAIN 531-595; note="SLH"; evidence="ECO:0000259|PROSITE:PS51272"
	alr3338	Q8YRV4	449	Phosphoglycerate mutase; Associated terms: catalytic activity [GO:0003824]; Molecular function: catalytic activity [GO:0003824]; Keywords: Protein families: Phosphoglycerate mutase family
	alr3729	Q8YQT8	138	Alr3729 protein; Biological process: polyketide metabolic process [GO:0030638]; Associated terms: polyketide metabolic process [GO:0030638]
	alr4380*	Q8YP22	326	Delta-aminolevulinic acid dehydratase (EC 4.2.1.24) ; Biological process: porphyrin-containing compound biosynthetic process [GO:0006779]; Associated terms: metal ion binding [GO:0046872]; porphobilinogen synthase activity [GO:0004655]; porphyrin-containing compound biosynthetic process [GO:0006779]; Molecular function: metal ion binding [GO:0046872]; porphobilinogen synthase activity [GO:0004655]; Keywords: Lyase; Magnesium; Metal-binding; Porphyrin biosynthesis; Zinc; Protein families: ALAD family
	alr4566*	Q8YNJ9	384	NADH-dependent butanol dehydrogenase; Associated terms: metal ion binding [GO:0046872]; oxidoreductase activity [GO:0016491]; Molecular function: metal ion binding [GO:0046872]; oxidoreductase activity [GO:0016491]; Domain features: DOMAIN 9-362; note="Fe-ADH"; evidence="ECO:0000259|Pfam:PF00465"
	alr7200*	Q8YKU1	539	Alr7200 protein; Associated terms: ATP binding [GO:0005524]; Molecular function: ATP binding [GO:0005524]; Domain features: DOMAIN 279-408; note="AAA"; evidence="ECO:0000259|SMART:SM00382" Keywords: Plasmid
	ccmK*	Q8YYI1	114	Carbon dioxide concentrating mechanism protein; Subcellular location: Cell inner membrane {ECO:0000255|HAMAP-Rule:MF_01701}; Peripheral membrane protein {ECO:0000255|HAMAP-Rule:MF_01701}; Domain features: DOMAIN 3-81; note="BMC"; evidence="ECO:0000259|SMART:SM00877"
	cysA*	Q8Z0H0	338	Sulfate/thiosulfate import ATP-binding protein CysA (EC 7.3.2.3) (Sulfate-transporting ATPase); Function: Part of the ABC transporter complex CysAWTP involved in sulfate/thiosulfate

				import. Responsible for energy coupling to the transport system. {ECO:0000255|HAMAP-Rule:MF_01701}; Cellular component: ATP-binding cassette (ABC) transporter complex [GO:0043190]; Associated terms: ATP-binding cassette (ABC) transporter complex [GO:0043190]; ATP binding [GO:0005524]; ATPase activity [GO:0016887]; ATPase-coupled sulfate transmembrane transporter activity [GO:0015419]; ATPase-coupled thiosulfate transmembrane transporter activity [GO:0102025]; Molecular function: ATPase activity [GO:0016887]; ATPase-coupled sulfate transmembrane transporter activity [GO:0015419]; ATPase-coupled thiosulfate transmembrane transporter activity [GO:0102025]; ATP binding [GO:0005524]; Domain features: DOMAIN 3-233; note="ABC transporter"; evidence="ECO:0000255|HAMAP-Rule:MF_01701" Keywords: ATP-binding; Cell inner membrane; Cell membrane; Membrane; Nucleotide-binding; Sulfate transport; Translocase; Transport; Protein families: ABC transporter superfamily, Sulfate/tungstate importer (TC 3.A.1.6) family
Organo-nitrogen metabolism	all0666*	Q8YZ21	348	All0666 protein; Cross-reference (InterPro): DUF1822 (This entry includes a group of bacterial proteins, including EipB from Brucella. EipB is a periplasmic protein that functions as part of a system required for cell envelope homeostasis)
	all0667*	Q8YZ20	481	All0667 protein; Protein-protein interaction databases (String): Three gene neighborhood (all0666, tplA, alr0841)
	all2425	Q8YUC7	255	All2425 protein; Domain features: DOMAIN 128-243; note="Peptidase_M15_3"; evidence="ECO:0000259|Pfam:PF08291"
	all2500	Q8YU55	428	Carboxyl-terminal protease; Associated terms: serine-type peptidase activity [GO:0008236]; Molecular function: serine-type peptidase activity [GO:0008236]; Domain features: DOMAIN 106-190; note="PDZ"; evidence="ECO:0000259|PROSITE:PS50106" Keywords: Coiled coil; Hydrolase; Protease; Serine protease; Protein families: Peptidase S41A family
	all4737*	Q8YN33	223	All4737 protein; Associated terms: cofactor binding [GO:0048037]; Molecular function: cofactor binding [GO:0048037]; Family and domain databases (InterPro): FMN-binding split barrel, Pyridoxamine 5'-phosphate oxidase-related.
	all4999	Q8YMD5	597	N-acetylmuramoyl-L-alanine amidase ; Biological process: peptidoglycan catabolic process [GO:0009253]; Associated terms: N-acetylmuramoyl-L-alanine amidase activity [GO:0008745]; peptidoglycan catabolic process [GO:0009253]; Molecular function: N-acetylmuramoyl-L-alanine amidase activity [GO:0008745]; Domain features: DOMAIN 237-295; note="SH3b"; evidence="ECO:0000259|SMART:SM00287"; DOMAIN 478-590; note="MurNAc-LAA"; evidence="ECO:0000259|SMART:SM00646"
	all7011	Q8YLC4	323	All7011 protein; Associated terms: ATP binding [GO:0005524]; metal ion binding [GO:0046872]; Molecular function: ATP binding [GO:0005524]; metal ion binding [GO:0046872]; Domain features: DOMAIN 129-320; note="ATP-grasp"; evidence="ECO:0000259|PROSITE:PS50975" Keywords: ATP-binding; Nucleotide-binding; Plasmid
	alr0668*	Q8YZ19	198	Alr0668 protein; Isolated within the heterocyst fraction.[9]
	alr0669*	Q8YZ18	295	Alr0669 protein; Domain features: DOMAIN 26-76; note="PG_binding_1"; evidence="ECO:0000259|Pfam:PF01471"; Family and domain databases (InterPro): PGBD superfamily (This superfamily represents peptidoglycan binding domain (PGBD). PGBD may have a general peptidoglycan binding function. It has a core structure consisting of a closed, three-helical bundle with a

				left-handed twist. It is found at the N or C terminus of a variety of enzymes involved in bacterial cell wall degradation)
	alr2927*	Q8YT00	132	Alr2927 protein; Domain features: DOMAIN 48-112; note="PPC"; evidence="ECO:0000259|Pfam:PF04151"
	alr3301*	Q8YRZ1	277	Alr3301 protein; Keywords: Coiled coil; Associated to heterocyst differentiation,[10] and to nitrogen depravation.[11]
	alr3804*	Q8YQL7	383	Deoxyhypusine synthase-like protein (EC 2.5.-.-) ; Biological process: peptidyl-lysine modification to peptidyl-hypusine [GO:0008612]; Associated terms: transferase activity, transferring alkyl or aryl (other than methyl) groups [GO:0016765]; peptidyl-lysine modification to peptidyl-hypusine [GO:0008612]; Molecular function: transferase activity, transferring alkyl or aryl (other than methyl) groups [GO:0016765]; Keywords: Transferase; Protein families: Deoxyhypusine synthase family
	asl0662*	Q8YZ25	59	Asl0662 protein; Related to heterocyst and nitrogen starvation. [11]
	cynS	P58703	146	Cyanate hydratase (Cyanase) (EC 4.2.1.104) (Cyanate hydrolase) (Cyanate lyase); Function: Catalyzes the reaction of cyanate with bicarbonate to produce ammonia and carbon dioxide. {ECO:0000255|HAMAP-Rule:MF_00535}; Subcellular location: Cytoplasm {ECO:0000255|HAMAP-Rule:MF_00102}; Biological process: cyanate metabolic process [GO:0009439]; Associated terms: cyanate hydratase activity [GO:0008824]; DNA binding [GO:0003677]; cyanate metabolic process [GO:0009439]; Molecular function: cyanate hydratase activity [GO:0008824]; DNA binding [GO:0003677]; Keywords: Lyase; Protein families: Cyanase family
	dapB	Q8YU19	278	4-hydroxy-tetrahydrodipicolinate reductase (HTPA reductase) (EC 1.17.1.8); Function: Catalyzes the conversion of 4-hydroxy-tetrahydrodipicolinate (HTPA) to tetrahydrodipicolinate. {ECO:0000255|HAMAP-Rule:MF_00102}; Subcellular location: Cytoplasm {ECO:0000250|UniProtKB:P9WN39}; Biological process: diaminopimelate biosynthetic process [GO:0019877]; lysine biosynthetic process via diaminopimelate [GO:0009089]; Cellular component: cytoplasm [GO:0005737]; Associated terms: cytoplasm [GO:0005737]; 4-hydroxy-tetrahydrodipicolinate reductase [GO:0008839]; NAD binding [GO:0051287]; NADP binding [GO:0050661]; oxidoreductase activity, acting on CH or CH2 groups, NAD or NADP as acceptor [GO:0016726]; diaminopimelate biosynthetic process [GO:0019877]; lysine biosynthetic process via diaminopimelate [GO:0009089]; Molecular function: 4-hydroxy-tetrahydrodipicolinate reductase [GO:0008839]; NAD binding [GO:0051287]; NADP binding [GO:0050661]; oxidoreductase activity, acting on CH or CH2 groups, NAD or NADP as acceptor [GO:0016726]; Keywords: Amino-acid biosynthesis; Cytoplasm; Diaminopimelate biosynthesis; Lysine biosynthesis; NAD; NADP; Oxidoreductase; Protein families: DapB family
	glnA*	P00964	474	Glutamine synthetase (GS) (EC 6.3.1.2) (Glutamate--ammonia ligase) (Glutamine synthetase I beta) (GSI beta); Function: Involved in nitrogen metabolism via ammonium assimilation. Catalyzes the ATP-dependent biosynthesis of glutamine from glutamate and ammonia. {ECO:0000250|UniProtKB:P77961}; Biological process: glutamine biosynthetic process [GO:0006542]; heterocyst differentiation [GO:0043158]; nitrogen fixation [GO:0009399]; Cellular component: cytoplasm [GO:0005737]; Associated terms: cytoplasm [GO:0005737]; ATP binding [GO:0005524]; glutamate-ammonia ligase activity [GO:0004356]; metal ion binding [GO:0046872]; glutamine biosynthetic process [GO:0006542]; heterocyst differentiation [GO:0043158]; nitrogen fixation [GO:0009399]; Molecular function: ATP binding

				[GO:0005524]; glutamate-ammonia ligase activity [GO:0004356]; metal ion binding [GO:0046872]; Keywords: ATP-binding; Cytoplasm; Direct protein sequencing; Heterocyst; Ligase; Magnesium; Metal-binding; Nitrogen fixation; Nucleotide-binding; Phosphoprotein; Protein families: Glutamine synthetase family
	leuC	Q8YX02	467	3-isopropylmalate dehydratase large subunit (EC 4.2.1.33) (Alpha-IPM isomerase) (IPMI) (Isopropylmalate isomerase); Function: Catalyzes the isomerization between 2-isopropylmalate and 3-isopropylmalate, via the formation of 2-isopropylmaleate. {ECO:0000255|HAMAP-Rule:MF_01026}; Subcellular location: Cytoplasm {ECO:0000255|HAMAP-Rule:MF_00451}; Biological process: leucine biosynthetic process [GO:0009098]; Associated terms: 3-isopropylmalate dehydratase activity [GO:0003861]; 4 iron, 4 sulfur cluster binding [GO:0051539]; metal ion binding [GO:0046872]; leucine biosynthetic process [GO:0009098]; Molecular function: 3-isopropylmalate dehydratase activity [GO:0003861]; 4 iron, 4 sulfur cluster binding [GO:0051539]; metal ion binding [GO:0046872]; Keywords: 4Fe-4S; Amino-acid biosynthesis; Branched-chain amino acid biosynthesis; Iron; Iron-sulfur; Leucine biosynthesis; Lyase; Metal-binding; Protein families: Aconitase/IPM isomerase family, LeuC type 1 subfamily
	ndk	Q8YRP2	149	Nucleoside diphosphate kinase (NDK) (NDP kinase) (EC 2.7.4.6) (Nucleoside-2-P kinase); Function: Major role in the synthesis of nucleoside triphosphates other than ATP. The ATP gamma phosphate is transferred to the NDP beta phosphate via a ping-pong mechanism, using a phosphorylated active-site intermediate. {ECO:0000255|HAMAP-Rule:MF_00451}; Subcellular location: Cytoplasm {ECO:0000255|HAMAP-Rule:MF_00181}; Biological process: CTP biosynthetic process [GO:0006241]; GTP biosynthetic process [GO:0006183]; UTP biosynthetic process [GO:0006228]; Cellular component: cytoplasm [GO:0005737]; Associated terms: cytoplasm [GO:0005737]; ATP binding [GO:0005524]; metal ion binding [GO:0046872]; nucleoside diphosphate kinase activity [GO:0004550]; CTP biosynthetic process [GO:0006241]; GTP biosynthetic process [GO:0006183]; UTP biosynthetic process [GO:0006228]; Molecular function: ATP binding [GO:0005524]; metal ion binding [GO:0046872]; nucleoside diphosphate kinase activity [GO:0004550]; Keywords: ATP-binding; Cytoplasm; Kinase; Magnesium; Metal-binding; Nucleotide metabolism; Nucleotide-binding; Phosphoprotein; Transferase; Protein families: NDK family
	pepA	Q8Z064	491	Probable cytosol aminopeptidase (EC 3.4.11.1) (Leucine aminopeptidase) (LAP) (EC 3.4.11.10) (Leucyl aminopeptidase); Function: Presumably involved in the processing and regular turnover of intracellular proteins. Catalyzes the removal of unsubstituted N-terminal amino acids from various peptides. {ECO:0000255|HAMAP-Rule:MF_00181}; Cellular component: cytoplasm [GO:0005737]; Associated terms: cytoplasm [GO:0005737]; aminopeptidase activity [GO:0004177]; manganese ion binding [GO:0030145]; metalloexopeptidase activity [GO:0008235]; Molecular function: aminopeptidase activity [GO:0004177]; manganese ion binding [GO:0030145]; metalloexopeptidase activity [GO:0008235]; Keywords: Aminopeptidase; Cytoplasm; Hydrolase; Manganese; Metal-binding; Protease; Protein families: Peptidase M17 family
Nucleic acid metabolism	alr4692*	Q8YN78	155	Transcriptional regulator; Associated terms: DNA binding [GO:0003677]; DNA-binding transcription factor activity [GO:0003700]; Molecular function: DNA binding [GO:0003677]; DNA-binding transcription factor activity [GO:0003700]; Domain features: DOMAIN 20-152; note="HTH marR-type";

				evidence="ECO:0000259|PROSITE:PS50995" Keywords: DNA-binding; Transcription; Transcription regulation
	alr7083*	Q8YL52	372	Chromosome partitioning protein, ParB family; Associated terms: DNA binding [GO:0003677]; Molecular function: DNA binding [GO:0003677]; Domain features: DOMAIN 61-147; note="ParB"; evidence="ECO:0000259|SMART:SM00470" Keywords: Coiled coil; Plasmid; Protein families: ParB family
	alr7311*	Q8YKI6	404	Alr7311 protein; Subcellular location: Cytoplasm {ECO:0000255|HAMAP-Rule:MF_00054}; Biological process: DNA-templated transcription, initiation [GO:0006352]; Associated terms: DNA-binding transcription factor activity [GO:0003700]; DNA-templated transcription, initiation [GO:0006352]; Molecular function: DNA-binding transcription factor activity [GO:0003700]; Domain features: DOMAIN 308-351; note="Sigma70_r4"; evidence="ECO:0000259|Pfam:PF04545" Keywords: Plasmid
	fusA	Q8YP62	692	Elongation factor G (EF-G); Function: Catalyzes the GTP-dependent ribosomal translocation step during translation elongation. During this step, the ribosome changes from the pre-translocational (PRE) to the post-translocational (POST) state as the newly formed A-site-bound peptidyl-tRNA and P-site-bound deacylated tRNA move to the P and E sites, respectively. Catalyzes the coordinated movement of the two tRNA molecules, the mRNA and conformational changes in the ribosome. {ECO:0000255|HAMAP-Rule:MF_00054}; Subcellular location: Cytoplasm {ECO:0000256|HAMAP-Rule:MF_00839}; Cellular component: cytoplasm [GO:0005737]; Associated terms: cytoplasm [GO:0005737]; GTP binding [GO:0005525]; GTPase activity [GO:0003924]; translation elongation factor activity [GO:0003746]; Molecular function: GTPase activity [GO:0003924]; GTP binding [GO:0005525]; translation elongation factor activity [GO:0003746]; Domain features: DOMAIN 8-282; note="tr-type G" Keywords: Cytoplasm; Elongation factor; GTP-binding; Nucleotide-binding; Protein biosynthesis; Protein families: TRAFAC class translation factor GTPase superfamily, Classic translation factor GTPase family, EF-G/EF-2 subfamily
	hpf	Q8YSA5	213	Ribosome hibernation promoting factor (HPF); Function: Required for dimerization of active 70S ribosomes into 100S ribosomes in stationary phase; 100S ribosomes are translationally inactive and sometimes present during exponential growth. {ECO:0000256|HAMAP-Rule:MF_00839}; Protein L1 is also a translational repressor protein, it controls the translation of the L11 operon by binding to its mRNA. {ECO:0000255|HAMAP-Rule:MF_01318}; ; Biological process: primary metabolic process [GO:0044238]; regulation of translation [GO:0006417]; Cellular component: cytoplasm [GO:0005737]; Associated terms: cytoplasm [GO:0005737]; primary metabolic process [GO:0044238]; regulation of translation [GO:0006417]; Domain features: DOMAIN 130-184; note="Ribosom_S30AE_C"; evidence="ECO:0000259|Pfam:PF16321" Keywords: Coiled coil; Cytoplasm; Translation regulation; Protein families: HPF/YfiA ribosome-associated protein family, Long HPF subfamily
	rpl1	Q8YLJ7	238	50S ribosomal protein L1; Function: Binds directly to 23S rRNA. The L1 stalk is quite mobile in the ribosome, and is involved in E site tRNA release. {ECO:0000255|HAMAP-Rule:MF_01318}; Biological process: regulation of translation [GO:0006417]; translation [GO:0006412]; Cellular component: large ribosomal subunit [GO:0015934]; Associated terms: large ribosomal subunit [GO:0015934]; rRNA binding [GO:0019843]; structural constituent of ribosome [GO:0003735]; tRNA binding [GO:0000049]; regulation of translation [GO:0006417]; translation

				[GO:0006412]; Molecular function: rRNA binding [GO:0019843]; structural constituent of ribosome [GO:0003735]; tRNA binding [GO:0000049]; Keywords: RNA-binding; Repressor; Ribonucleoprotein; Ribosomal protein; Translation regulation; rRNA-binding; tRNA-binding; Protein families: Universal ribosomal protein uL1 family
	rplN	Q8YPI9	122	50S ribosomal protein L14; Function: Binds to 23S rRNA. Forms part of two intersubunit bridges in the 70S ribosome. {ECO:0000255|HAMAP-Rule:MF_01367}; Biological process: translation [GO:0006412]; Cellular component: large ribosomal subunit [GO:0015934]; Associated terms: large ribosomal subunit [GO:0015934]; rRNA binding [GO:0019843]; structural constituent of ribosome [GO:0003735]; translation [GO:0006412]; Molecular function: rRNA binding [GO:0019843]; structural constituent of ribosome [GO:0003735]; Keywords: RNA-binding; Ribonucleoprotein; Ribosomal protein; rRNA-binding; Protein families: Universal ribosomal protein uL14 family
	rpoB	P22703	1131	DNA-directed RNA polymerase subunit beta (RNAP subunit beta) (EC 2.7.7.6) (RNA polymerase subunit beta) (Transcriptase subunit beta); Function: DNA-dependent RNA polymerase catalyzes the transcription of DNA into RNA using the four ribonucleoside triphosphates as substrates. {ECO:0000255|HAMAP-Rule:MF_01321}; Biological process: transcription, DNA-templated [GO:0006351]; Associated terms: DNA binding [GO:0003677]; DNA-directed 5'-3' RNA polymerase activity [GO:0003899]; ribonucleoside binding [GO:0032549]; transcription, DNA-templated [GO:0006351]; Molecular function: DNA binding [GO:0003677]; DNA-directed 5'-3' RNA polymerase activity [GO:0003899]; ribonucleoside binding [GO:0032549]; Keywords: DNA-directed RNA polymerase; Nucleotidyltransferase; Transcription; Transferase; Protein families: RNA polymerase beta chain family
	rpoC2	P22705	1355	DNA-directed RNA polymerase subunit beta' (RNAP subunit beta') (EC 2.7.7.6) (RNA polymerase subunit beta') (Transcriptase subunit beta'); Function: DNA-dependent RNA polymerase catalyzes the transcription of DNA into RNA using the four ribonucleoside triphosphates as substrates. {ECO:0000255|HAMAP-Rule:MF_01324}; With S5 and S12 plays an important role in translational accuracy. {ECO:0000255|HAMAP-Rule:MF_01306}; ; Biological process: transcription, DNA-templated [GO:0006351]; Associated terms: DNA binding [GO:0003677]; DNA-directed 5'-3' RNA polymerase activity [GO:0003899]; zinc ion binding [GO:0008270]; transcription, DNA-templated [GO:0006351]; Molecular function: DNA binding [GO:0003677]; DNA-directed 5'-3' RNA polymerase activity [GO:0003899]; zinc ion binding [GO:0008270]; Keywords: DNA-directed RNA polymerase; Metal-binding; Nucleotidyltransferase; Transcription; Transferase; Zinc; Protein families: RNA polymerase beta' chain family, RpoC2 subfamily
	rpsD	Q8YTI0	202	30S ribosomal protein S4; Function: One of the primary rRNA binding proteins, it binds directly to 16S rRNA where it nucleates assembly of the body of the 30S subunit. {ECO:0000255|HAMAP-Rule:MF_01306}; Located at the back of the 30S subunit body where it stabilizes the conformation of the head with respect to the body. {ECO:0000255|HAMAP-Rule:MF_01307}; ; Biological process: translation [GO:0006412]; Cellular component: small ribosomal subunit [GO:0015935]; Associated terms: small ribosomal subunit [GO:0015935]; rRNA binding [GO:0019843]; structural constituent of ribosome [GO:0003735]; translation [GO:0006412]; Molecular function: rRNA binding [GO:0019843];

				structural constituent of ribosome [GO:0003735]; Domain features: DOMAIN 90-152; note="S4 RNA-binding"; evidence="ECO:0000255|HAMAP-Rule:MF_01306" Keywords: RNA-binding; Ribonucleoprotein; Ribosomal protein; rRNA-binding; Protein families: Universal ribosomal protein uS4 family
	rpsE	Q8YPJ5	174	30S ribosomal protein S5; Function: With S4 and S12 plays an important role in translational accuracy. {ECO:0000255|HAMAP-Rule:MF_01307}; Biological process: translation [GO:0006412]; Cellular component: small ribosomal subunit [GO:0015935]; Associated terms: small ribosomal subunit [GO:0015935]; rRNA binding [GO:0019843]; structural constituent of ribosome [GO:0003735]; translation [GO:0006412]; Molecular function: rRNA binding [GO:0019843]; structural constituent of ribosome [GO:0003735]; Domain features: DOMAIN 18-81; note="S5 DRBM"; evidence="ECO:0000255|HAMAP-Rule:MF_01307" Keywords: RNA-binding; Ribonucleoprotein; Ribosomal protein; rRNA-binding; Protein families: Universal ribosomal protein uS5 family
	rpsG	Q8YP61	156	30S ribosomal protein S7; Function: One of the primary rRNA binding proteins, it binds directly to 16S rRNA where it nucleates assembly of the head domain of the 30S subunit. Is located at the subunit interface close to the decoding center, probably blocks exit of the E-site tRNA. {ECO:0000255|HAMAP-Rule:MF_00480; Biological process: translation [GO:0006412]; Cellular component: small ribosomal subunit [GO:0015935]; Associated terms: small ribosomal subunit [GO:0015935]; rRNA binding [GO:0019843]; structural constituent of ribosome [GO:0003735]; tRNA binding [GO:0000049]; translation [GO:0006412]; Molecular function: rRNA binding [GO:0019843]; structural constituent of ribosome [GO:0003735]; tRNA binding [GO:0000049]; Keywords: RNA-binding; Ribonucleoprotein; Ribosomal protein; rRNA-binding; tRNA-binding; Protein families: Universal ribosomal protein uS7 family
	rpsN	Q8YQ66	100	30S ribosomal protein S14; Function: Binds 16S rRNA, required for the assembly of 30S particles and may also be responsible for determining the conformation of the 16S rRNA at the A site. {ECO:0000255|HAMAP-Rule:MF_00537}; Probably participates in protein translocation into and across both the cytoplasmic and thylakoid membranes in cyanobacterial cells. {ECO:0000255|HAMAP-Rule:MF_01382}; Subcellular location: Cell inner membrane {ECO:0000255|HAMAP-Rule:MF_01382}; Peripheral membrane protein {ECO:0000255|HAMAP-Rule:MF_01382}; Cytoplasmic side {ECO:0000255|HAMAP-Rule:MF_01382}. Cellular thylakoid membrane {ECO:0000255|HAMAP-Rule:MF_01382}; Peripheral membrane protein {ECO:0000255|HAMAP-Rule:MF_01382}; Cytoplasmic side {ECO:0000255|HAMAP-Rule:MF_01382}. Cytoplasm {ECO:0000255|HAMAP-Rule:MF_01382}; Biological process: translation [GO:0006412]; Cellular component: ribosome [GO:0005840]; Associated terms: ribosome [GO:0005840]; rRNA binding [GO:0019843]; structural constituent of ribosome [GO:0003735]; translation [GO:0006412]; Molecular function: rRNA binding [GO:0019843]; structural constituent of ribosome [GO:0003735]; Keywords: RNA-binding; Ribonucleoprotein; Ribosomal protein; rRNA-binding; Protein families: Universal ribosomal protein uS14 family
	secA	Q8YMS8	930	Protein translocase subunit SecA; Function: Part of the Sec protein translocase complex. Interacts with the SecYEG preprotein conducting channel. Has a central role in coupling the hydrolysis of ATP to the transfer of proteins into and across the cell membrane,

				serving as an ATP-driven molecular motor driving the stepwise translocation of polypeptide chains across the membrane. {ECO:0000255|HAMAP-Rule:MF_01382}; Biological process: intracellular protein transmembrane transport [GO:0065002]; protein import [GO:0017038]; protein targeting [GO:0006605]; Cellular component: cytoplasm [GO:0005737]; plasma membrane [GO:0005886]; thylakoid membrane [GO:0042651]; Associated terms: cytoplasm [GO:0005737]; plasma membrane [GO:0005886]; thylakoid membrane [GO:0042651]; ATP binding [GO:0005524]; intracellular protein transmembrane transport [GO:0065002]; protein import [GO:0017038]; protein targeting [GO:0006605]; Molecular function: ATP binding [GO:0005524]; Keywords: ATP-binding; Cell inner membrane; Cell membrane; Cytoplasm; Membrane; Nucleotide-binding; Protein transport; Thylakoid; Translocation; Transport; Protein families: SecA family
Photosynthesis	all7255	Q8YKN8	499	Zeta-carotene desaturase; Transmembrane; Biological process: carotenoid biosynthetic process [GO:0016117]; Associated terms: oxidoreductase activity [GO:0016491]; carotenoid biosynthetic process [GO:0016117]; Molecular function: oxidoreductase activity [GO:0016491]; Domain features: DOMAIN 13-474; note="Amino_oxidase"; evidence="ECO:0000259|Pfam:PF01593" Keywords: Carotenoid biosynthesis; Oxidoreductase; Plasmid; Protein families: Carotenoid/retinoid oxidoreductase family
	all7348*	Q8YKF0	460	All7348 protein; Subcellular location: Cellular thylakoid membrane {ECO:0000250}; Peripheral membrane protein {ECO:0000250}; Cytoplasmic side {ECO:0000250}. Note=Anchors the phycobilisome perpendicularly to the cytoplasmic surface of the thylakoid membrane. {ECO:0000250}; Cellular component: integral component of membrane [GO:0016021]; Associated terms: integral component of membrane [GO:0016021]; 2 iron, 2 sulfur cluster binding [GO:0051537]; chlorophyllide a oxygenase [overall] activity [GO:0010277]; Molecular function: 2 iron, 2 sulfur cluster binding [GO:0051537]; chlorophyllide a oxygenase [overall] activity [GO:0010277]; Domain features: DOMAIN 11-122; note="Rieske"; evidence="ECO:0000259|PROSITE:PS51296" Keywords: Membrane; Plasmid; Transmembrane; Transmembrane helix
	apcE*	P80559	1132	Phycobiliprotein ApcE (Anchor polypeptide) (PBS-anchor protein) (Phycobilisome linker polypeptide); Function: This protein is postulated to act both as terminal energy acceptor (by its phycobilin-like domains) and as a linker polypeptide (by its repeats and arms) that stabilizes the phycobilisome core architecture. Has intrinsic bilin lyase activity (By similarity). {ECO:0000250}; Linker polypeptides determine the state of aggregation and the location of the disk-shaped phycobiliprotein units within the phycobilisome and modulate their spectroscopic properties in order to mediate a directed and optimal energy transfer. {ECO:0000250}; Subcellular location: Cellular thylakoid membrane {ECO:0000250}; Peripheral membrane protein {ECO:0000250}; Cytoplasmic side {ECO:0000250}; Biological process: oxidation-reduction process [GO:0055114]; photosynthesis [GO:0015979]; protein-chromophore linkage [GO:0018298]; Cellular component: phycobilisome [GO:0030089]; Associated terms: phycobilisome [GO:0030089]; lyase activity [GO:0016829]; oxidation-reduction process [GO:0055114]; photosynthesis [GO:0015979]; protein-chromophore linkage [GO:0018298]; Molecular function: lyase activity [GO:0016829]; Domain features: DOMAIN 253-433; note="PBS-linker 1"; evidence="ECO:0000255|PROSITE-ProRule:PRU00775"; DOMAIN 514-692; note="PBS-linker 2"; evidence="ECO:0000255|PROSITE-ProRule:PRU00775";

				DOMAIN 709-887; note="PBS-linker 3"; evidence="ECO:0000255|PROSITE-ProRule:PRU00775"; DOMAIN 940-1121; note="PBS-linker 4"; evidence="ECO:0000255|PROSITE-ProRule:PRU00775" Keywords: 3D-structure; Bile pigment; Chromophore; Direct protein sequencing; Electron transport; Lyase; Membrane; Photosynthesis; Phycobilisome; Repeat; Thylakoid; Transport; Protein families: Phycobilisome linker protein family
	cpcG3	P29988	237	Phycobilisome rod-core linker polypeptide CpcG3 (L-RC 27.2); Function: Rod-core linker protein required for attachment of phycocyanin to allophycocyanin in cores of phycobilisomes. {ECO:0000250}; Subcellular location: Cellular thylakoid membrane {ECO:0000255|HAMAP-Rule:MF_01351}; Peripheral membrane protein {ECO:0000255|HAMAP-Rule:MF_01351}; Biological process: photosynthesis [GO:0015979]; Cellular component: phycobilisome [GO:0030089]; Associated terms: phycobilisome [GO:0030089]; photosynthesis [GO:0015979]; Domain features: DOMAIN 11-191; note="PBS-linker"; evidence="ECO:0000255|PROSITE-ProRule:PRU00775" Keywords: Membrane; Photosynthesis; Phycobilisome; Thylakoid; Protein families: Phycobilisome linker protein family
	ndhI	Q9WWM6	194	NAD(P)H-quinone oxidoreductase subunit I (EC 7.1.1.-) (NAD(P)H dehydrogenase I subunit I) (NDH-1 subunit I) (NDH-I); Function: NDH-1 shuttles electrons from an unknown electron donor, via FMN and iron-sulfur (Fe-S) centers, to quinones in the respiratory and/or the photosynthetic chain. The immediate electron acceptor for the enzyme in this species is believed to be plastoquinone. Couples the redox reaction to proton translocation, and thus conserves the redox energy in a proton gradient. {ECO:0000255|HAMAP-Rule:MF_01351}; Subcellular location: Cellular thylakoid membrane {ECO:0000250}; Peripheral membrane protein {ECO:0000250}; Cytoplasmic side {ECO:0000250}. Note=Forms the periphery of the phycobilisome rod. {ECO:0000250}; Biological process: photosynthesis, light reaction [GO:0019684]; Cellular component: thylakoid membrane [GO:0042651]; Associated terms: thylakoid membrane [GO:0042651]; 4 iron, 4 sulfur cluster binding [GO:0051539]; iron ion binding [GO:0005506]; NADH dehydrogenase (ubiquinone) activity [GO:0008137]; quinone binding [GO:0048038]; photosynthesis, light reaction [GO:0019684]; Molecular function: 4 iron, 4 sulfur cluster binding [GO:0051539]; iron ion binding [GO:0005506]; NADH dehydrogenase (ubiquinone) activity [GO:0008137]; quinone binding [GO:0048038]; Domain features: DOMAIN 55-84; note="4Fe-4S ferredoxin-type 1"; evidence="ECO:0000255|HAMAP-Rule:MF_01351"; DOMAIN 95-124; note="4Fe-4S ferredoxin-type 2"; evidence="ECO:0000255|HAMAP-Rule:MF_01351" Keywords: 4Fe-4S; Iron; Iron-sulfur; Membrane; Metal-binding; NAD; NADP; Plastoquinone; Quinone; Repeat; Thylakoid; Translocase; Protein families: Complex I 23 kDa subunit family
	pecA*	P35796	162	Phycoerythrocyanin alpha chain; Function: Light-harvesting photosynthetic bile pigment-protein from the phycobiliprotein complex; Subcellular location: Cellular thylakoid membrane {ECO:0000250}; Peripheral membrane protein {ECO:0000250}; Cytoplasmic side {ECO:0000250}. Note=Forms the periphery of the phycobilisome rod. {ECO:0000250}; Biological process: oxidation-reduction process [GO:0055114]; photosynthesis [GO:0015979]; protein-chromophore linkage [GO:0018298]; Cellular component: phycobilisome [GO:0030089]; Associated terms: phycobilisome [GO:0030089]; oxidation-reduction process

				[GO:0055114]; photosynthesis [GO:0015979]; protein-chromophore linkage [GO:0018298]; Keywords: Bile pigment; Chromophore; Electron transport; Membrane; Photosynthesis; Phycobilisome; Thylakoid; Transport; Protein families: Phycobiliprotein family
	pecB	P35797	172	Phycoerythrocyanin subunit beta; Function: Light-harvesting photosynthetic bile pigment-protein from the phycobiliprotein complex; Subcellular location: Cellular thylakoid membrane; Peripheral membrane protein; Cytoplasmic side. Note=This protein occurs in the rod, it is associated with phycoerythrocyanin; Biological process: oxidation-reduction process [GO:0055114]; photosynthesis [GO:0015979]; protein-chromophore linkage [GO:0018298]; Cellular component: phycobilisome [GO:0030089]; Associated terms: phycobilisome [GO:0030089]; oxidation-reduction process [GO:0055114]; photosynthesis [GO:0015979]; protein-chromophore linkage [GO:0018298]; Keywords: Bile pigment; Chromophore; Electron transport; Membrane; Photosynthesis; Phycobilisome; Thylakoid; Transport; Protein families: Phycobiliprotein family
	pecC	P31329	278	Phycobilisome 34.5 kDa linker polypeptide, phycoerythrocyanin-associated, rod; Function: Rod linker protein, associated with phycoerythrocyanin. Linker polypeptides determine the state of aggregation and the location of the disk-shaped phycobiliprotein units within the phycobilisome and modulate their spectroscopic properties in order to mediate a directed and optimal energy transfer; Subcellular location: Cellular thylakoid membrane {ECO:0000250}; Multi-pass membrane protein {ECO:0000250}; Transmembrane; Biological process: photosynthesis [GO:0015979]; Cellular component: phycobilisome [GO:0030089]; Associated terms: phycobilisome [GO:0030089]; photosynthesis [GO:0015979]; Domain features: DOMAIN 2-178; note="PBS-linker"; evidence="ECO:0000255|PROSITE-ProRule:PRU00775"; DOMAIN 226-278; note="CpcD-like"; evidence="ECO:0000255|PROSITE-ProRule:PRU00771" Keywords: Direct protein sequencing; Membrane; Photosynthesis; Phycobilisome; Thylakoid; Protein families: Phycobilisome linker protein family
	alr1129	Q8YXT2	325	Alr1129 protein; Domain features: DOMAIN 5-76; note="PRC"; evidence="ECO:0000259|Pfam:PF05239"; DOMAIN 85-163; note="PRC"; evidence="ECO:0000259|Pfam:PF05239"
	psaL	P58577	172	Photosystem I reaction center subunit XI (PSI subunit V) (PSI-L); Subcellular location: Cellular thylakoid membrane {ECO:0000255|HAMAP-Rule:MF_01495}; Multi-pass membrane protein {ECO:0000255|HAMAP-Rule:MF_01495}; Transmembrane; Biological process: photosynthesis [GO:0015979]; Cellular component: integral component of membrane [GO:0016021]; photosystem I reaction center [GO:0009538]; thylakoid membrane [GO:0042651]; Associated terms: integral component of membrane [GO:0016021]; photosystem I reaction center [GO:0009538]; thylakoid membrane [GO:0042651]; photosynthesis [GO:0015979]; Keywords: 3D-structure; Membrane; Photosynthesis; Photosystem I; Thylakoid; Transmembrane; Transmembrane helix; Protein families: PsaL family
	psbB	P20093	509	Photosystem II CP47 reaction center protein (PSII 47 kDa protein) (Protein CP-47); Function: One of the components of the core complex of photosystem II (PSII). It binds chlorophyll and helps catalyze the primary light-induced photochemical processes of PSII. PSII is a light-driven water: plastoquinone oxidoreductase, using light energy to abstract electrons from H(2)O, generating

				O(2) and a proton gradient subsequently used for ATP formation. {ECO:0000255|HAMAP-Rule:MF_01495}; Biological process: photosynthetic electron transport in photosystem II [GO:0009772]; protein-chromophore linkage [GO:0018298]; Cellular component: integral component of membrane [GO:0016021]; photosystem II [GO:0009523]; thylakoid membrane [GO:0042651]; Associated terms: integral component of membrane [GO:0016021]; photosystem II [GO:0009523]; thylakoid membrane [GO:0042651]; chlorophyll binding [GO:0016168]; electron transporter, transferring electrons within the cyclic electron transport pathway of photosynthesis activity [GO:0045156]; photosynthetic electron transport in photosystem II [GO:0009772]; protein-chromophore linkage [GO:0018298]; Molecular function: chlorophyll binding [GO:0016168]; electron transporter, transferring electrons within the cyclic electron transport pathway of photosynthesis activity [GO:0045156]; Keywords: Chlorophyll; Chromophore; Membrane; Photosynthesis; Photosystem II; Thylakoid; Transmembrane; Transmembrane helix; Protein families: PsbB/PsbC family, PsbB subfamily
Signal domine	all0050*	Q8Z0P0	345	All0050 protein; Keywords: Signal
	all1755	Q8YW61	132	All1755 protein; Keywords: Signal
	all1783*	Q8YW33	201	All1783 protein; Keywords: Signal
	all4130	Q8YPR2	301	Binding protein of ABC transporter component; Domain features: DOMAIN 36-269; note="PBPb"; evidence="ECO:0000259|SMART:SM00062" Keywords: Signal
	alr0490	Q8YZH0	225	Alr0490 protein; Keywords: Signal
	alr1548	Q8YWQ6	312	Alr1548 protein; Domain features: DOMAIN 214-281; note="TPR_REGION"; evidence="ECO:0000259|PROSITE:PS50293" Keywords: Coiled coil; Signal
	alr3932	Q8YQA1	231	Alr3932 protein; Keywords: Signal
	alr7326	Q8YKH2	173	Alr7326 protein; Keywords: Plasmid; Signal
	alr7345	Q8YKF3	303	Alr7345 protein; Associated terms: methyltransferase activity [GO:0008168]; Molecular function: methyltransferase activity [GO:0008168]; Domain features: DOMAIN 142-201; note="Methyltransf_11"; evidence="ECO:0000259|Pfam:PF08241" Keywords: Plasmid; Signal
	all2086	Q8YV95	564	All2086 protein
	all2262	Q8YUS2	142	All2262 protein; Keywords: Coiled coil
	all2480	Q8YU74	283	Beta-lactamase; Associated terms: penicillin binding [GO:0008658]; Molecular function: penicillin binding [GO:0008658]; Domain features: DOMAIN 64-274; note="Transpeptidase"; evidence="ECO:0000259|Pfam:PF00905" Keywords: 3D-structure
	all2965*	Q8YSW4	162	All2965 protein
Non-clustered proteins	alr0436	Q8YZM1	470	Alr0436 protein
	alr4359	Q8YP41	418	Alr4359 protein; Domain features: DOMAIN 43-215; note="VWFA"; evidence="ECO:0000259|PROSITE:PS50234"
	alr7233	Q8YKR0	341	Alr7233 protein; Keywords: Plasmid
	alr7300	Q8YKJ5	269	Alr7300 protein; Keywords: Plasmid
	alr7312*	Q8YKI5	383	Alr7312 protein; Keywords: Plasmid

Figure 1B specific information:

FTIR peaks specific information

The FTIR spectra present the characteristic bands of PS: C–H stretching vibration (3070 cm^{-1} and 3028 cm^{-1}), C–H_2 stretching vibration (2924 cm^{-1} and 2854 cm^{-1}) and stretching (1646 cm^{-1}, 1556 cm^{-1}, 1456 cm^{-1}) of the benzene ring;[12] G7: N-H stretching of primary and secondary amine groups stretching (3408 cm^{-1} and 3292 cm^{-1}), C-H stretching (2934 cm^{-1} and 2866 cm^{-1}), C = O stretching of primary amide (1650 cm^{-1}) H-C-H asymmetric, N-H bending/C-N stretching secondary amide (1562 cm^{-1}), H-C-H scissor (1452 cm^{-1}), H-C-H asymmetric (1368 cm^{-1}) and C–O stretching vibration (1060 cm^{-1}).[13] The suspension containing both nanopolymers shows the characteristic peaks from each one: from PS the C-H stretching vibration (3086 cm^{-1} and 3031 cm^{-1}), C–H_2 stretching vibration (2924 cm^{-1} and 2856 cm^{-1}) and stretching of the benzene ring (1646 cm^{-1}, 1556 cm^{-1}, 1456 cm^{-1}) and from the G7, N-H stretching of primary and secondary amine groups stretching (3408 cm^{-1} and 3288 cm^{-1}), C–H_2 stretching vibration shared with PS, C = O stretching of primary amide, N-H bending/C-N stretching secondary amide and H-C-H scissor (which three peaks overlapped with those corresponding to the benzene ring), H-C-H asymmetric (1368 cm^{-1}) and C–O stretching vibration (1030 cm^{-1}). Thus, the chemical surface of the aggregates rather than being homogeneous appear to present an irregular surface presenting region with characteristics corresponding to G7 and others corresponding to PS-NPs, which surface net charge prevails over the G7 positive charge due to its higher concentration and dimensions.

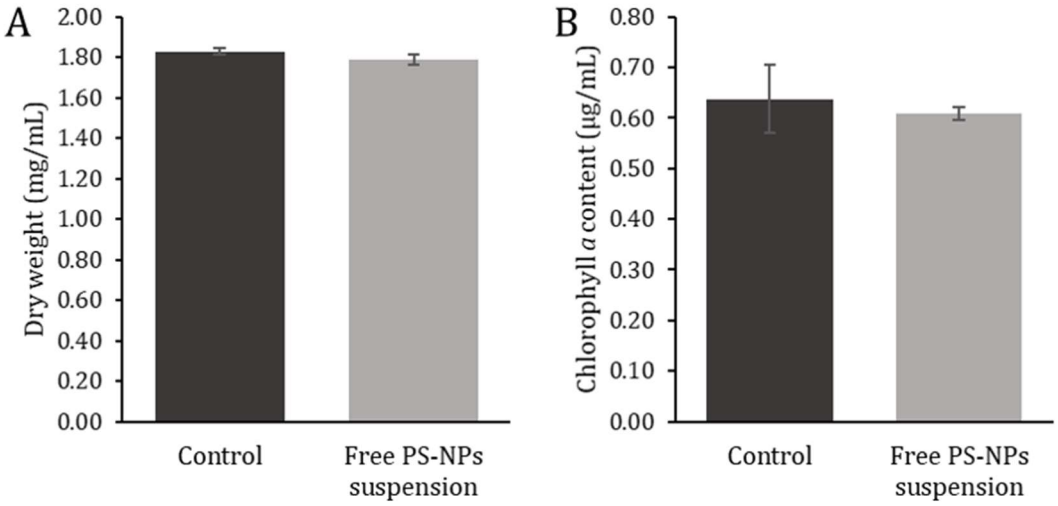

Figure S1: Effect of free PS-NPs suspension on *Anabaena* sp. PCC7120 growth for 72 h at ~ 65 µmol photons m^2 s^{-1} on a rotary shaker in AA/8 + N in terms of growth inhibition (A) and chlorophyll *a* content (B). Different letters indicate treatments that are significantly different (Tukey's HSD, $p < 0.05$).

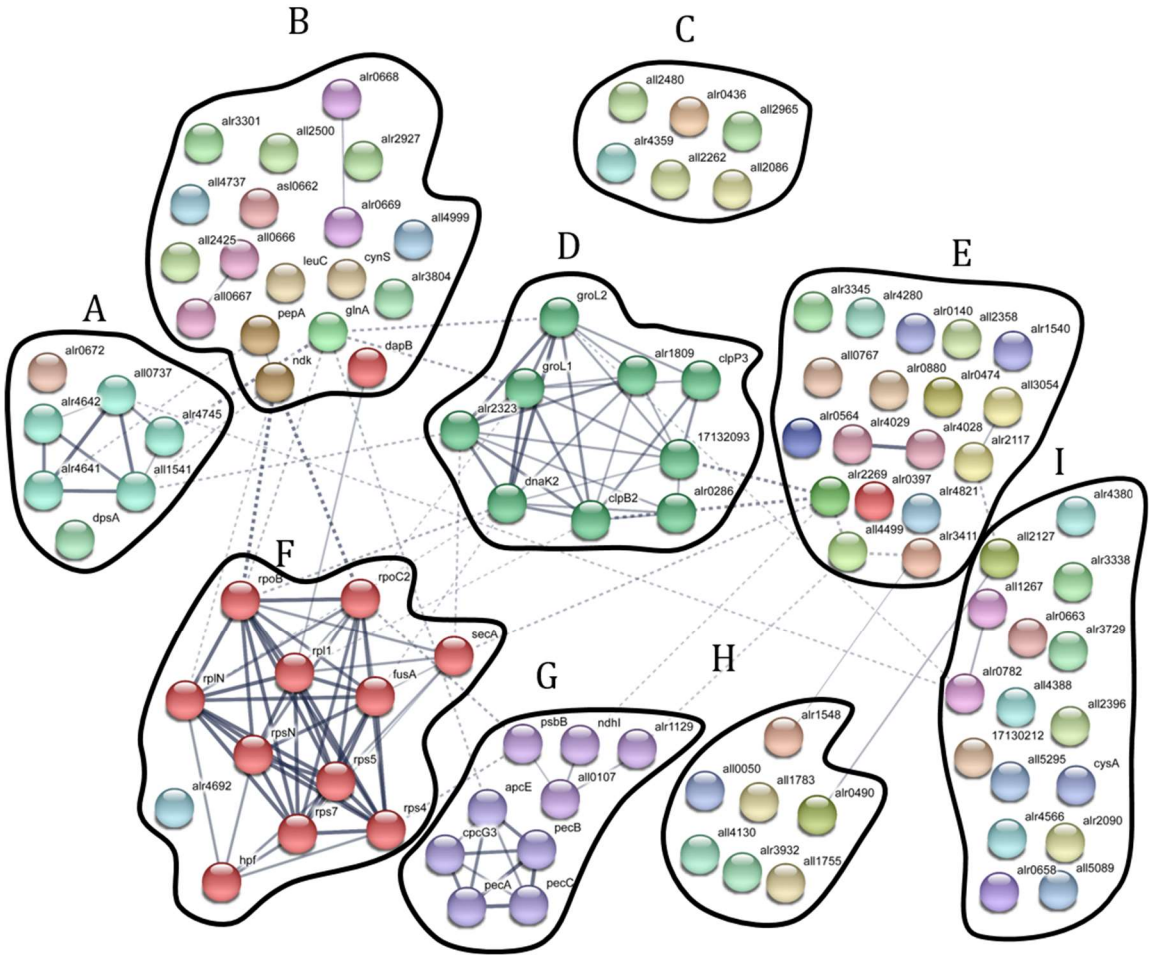

Figure S2: Protein-protein interaction network from STRING software clustered by MCL algorithm (inflation parameter = 3) complemented with Uniprot protein information. Proteins were allocated into 9 categories: Oxidative stress (A), Organo-nitrogen metabolism (B), No clustered proteins (C), Stress response (D), Surface location (E), Nucleic acid metabolism (F), Photosynthesis (G), Signal domain (H) and Carbon metabolism and energy (I).

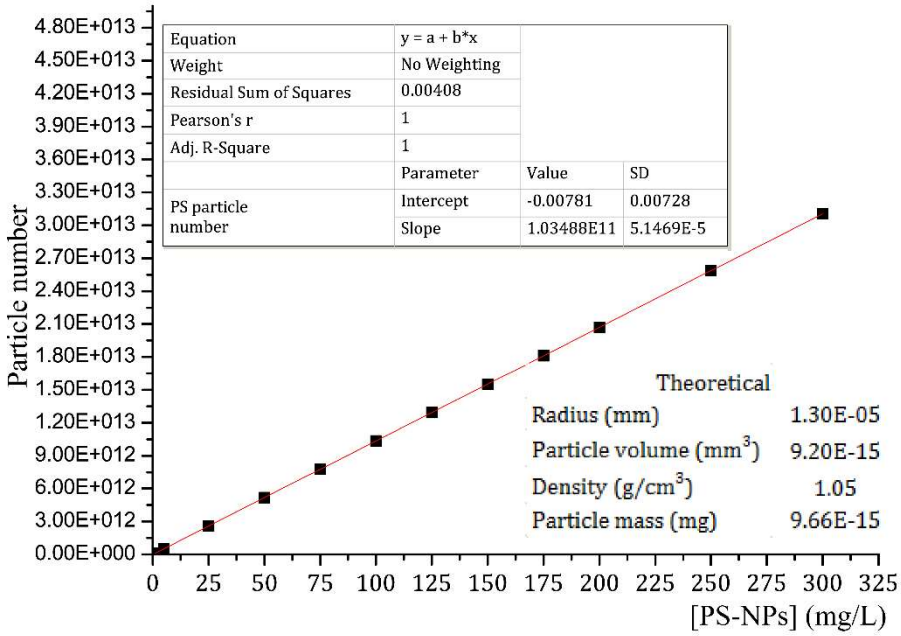

Figure S3: Theoretical linear regression between PS-NPs particle number and concentration as well as the correspondent related parameters.

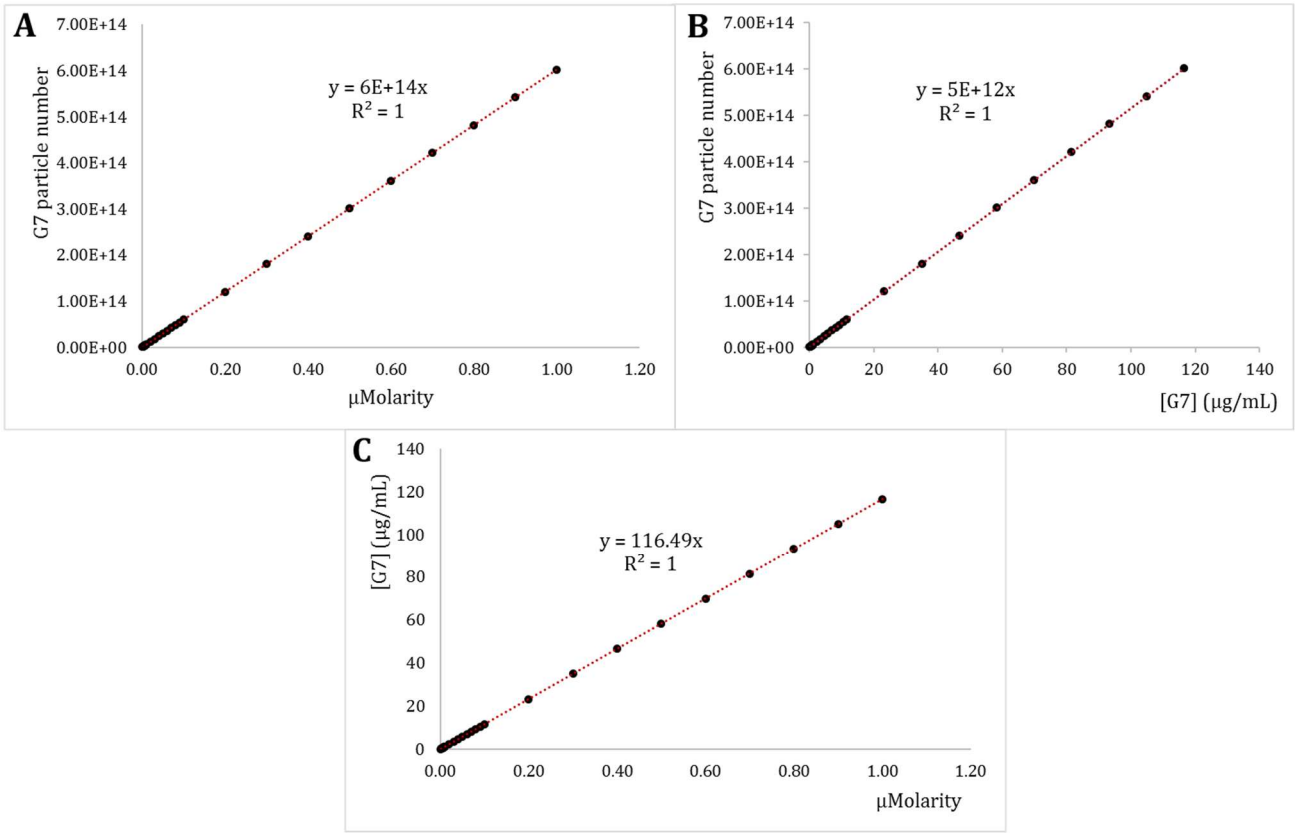

Figure S4: Theoretical linear regressions between G7 particle number and concentration (in term of µM or mg/L) as well as the corresponding related parameters.

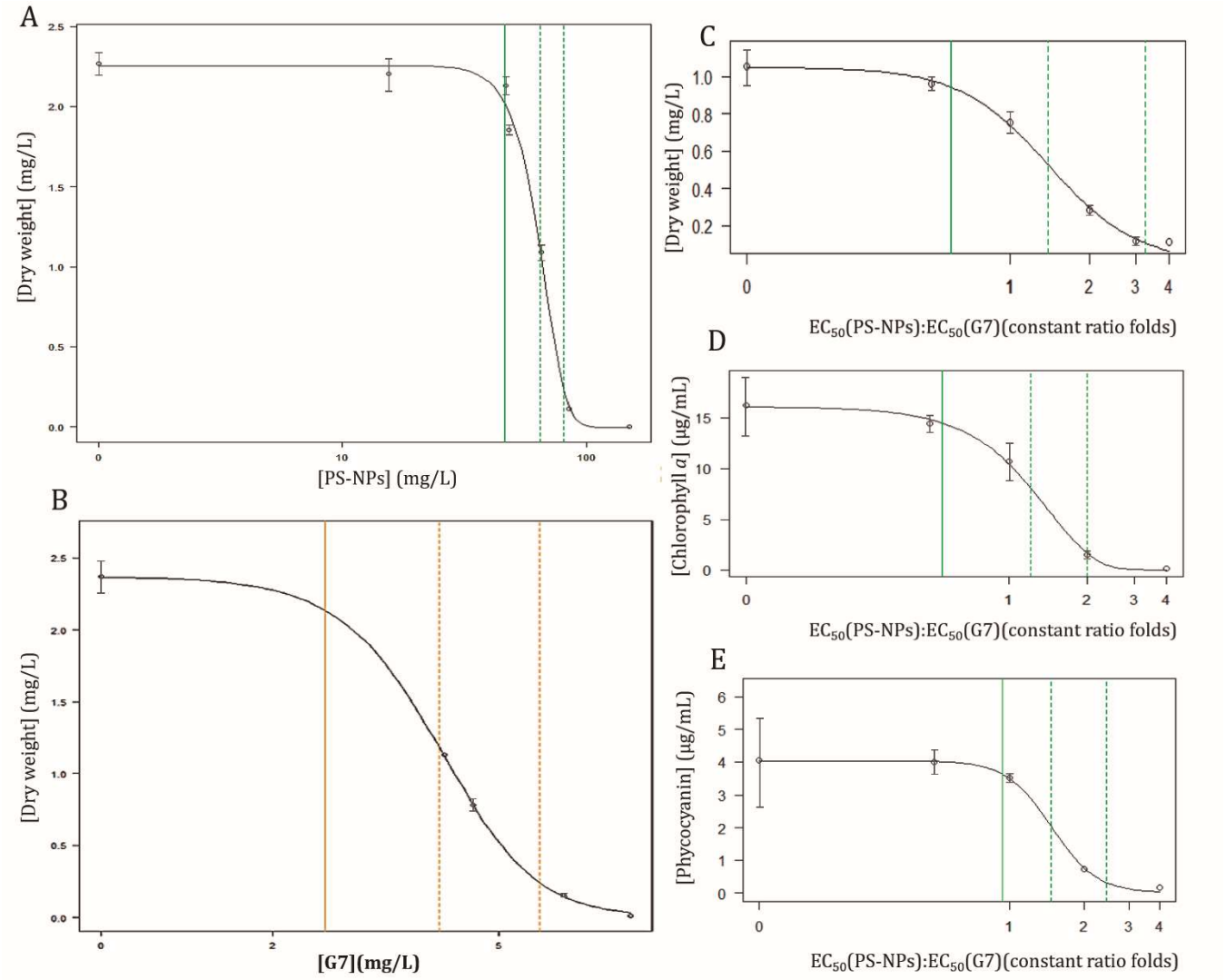

Figure S5: Individual dose-response curves (DRC) for growth inhibition of *Anabaena* exposed to PS-NPs (A) and G7 (B) for 72 h. Binary mixture DRC for growth inhibition (C), for chlorophyll *a* concentration (D) and for phycocyanin concentration decrease (E).

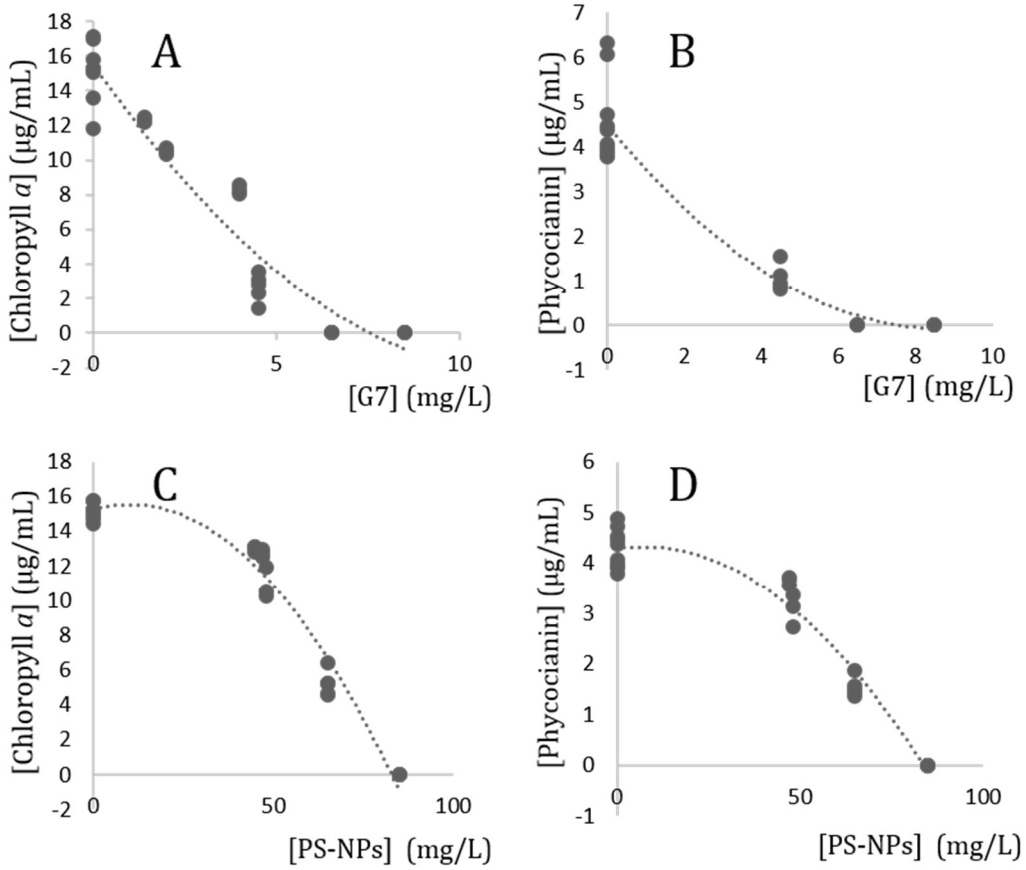

Figure S6: Dose-response curves (DRC) of *Anabaena* sp. PCC 7120 exposed to G7 PAMAM dendrimers (A, B), PS-NPs (C, D) and their mixture in the ratio 1:1 (EC_{50} for growth inhibition) (E, F) in terms of chlorophyll *a* (A, C) and phycocyanin content (B, D).

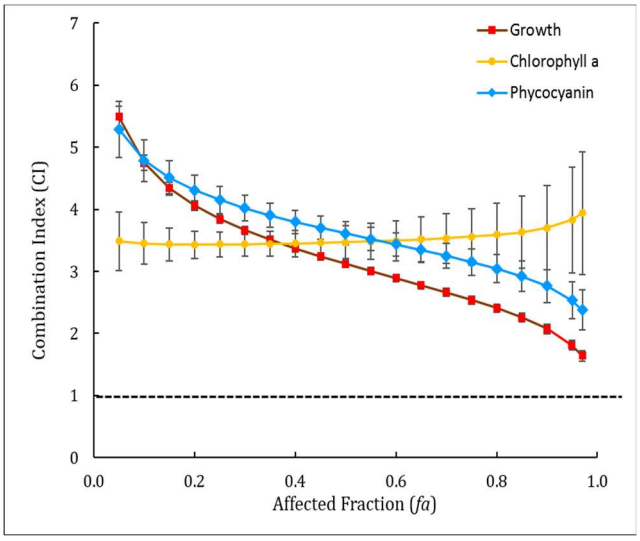

Figure S7: Combination index plot for binary combinations of PS-NPs and G7 in a constant ratio corresponding to the EC_{50} of both nanopolymers for growth inhibition; CI values are plotted as a function of the growth inhibition, decrease in chlorophyll a concentration and decrease in phycocyanin concentration (through all effect levels, fa). CI > 1 indicates antagonism and the dashed line additivity (CI = 1)

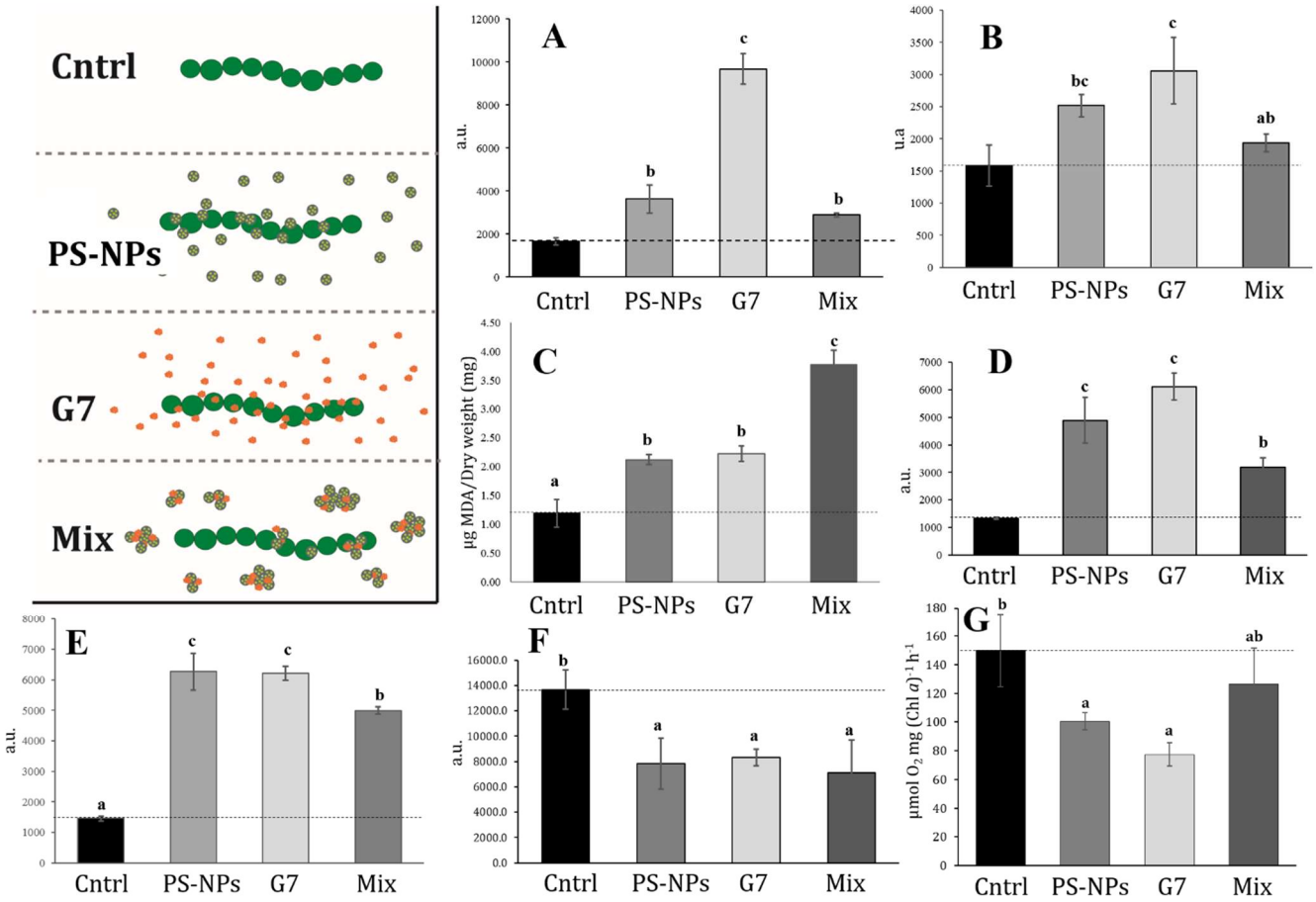

Figure S8: Physiological response of *Anabaena* sp. PCC7120 after its exposure to PAMAM dendrimer of generation 7 (G7) and polystyrene nanoparticles (PS-NPs), their mixture (Mix) and non-exposed cultures (Cntrl). Measurements were conducted by fluorimetry using a set of fluorochromes to evaluate: intracellular ROS formation by using 2 different fluorochromes [H_2DCF DA for general ROS formation (A), DHR 123 for H_2O_2 formation (B)], lipid peroxidation (C) by quantification of TBARS, membrane integrity by propidium iodide (D), cytoplasmic membrane potential (E) by DiBAC$_4$(3)), intracellular pH (F)by using BCECF AM and photosynthesis (G). Different letters indicate treatments that are significantly different (Tukey's HSD, $p < 0.05$).

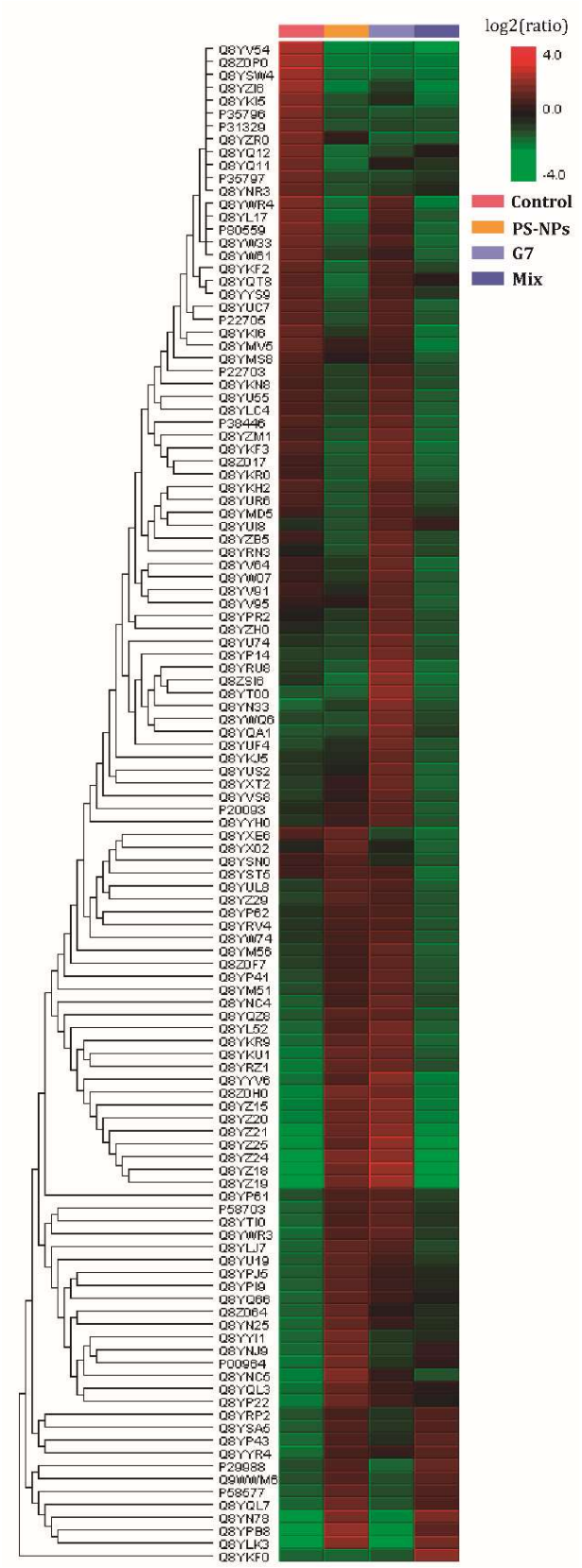

Figure S9: Heatmap with phylogenetic tree representing the proteomic response of *Anabaena* sp. PCC7120 in which at least one treatment induced significant change (FC <0.83 or >1.2, p <0.01) with respect to the control (p<0.01) after its exposure to PAMAM dendrimer of generation 7 (G7), polystyrene nanoparticles (PS-NPs) and the combination of both nanopolymers (Mix).

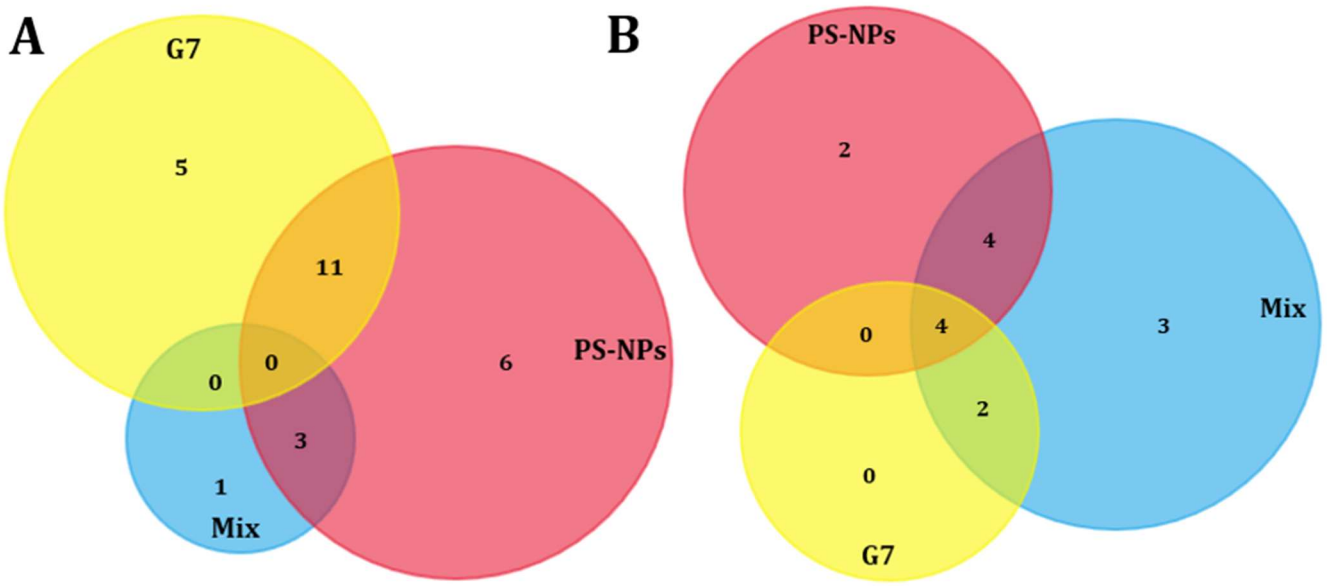

Upregulated (A)						
PS-NPs	**G7**	**Mix**	**PS-NPs & G7**	**PS-NPs & Mix**	**G7 & Mix**	**PS-NPs, G7 & Mix**
GlnA	All7222	All7348	Alr0663	All5295	-	-
CcmK	Alr7083	-	Alr0672	Alr4692	-	-
Alr4641	All0737	-	Alr0668	Alr4280	-	-
Alr4566	Alr2927	-	Alr0669	-	-	-
DpsA	All4737	-	Alr4380	-	-	-
Alr3804	-	-	Alr3301	-	-	-
-	-	-	Asl0662	-	-	-
-	-	-	Alr7200	-	-	-
-	-	-	All0667	-	-	-
-	-	-	CysA	-	-	-
-	-	-	All0666	-	-	-
Downregulated (B)						
PS-NPs	**G7**	**Mix**	**PS-NPs & G7**	**PS-NPs & Mix**	**G7 & Mix**	**PS-NPs, G7 & Mix**
Alr4029	-	All1783	-	ApcE	PecA	All0050
Alr4028	-	Alr7311	-	All7121	Alr0397	All2965
-	-	Alr4821	-	Alr7312	-	Alr0474
				Alr1540		All2127

Figure S10: Venn diagram of DEPs upregulated (A) and downregulated (B) upon the exposure of *Anabaena* sp. PCC7120 for 72 h to PS-NPs, G7 and their combined exposure (Mix) (FC <0.5 or >2, p <0.01). The table shows the DEPs clustered based on the Venn diagram distribution.

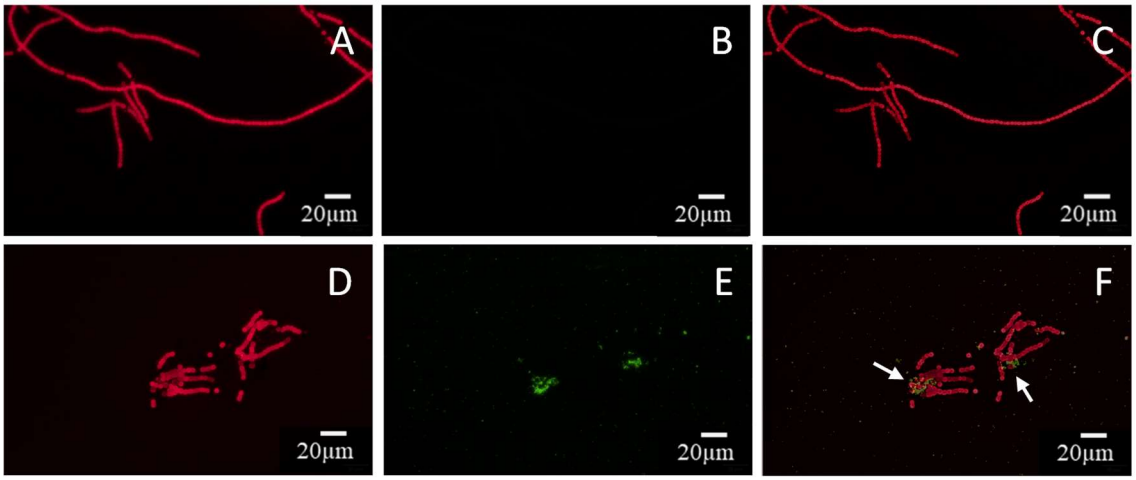

Figure S11: Fluorescence microscopy images (left to right): chlorophyll a fluorescence (red), PS-NPs fluorescence (green), and red/green fluorescence overlay. Images show *Anabaena* sp. PCC7120 cells after six days -control- (A, B, C) *and Anabaena* sp. PCC7120 cells after six days of exposure to the mixture PS-NPs + G7 (D, E, F). White arrows in the overlay images indicate heteroaggregates of PS-NPs and G7 adhered to sites of filament fragmentation.

References (SI)

1 M. Moreno, J. Escobar, A. Izquierdo-álvarez, A. Gil, S. Pérez, J. Pereda, I. Zapico, M. Vento, L. Sabater, A. Marina, A. Martínez-ruiz and J. Sastre, Disulfide stress: a novel type of oxidative stress in acute pancreatitis, *Free Radic. Biol. Med.*, 2014, **70**, 265–277.

2 A. Shevchenko, M. Wilm, O. Vorm and M. Mann, Mass Spectrometric Sequencing of Proteins from Silver-Stained Polyacrylamide Gels, *Anal. Chem.*, 1996, **68**, 850–858.

3 X. Zhou, W. Xiao, Z. Su, J. Cheng, C. Zheng and Z. Zhang, Hippocampal Proteomic Alteration in Triple Transgenic Mouse Model of Alzheimer ' s Disease and Implication of PINK 1 Regulation in Donepezil Treatment, *J. Proteomics*, 2019, **18**, 1542−1552.

4 C. C. Clement, W. Wang, M. Dzieciatkowska, M. Cortese, K. C. Hansen, A. Bece, S. Thangaswamy, I. Nizamutdinova and J. Moon, Quantitative Profiling of the Lymph Node Clearance Capacity, *Sci. Rep.*, 2018, **8**, 1–16.

5 Y. Zou, P. Gong, W. Zhao, J. Zhang, X. Wu and C. Xin, Neurochemistry International Quantitative iTRAQ-based proteomic analysis of piperine protected cerebral ischemia / reperfusion injury in rat brain, *Neurochem. Int.*, 2019, **124**, 51–61.

6 V. C. Sein-echaluce, A. González, M. Napolitano, I. Luque, F. Barja, M. L. Peleato and M. F. Fillat, Zur (FurB) is a key factor in the control of the oxidative stress response in Anabaena sp . PCC 7120, *Environ. Microbiol.*, 2017, **17**, 2006–2017.

7 H. Jin, R. Kim and D. Bhaya, Deciphering proteolysis pathways for the error-prone DNA polymerase in cyanobacteria, *Environ. Microbiol.*, 2020, **00**, 1–13.

8 S. Moslavac, R. Bredemeier, O. Mirus, B. Granvogl, L. A. Eichacker and E. Schleiff, Proteomic Analysis of the Outer Membrane of Anabaena sp . Strain PCC 7120, *J. Proteome Res.*, 2005, **4**, 1330–1338.

9 Sunčana Moslavac, Ludwig-Maximilians-Universität, 2007.

10 S. Ehira and S. Miyazaki, Regulation of Genes Involved in Heterocyst Differentiation in the Cyanobacterium Anabaena sp. Strain PCC 7120 by a Group 2 Sigma Factor SigC, *Life*, 2015, 587–603.

11 S. Ehira, M. Ohmori and N. Sato, Genome-wide Expression Analysis of the Responses to Nitrogen Deprivation in the Heterocyst-forming Cyanobacterium Anabaena sp . Strain PCC 7120, *DNA Res.*, 2003, **113**, 97–113.
12 L. Tian, Q. Chen, W. Jiang, L. Wang, H. Xie, N. Kalogerakis, Y. Ma and R. Ji, A carbon-14 radiotracer-based study on the phototransformation of polystyrene nanoplastics in water versus in air †, *Environ. Sci. Nano*, , DOI:10.1039/c9en00662a.
13 M. Gholami, R. Mohammadi, M. Arzanlou, F. A. Dourbash, E. Kouhsari, G. Majidi, S. M. Mohseni and S. Nazari, In vitro antibacterial activity of poly (amidoamine) -G7 dendrimer, *BMC Infect. Dis.*, 2017, **17**, 1–11.